NSF/RA-800625

PB82-147844

	80-SM-14
	10. Project/Task/Work Unit No
·ing	11. Contract(C) or Grant(G) No. (C) (G) PFR7822865
ɜnce (EAS)	13. Type of Report & Period C 14.

ɪs Program (OPRM)
ɜnce Foundation
DC 20550

elastic models were developed for evaluating natural
bration of a wide class of earth dams in a direction
The nonhomogeneity of the dam materials was considered
al (axial) deviations. Dynamic properties of three re
fornia estimated from their earthquake records and the
[illegible] from the suggested model

PRINCETON UNIVERSITY

Department of Civil Engineering

50272-101

REPORT DOCUMENTATION PAGE	1. REPORT NO. NSF/RA-800625	2.	3. Recipient's Accession No. PB82 147844
4. Title and Subtitle: Earthquake Induced Longitudinal Vibration in Earth Dams			5. Report Date: December 1980 6. 008196
7. Author(s): A.M. Abdel-Ghaffer			8. Performing Organization Rept. No. 80-SM-14
9. Performing Organization Name and Address: Princeton University, Department of Civil Engineering, Princeton, NJ 08544			10. Project/Task/Work Unit No. 11. Contract(C) or Grant(G) No. (C) (G) PFR7822865
12. Sponsoring Organization Name and Address: Engineering and Applied Science (EAS), National Science Foundation, 1800 G Street, N.W., Washington, DC 20550			13. Type of Report & Period Covered 14.

15. Supplementary Notes
Submitted by: Communications Program (OPRM)
National Science Foundation
Washington, DC 20550

16. Abstract (Limit: 200 words)

Two-dimensional analytical elastic models were developed for evaluating natural frequencies and modes of vibration of a wide class of earth dams in a direction parallel to the dam axis. The nonhomogeneity of the dam materials was considered as well as both shear and normal (axial) deviations. Dynamic properties of three real earth dams in Southern California estimated from their earthquake records and the dynamic test results of one dam, are compared with those from the suggested models. It was found that the models in which both the shear modulus and the modulus of elasticity of the dam material vary along the depth provide the most appropriate representations for predicting the dynamic characteristics. The theoretical results from some of the models compared favorably with the experimental and earthquake data. An analysis of real earthquake performance of an earth dam, in the longitudinal direction, yielded data on the shear moduli, damping factors, and nonlinear constitutive relations for the dam materials; Ramberg-Osgood nonlinear stress-strain curves were then fitted to these data. As a result of the study, a qualitative picture is presented of the distribution of dynamic strains and stresses and stresses within an earth dam during an earthquake.

17. Document Analysis a. Descriptors

Earthquake resistant structures
Earth dams
Dynamic structural analysis
Model tests
Stress-strain curves
Shear modulus
Modulus of elasticity

b. Identifiers/Open-Ended Terms

Southern California
A.M. Abdel-Ghaffar, /PI

c. COSATI Field/Group

18. Availability Statement	19. Security Class (This Report)	21. No. of Pages
NTIS	20. Security Class (This Page)	22. Price

PRINCETON UNIVERSITY
CIVIL ENGINEERING DEPARTMENT
STRUCTURES AND MECHANICS PROGRAMS
(Earthquake and Geotechnical Engineering)

EARTHQUAKE INDUCED LONGITUDINAL VIBRATION IN EARTH DAMS

by

Ahmed M. Abdel-Ghaffar

REPORT NO. 80-SM-14

DECEMBER 1980

A Report on Research Conducted under Grant

from the National Science Foundation

PRINCETON, NEW JERSEY

This report is based on research conducted under Grant No. PFR78-22865 from the National Science Foundation. Any opinions, findings and conclusions or recommendations expressed in this publication are those of the author and do not necessarily reflect the views of the National Science Foundation.

TABLE OF CONTENTS

ACKNOWLEDGMENTS

This research was supported by a grant (PFR78-22865) from the National Science Foundation (Research Initiation in Earthquake Engineering Hazards Mitigation), with Dr. William W. Hakala as the Program Manager.

The author is grateful to Mr. Aik-Siong Koh, a graduate student in the Civil Engineering Department at Princeton University, for his research assistance and for the computer-plotting of most of the curves in this report.

The assistance provided by both the Department of Materials Engineering at the University of Illinois at Chicago Circle (1978-1979) and the Department of Civil Engineering at Princeton University (1979-1980) is greatly appreciated. Appreciation is extended to the School of Engineering and Applied Science at Princeton University.

The author also acknowledges the valuable discussions and suggestions given by Dr. Attila Askar of the Bagazici University in Turkey.

Sincere thanks are given to Ms. Anne Chase for her skillful typing of the manuscript and for help in preparing the final report.

ABSTRACT

Two-dimensional analytical elastic models are developed for evaluating dynamic characteristics, namely natural frequencies and modes of vibration of a wide class of earth dams in a direction parallel to the dam axis. In these models the nonhomogeneity of the dam materials is taken into account by assuming a specific variation of the stiffness properties along the depth (due to the continuous increase in confining pressure). In addition, both shear and normal (axial) deformations are considered. Cases having constant elastic moduli, linear and trapezoidal variations of elastic moduli, and elastic moduli increasing as the one-half, one-third, two-fifths, and a general $(\ell/m)^{th}$ powers of the depth are studied. Dynamic properties of three real earth dams in a seismically active area (Southern California) estimated from their earthquake records (input ground motion and crest response in the longitudinal direction) as well as results from full-scale dynamic tests on one of these dams (including ambient and forced vibration tests) are compared with those from the suggested models. It was found that the models in which the shear modulus and the modulus of elasticity of the dam material vary along the depth are the most appropriate representations for predicting the dynamic characteristics. The agreement between the experimental and earthquake data and the theoretical results from some of the models is reasonably good. Based on the analytical models, a rational procedure is developed to estimate dynamic stresses and strains and corresponding elastic moduli and damping factors for earth dams from their hysteretic responses to real earthquakes, utilizing the hysteresis loops from the filtered crest and base records. This leads to a study of the nonlinear behavior in terms of the variation of stiffness and damping properties with

the strain levels of different loops. Finally, an analysis of real earthquake performance of an earth dam, in the longitudinal direction, yields data on the shear moduli, damping factors, and nonlinear constitutive relations for the dam materials; the Ramberg-Osgood nonlinear stress-strain curves are then fitted to these data.

CHAPTER I

INTRODUCTION

Designing a dam to resist earthquake damage is probably one of the most difficult tasks to be faced by the geotechnical and earthquake engineer. The information available concerning the performance of earth dams in particular during earthquakes is meager and offers little assistance to engineers planning a dam in a region of seismic activity. As relatively few earth dams have been subjected to strong earthquakes, it is dangerous to draw any specific conclusions regarding their performance or the likelihood of any particular modes of damage to such dams during strong ground motion. However, the few existing recordings on and near dams may be of assistance in giving some indication of performance characteristics in particular instances.

In the majority of earth dams shaken by severe earthquakes, two primary types of damage have occurred (10,15,20,24,29,30): longitudinal cracks at the top of the embankment and transverse cracks sometimes accompanied by crest settlement. The longitudinal cracks appear to have been caused primarily by the horizontal component of the earthquake motion in the upstream-downstream direction, that is, the direction perpendicular to the longitudinal axis of the dam. In contrast, transverse cracking of an earth dam can result from longitudinal dynamic strains induced by earthquake motion in the longitudinal direction (as well as from differential settlements). Such cracks are of concern because they present a path for water to flow through the dam's core.

Over the last two decades, much emphasis has been placed on the dynamic response analysis of earth dams and their safety against earthquakes. Although some progress has been made in the development of analytical and numerical

techniques (9,11,12,13,14,17,18,19,21,22,23,24,28) for evaluating the response of earth dams subjected to earthquake motions, these techniques are still in a rudimentary state of development. For instance, the existing analytical techniques for earth dams still assume uniform shear beam, elastic behavior, with the nature of the response restricted to horizontal shear deformation in the upstream-downstream direction. Due to these restrictive assumptions, the dynamic response analyses have many limitations and cannot be used to examine the nature of stress distribution within an earth dam due to longitudinal or vertical ground motion. In addition, a three-dimensional finite element or finite difference technique would be very costly.

Although the existing dynamic analyses of the upstream-downstream motion of an earth dam (Refs. 10 to 15, 19, and 20) have the most notable importance to earthquake resistant design, there can be little doubt that the problem of earthquake-induced strains and stresses in earth dams from longitudinal vibration should be of vital concern to earthquake and soil engineers. The importance of this type of vibration is demonstrated by the following points:

1. Transverse cracking of an earth dam may result directly from the large dynamic strains induced by the earthquake itself. Cracks that reach the core would reduce the structural strength of the dam and could lead to concentrated leaks resulting in eventual failure of the dam.
2. Differential settlement of an earth dam may contribute significantly to transverse cracking. The portions located close to the abutments and, sometimes, the central portion of the dam are subjected to tensile strains when the dam is deformed by differential settlement. The levels which these strains reach are dependent upon the geometry and relative compressibility of the foundation, abutments and embank-

ment. When the dam is then shaken by an earthquake, the additional dynamic strains may cause cracks to develop even if the additional strains are not large. This is explained by the fact that the initial strains caused by differential settlement may not be apparent until triggered or augmented by the earthquake. Figure 1.1 illustrates the contribution from both the strains induced by differential settlement and the dynamic strains induced by earthquake longitudinal excitation.

3. In all cases where earth dams have been seriously damaged during an earthquake, the dams were constructed without the use of present compaction control techniques. However, there is evidence to support the contention that even a large, well-constructed, modern earth dam can be cracked transversely by an earthquake. The San Fernando earthquake of February 9, 1971 (M_L = 6.3) caused a transverse crack on the Santa Felicia Dam crest at the east abutment, Fig. 1.2, (Refs. 1,4). This dam is comparatively large (236.5 ft high) and was constructed with modern design details and construction methods. The depth of the crack, approximately one-sixteenth of an inch in width, is not known. Investigation has implied that this narrow crack was caused by the dynamic strains induced by longitudinal vibration resulting from the earthquake and not by any settlement. Fortunately, the crack does not seem to be structurally significant.

This report develops analytical elastic models for evaluating the dynamic characteristics of nonhomogeneous earth dams such as natural frequencies and mode shapes of vibration in the direction parallel to the dam axis. Both shear and axial deformations are considered, and the variation of stiffness properties along the depth of the dam is taken into account. Comparison of both real earthquake observations of three earth dams and experimental results

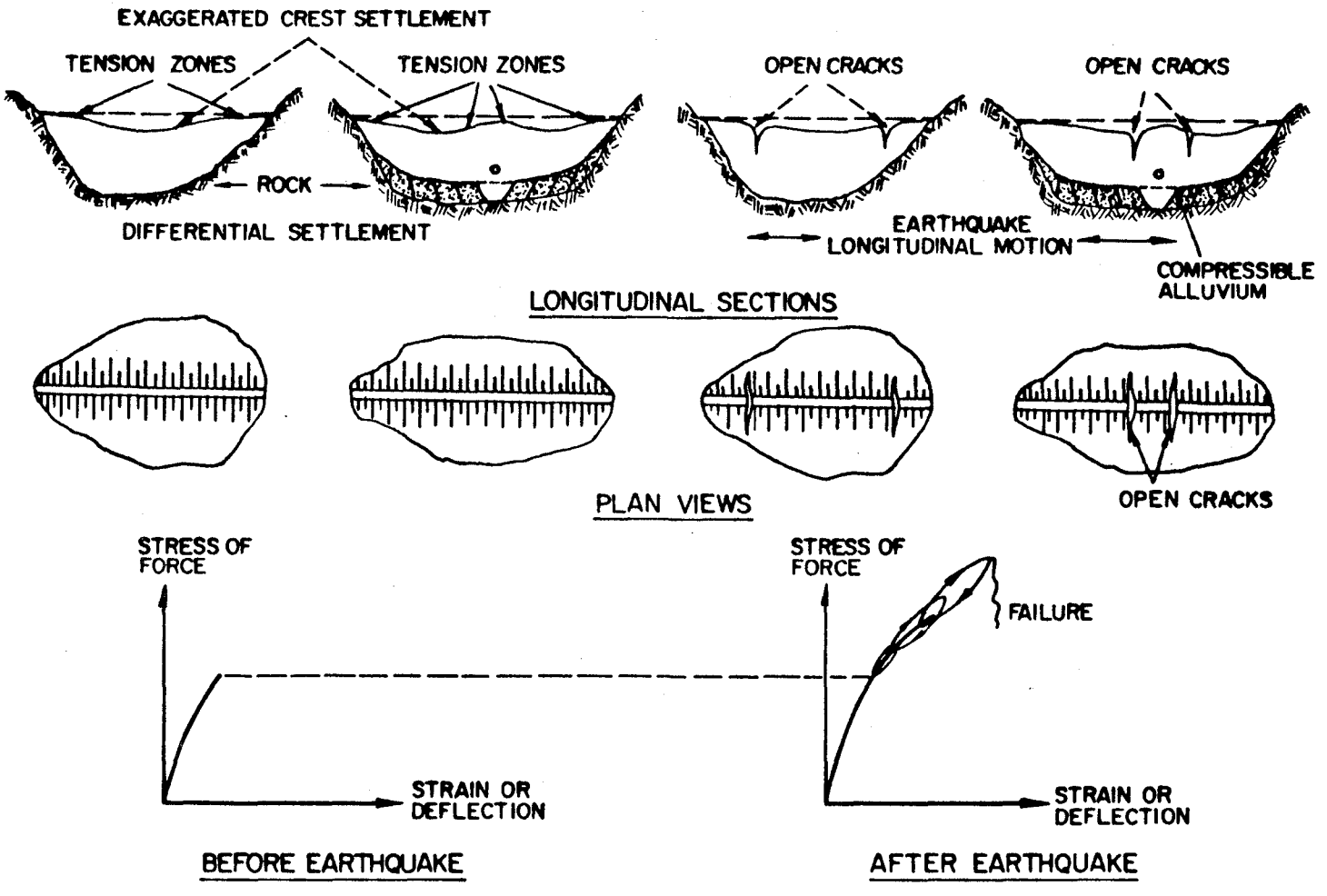

TYPICAL TRANSVERSE CRACKS IN EARTH DAMS DUE TO DIFFERENTIAL SETTLEMENT AND EARTHQUAKE LONGITUDINAL EXCITATIONS

Fig. 1.1 Effects of differential settlements and earthquake shakings.

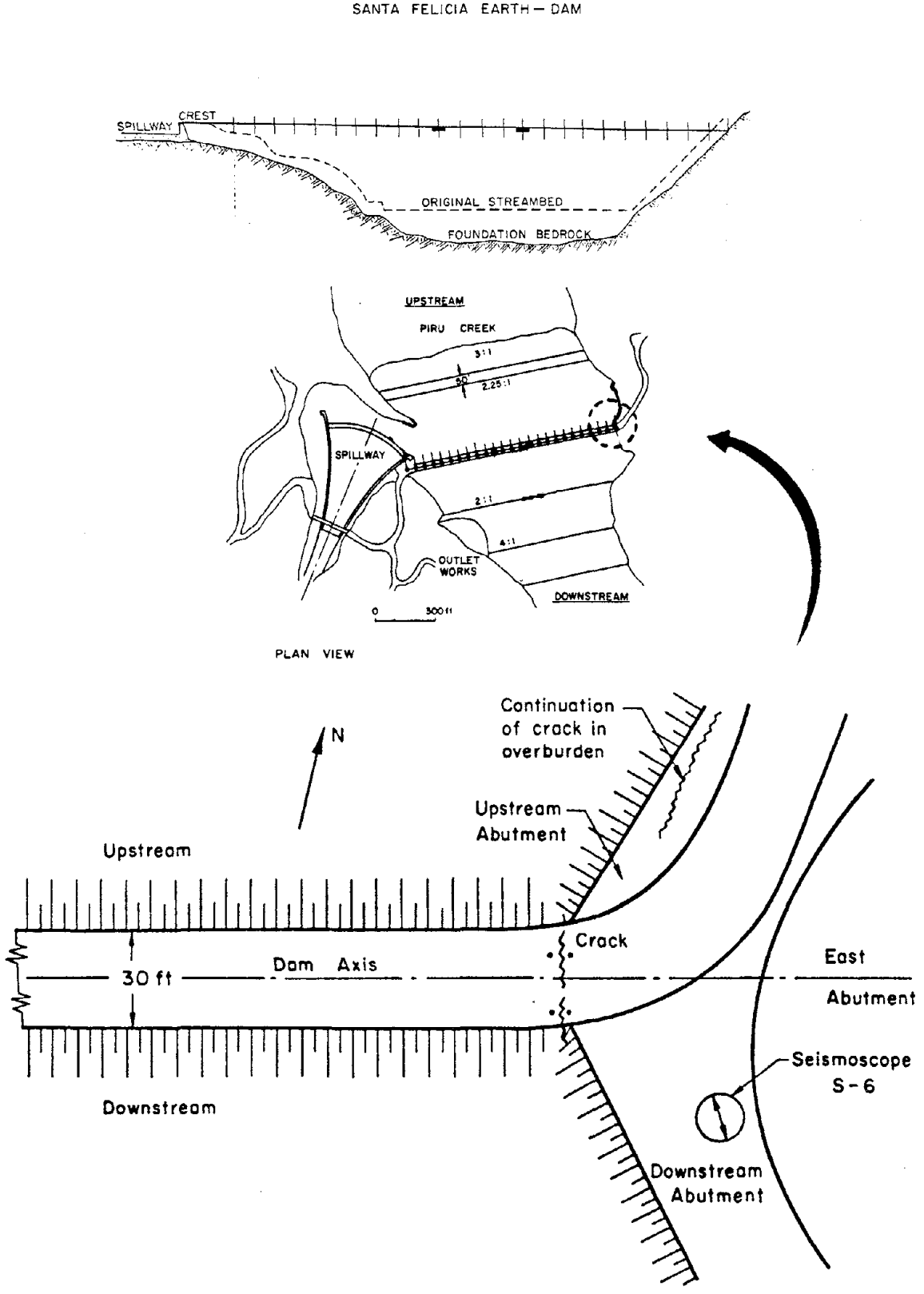

Fig. 1.2 The crack at the east abutment of Santa Felicia Dam as a result of the San Fernando earthquake of February 9, 1971.

(see Refs. 1,3,4,6,7,8) with the models' theoretical results have confirmed that these models are accurate enough to be used for estimating earthquake-induced longitudinal strains and stresses. In addition, the models and the full-scale response results help to reveal differences in the dynamic properties of dams under different loading conditions. Based on the analytical models, a rational procedure is developed to estimate dynamic stresses and strains and corresponding elastic moduli and damping factors for earth dams from their hysteretic responses to real earthquakes, utilizing the hysteresis loops from the filtered crest and base records. This leads to a study of the nonlinear behavior in terms of the variation of stiffness and damping properties with the strain levels of different loops. The report also utilizes the standard response spectra for estimating maximum earthquake-induced longitudinal strains and stresses. Finally, an analysis of real earthquake performance of an earth dam, in the longitudinal direction, yields data on the shear moduli, damping factors, and nonlinear constitutive relations for the dam materials; the Ramberg-Osgood nonlinear stress-strain curves are then fitted to these data. Although the assumption of elastic behavior during earthquakes is not strictly correct for earth dams, it provides a basis for establishing the natural frequencies of the dam, and it gives at least a qualitative picture of the distribution of dynamic strains and stresses within an earth dam during an earthquake.

CHAPTER II

FREE LONGITUDINAL VIBRATION OF NONHOMOGENEOUS EARTH DAMS

II-1. Simplifying Assumptions and Practical Considerations

In view of the fact that earth dams are large three-dimensional structures constructed from inelastic and nonhomogeneous materials, the determination of their dynamic characteristics such as the natural frequencies and modes of vibration is extremely difficult. As a result some simplifying assumptions are introduced.

1. The dam is represented by an elastic wedge of finite length (with symmetrical triangular section) in a rectangular canyon, resting on a rigid foundation (Fig. 2.1). This model is similar to the one often used to evaluate the dynamic characteristics of dams in the upstream-downstream direction (9,11,13,18,21,23). Closed form mathematical solutions for canyons of other shapes such as triangular, trapezoidal or parabolic are extremely difficult. Hence, in order to make use of the proposed solutions it is necessary to approximate a given dam's canyon shape to an equivalent rectangle.

2. The dam is modeled by a nonuniform elastic material that has uniform mass density ρ, a nonuniform cross section and variable stiffness or elastic moduli (G and E: the shear and elastic moduli) along the depth. Although the actual variation with depth (which is a function of the soil type, the method of construction and the geometry of the dam) has not been accurately measured in the field, some efforts (1,4,16,19,21,23) are encountered in the literature

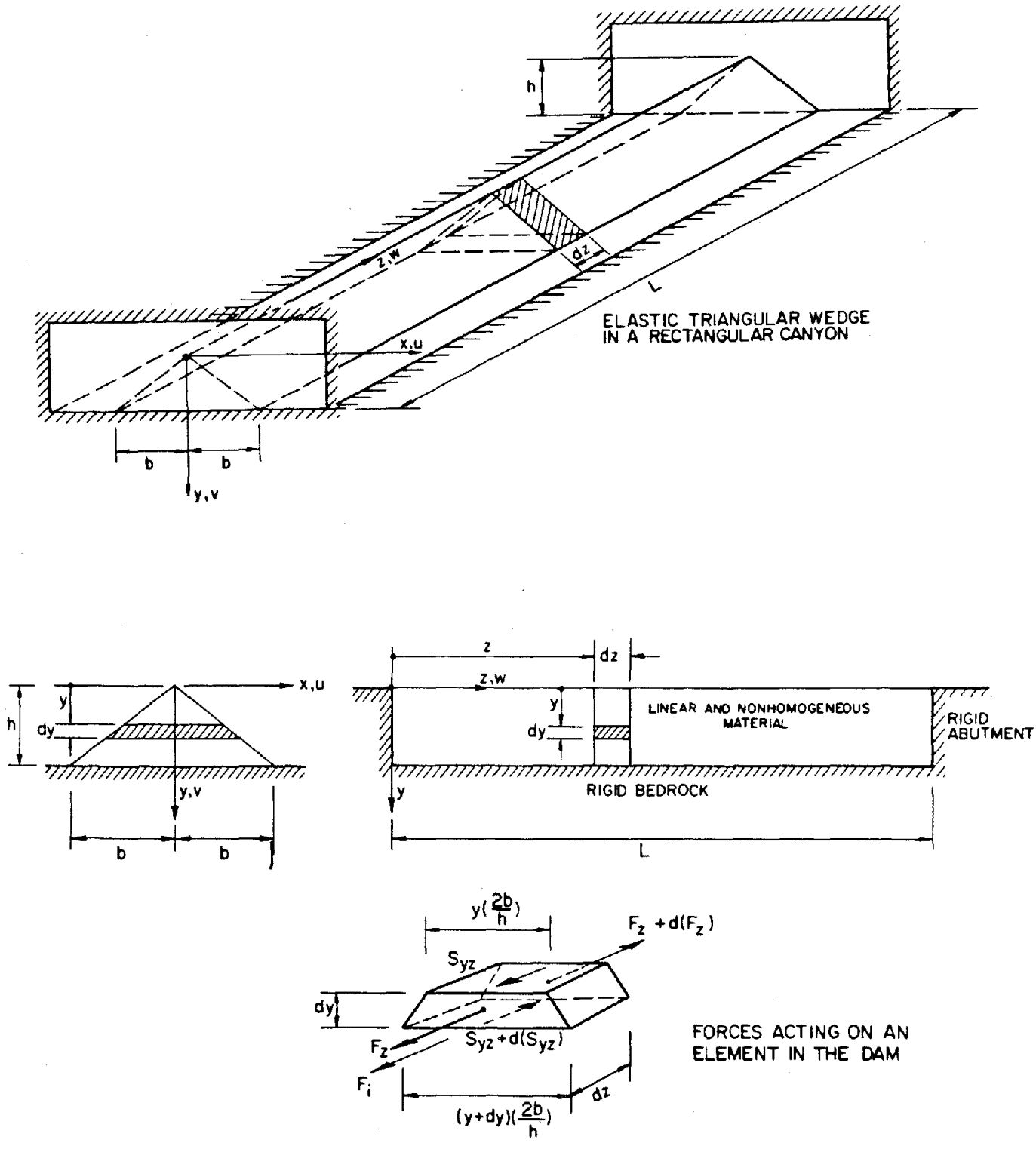

Fig. 2.1 The model considered in the longitudinal vibration analysis.

where the soil stiffness has been shown to vary in a continuous manner due to the continuous increase in normal stresses (or confining pressure). The continuous variation of soil stiffness may be represented by the following suggested relationships (Fig. 2.2):

A. Constant shear (or elastic) modulus (as a first order approximation):

$$G(y) = G = \text{constant}. \tag{2.1}$$

Dams constructed of homogeneous compacted earth fill consisting of material which is cohesive in nature can, at first approximation, be assumed to have a constant shear modulus (23).

B. Shear (or elastic) modulus increasing as the (ℓ/m)th power of the depth:

$$G(y) = G_0\left(\frac{y}{h}\right)^{\frac{\ell}{m}} , \tag{2.2}$$

where G_0 is the shear modulus of the dam material at the base and h is the height of the dam (Fig. 2.2). Four cases are considered:

B.1. Linear variation of shear (or elastic) modulus ($\ell = 1$ and $m = 1$) which may roughly account for the effect of confining pressure.

B.2. Shear (or elastic) modulus increasing as the square root of the depth ($\ell = 1$ and $m = 2$). If the low-amplitude shear modulus is proportional to the square-root of the confining pressure, this variation represents the case where the confining pressure is linearly proportional to the depth.

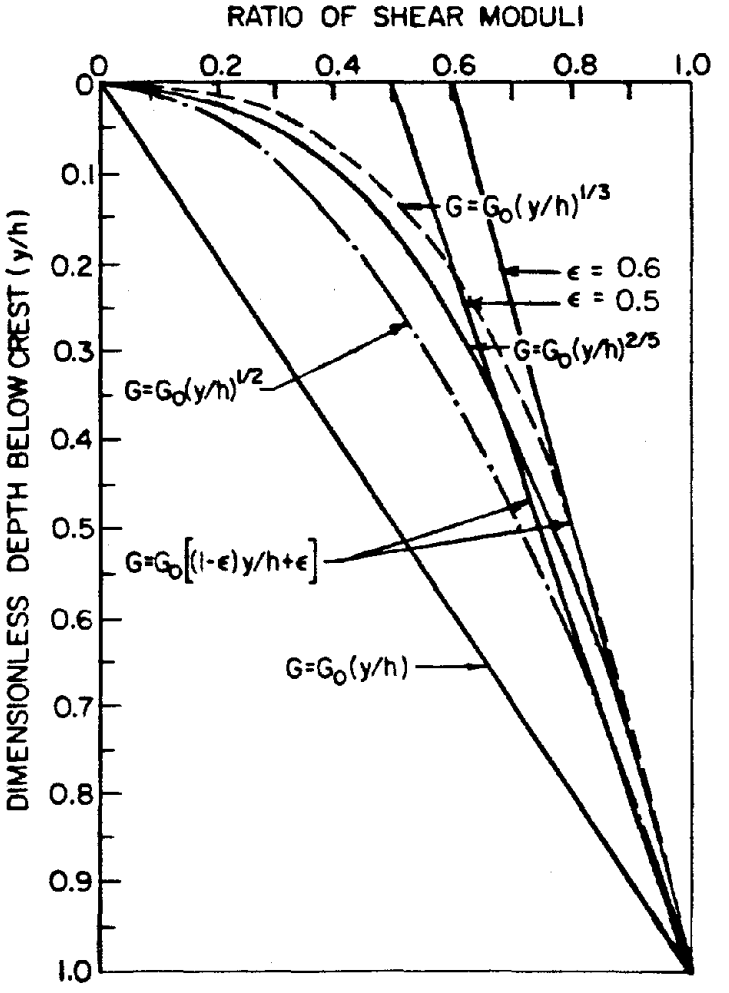

Fig. 2.2 Variation of stiffness properties along the depth of the dam.

B.3. Shear (or elastic) modulus increasing as the cube root of the depth (ℓ = 1 and m = 3). For earth dams consisting of cohesionless material, this case is most appropriate, because it has been shown that for such materials the shear modulus is approximately proportional to the cube root of the confining pressure (16,17,23,31).

B.4. Shear (or elastic) modulus increasing as the two-fifth power of the depth (ℓ = 2 and m = 5). This case was found by means of wave-velocity measurements (1,4) to be the most appropriate representation for the Santa Felicia earth dam (in Southern California).

C. Linear and truncated variation of shear (or elastic) modulus (Fig. 2.2):

$$G(y) = G_0\left[(1-\varepsilon)\frac{y}{h} + \varepsilon\right] \quad , \quad \varepsilon = \frac{G_1}{G_0} \tag{2.3}$$

where G_1 is the crest shear (or elastic) modulus of the dam material; this case is also possible from in-situ wave velocity measurements. Based on the results of both earthquake records and wave velocity measurements, of earth dams, reported in the U.S. and Japan (1,16,17,19,20,21,23,25 and 26) and based, also, on the estimated spatial distribution, within a dam, of the effective-confining stress (through finite element or finite difference analyses, e.g., Ref. 14), Table 2.1 presents suggestions (pertinent to the above-mentioned variations) for various types of earth dams.

Table 2.1. Suggested Stiffness Variations for Various Types of Earth Dams

Case	Stiffness Variation	Applicability
A	$G(y) = \text{constant}$	Appropriate for low-height (up to 80 ft high) earth dams constructed of: 1-Homogeneous compacted earth fill consisting of cohesive material, 2-Impervious soil (such as clays or clayey sands and gravels) and semi-pervious soil (such as silty sands and gravels).
B.1 B.2 B.3 B.4	$G(y) = G_0(y/h)$ $G(y) = G_0(y/h)^{1/2}$ $G(y) = G_0(y/h)^{1/3}$ $G(y) = G_0(y/h)^{2/5}$ $\Big\} G_0\left(\frac{y}{h}\right)^{\frac{\ell}{m}}$	Appropriate for zoned dams consisting of both pervious material (such as rock gravel) and impervious or semi-pervious soils. Examples are: 1-Zoned with adjacent pervious, impervious or semi-pervious sections (h = 50-200 ft) 2-Zoned with a wide or thin central impervious or semi-pervious core, and pervious or semi-pervious shells (h = 50-350 ft).
C	$G(y) = G_0\left[\left(1 - \frac{G_1}{G_0}\right)\frac{y}{h} + \frac{G_1}{G_0}\right]$	Appropriate for large homogeneous compacted earth fill (h = 80-200 ft) consisting of cohesive material. Also may be used for rockfill homogeneous dams (h = 50-300 ft), as well as dams founded on a soil stratum or soil strata.

3. Material linearity of the dam's soil is assumed. This is an acceptable assumption for small strains; in addition, it gives a qualitative picture of the dynamic characteristics. For large strains, no truly nonlinear solution exists. The effect of nonlinearity in the earthquake response calculation can be approximated by repeating the calculation and adjusting the soil moduli and damping factors according to the level of strain (27) or by using a piecewise, nonhomogeneous, linear representation for each hysteresis loop of the response (1.6).
4. Longitudinal deformations are due to shear and axial forces in the longitudinal direction, and the shear stress (or axial stress) is assumed uniformly distributed over a given horizontal (or vertical) plane of an element taken through the dam (Fig. 2.1-b).
5. The influence of the reservoir is assumed negligible.
6. The dam is assumed homogeneous in the sense that there is no distinction between the core and shell materials.
7. The longitudinal vibration problem is uncoupled from both the upstream-downstream and the vertical vibration problems. It will be shown later that during the full-scale vibration tests of Santa Felicia Dam (3) vibrational coupling among the three orthogonal directions was encountered at some frequencies higher than the fundamental frequency (which is usually primary in earthquake response analyses).

Although probably adequate for computing natural frequencies of vibration, the above assumptions place severe restrictions on the use of the models for obtaining accurate pictures of the stress distribution within a dam during an earthquake.

II-2. Free Vibration Analysis

Forces acting on an element in the longitudinal direction, as shown in Fig. (2.1-b), are:

1. Inertial force:

$$F_i = \rho\left(\frac{y + y + dy}{2}\right)\frac{2b}{h}\, dydz\, \frac{\partial^2 w}{\partial t^2} \simeq \rho y\left(\frac{2b}{h}\right)dydz\, \frac{\partial^2 w}{\partial t^2} \quad , \tag{2.4}$$

where $2b$ is the total width of the base of any cross section and $w(x,z;t)$ is the vibrational displacement at depth y in the z-direction.

2. Shear force:

$$S_{yz} = \tau_{yz} y\left(\frac{2b}{h}\right)dz = G(y)\frac{\partial w}{\partial y}\left(\frac{2b}{h}\right)ydz \quad , \tag{2.5}$$

where τ_{yz} and $\frac{\partial w}{\partial y}$ are the shear stress and strain, respectively, at depth y in the z-direction.

3. Axial (normal) force:

$$F_z = \sigma_z\left(\frac{y + y + dy}{2}\right)\frac{2b}{h}\, dy \simeq E(y)\frac{\partial w}{\partial z}\left(\frac{2b}{h}\right)ydy \tag{2.6}$$

where σ_z and $\frac{\partial w}{\partial z}$ are the longitudinal stress and strain, respectively, and $E(y)$ is the Young's (elastic) modulus of the dam material:

$$E(y) = 2(1 + \nu)G(y) = \eta G(y) \tag{2.7}$$

in which ν is the Poisson's ratio of the dam material.

For the equilibrium of an element (Fig. 2.1-b), one obtains

$$F_i = \frac{\partial}{\partial y}(S_{yz})dy + \frac{\partial}{\partial z}(F_z)dz \quad . \tag{2.8}$$

Substituting the forces from Eqs. 2.5 and 2.6 into Eq. 2.8, the equation of motion governing free longitudinal vibration of the dam is given by

$$\rho \frac{\partial^2 w}{\partial t^2} = \frac{1}{y}\frac{\partial}{\partial y}\left[G(y)\frac{\partial w}{\partial y}\, y\right] + \frac{1}{y}\frac{\partial}{\partial z}\left[\eta G(y)\frac{\partial w}{\partial z}\, y\right] \quad . \tag{2.9}$$

The differential equations for the three categories of Table 2.1 can then be written as:

$$\frac{\partial^2 w}{\partial t^2} = v_s^2\left[\frac{\partial^2 w}{\partial y^2} + \frac{1}{y}\frac{\partial w}{\partial y}\right] + \eta v_s^2 \frac{\partial^2 w}{\partial z^2} \tag{2.10}$$

$$\frac{\partial^2 w}{\partial t^2} = \frac{v_{s0}^2}{h^{\ell/m}}\left[y^{\ell/m}\frac{\partial^2 w}{\partial y^2} + \left(\frac{\ell}{m}+1\right)y^{\left(\frac{\ell}{m}-1\right)}\frac{\partial w}{\partial y}\right] + \frac{\eta v_{s0}^2}{h^{\ell/m}}\, y^{\ell/m}\frac{\partial^2 w}{\partial z^2} \quad \left(\text{for } \frac{\ell}{m} = 1, \frac{1}{2}, \frac{1}{3}, \frac{2}{5}\right) \tag{2.11}$$

$$\frac{\partial^2 w}{\partial t^2} = v_{s0}^2\left[(1-\varepsilon)\frac{y}{h} + \varepsilon\right]\frac{\partial^2 w}{\partial y^2} + \frac{v_{s0}^2}{y}\left[2(1-\varepsilon)\frac{y}{h} + \varepsilon\right]\frac{\partial w}{\partial y} + \eta v_{s0}^2\left[(1-\varepsilon)\frac{y}{h} + \varepsilon\right]\frac{\partial^2 w}{\partial z^2} \tag{2.12}$$

where $v_s = \sqrt{G/\rho}$ is the shear wave velocity for the case where G is constant, and $v_{s0} = \sqrt{G_0/\rho}$ is the shear wave velocity at the base of the dam material.

By the method of separation of variables [$w = Y(y)Z(z)T(t)$], the following equations are obtained for the time and space variables:

$$\ddot{T}(t) + \omega^2 T(t) = 0 \quad , \tag{2.13}$$

$$Z''(z) + \alpha^2 Z(z) = 0 \quad , \tag{2.14}$$

$$Y''(y) + \frac{1}{y}Y'(y) + \left(\frac{\omega^2}{v_s^2} - \eta\alpha^2\right)Y(y) = 0 \quad , \tag{2.15}$$

$$y^2Y'' + \left(1 + \frac{\ell}{m}\right)yY' + \left[\frac{\omega^2 h^{\ell/m}}{v_{s0}^2} y^{\left(2-\ell/m\right)} - \eta\alpha^2 y^2\right]Y = 0 \quad , \quad \left(\frac{\ell}{m} = 1, \frac{1}{2}, \frac{1}{3}, \frac{2}{5}\right) , \tag{2.16}$$

$$\left[(1-\varepsilon)y^2 + \varepsilon hy\right]Y'' + \left[2(1-\varepsilon)y + \varepsilon h\right]Y' + \left\{\frac{\omega^2 h}{v_{s0}^2} y - \eta\alpha^2\left[(1-\varepsilon)y^2 + \varepsilon hy\right]\right\}Y = 0, \tag{2.17}$$

where ω is the natural frequency and α is a constant (to be determined from the boundary conditions). The boundary conditions are:

$$\tau_{yz}(0,z;t) = G(0)\frac{\partial w}{\partial y}(0,z;t) = 0 \quad , \tag{2.18-a}$$

$$w(h,z;t) = 0 \quad , \tag{2.18-b}$$

$$w(y,0;t) = 0 \quad , \tag{2.18-c}$$

$$w(y,L;t) = 0 \quad . \tag{2.18-d}$$

In order to satisfy boundary conditions (2.18-c) and (2.18-d), one must have (from Eq. 2-14)

$$\alpha = \frac{r\pi}{L} \quad , \qquad r = 1,2,3,4,\ldots \quad . \tag{2.19}$$

Therefore, the mode shapes of longitudinal vibration in the z-direction can be given by

$$Z(z) = \sin\frac{r\pi}{L} z \quad , \qquad r = 1,2,3,\ldots \quad . \tag{2.20}$$

The mode shapes in the y-direction can be obtained by the solutions of Eqs. 2.15 through 2.17 and boundary conditions (2.18-a) and (2.18-b); Eq. 2.15 is the standard Bessel equation, while Eqs. 2.16 and 2.17 have no closed form (or special functional) solutions. The general solution of Eq. 2.15 is given by

$$Y(y) = C_1 J_0\left(\sqrt{\frac{\omega^2}{v_s^2} - \eta\alpha^2}\, y\right) + C_2 Y_0\left(\sqrt{\frac{\omega^2}{v_s^2} - \eta\alpha^2}\, y\right) \quad , \qquad (2.21)$$

where C_1 and C_2 are constants (to be determined from boundary conditions (2.18-a) and (2.18-b) and J_0 and Y_0 are Bessel functions of zero order, of first and second kinds, respectively. For finite displacement at the crest Y_0 is discarded. The frequency equation for the case where G is constant is thus given by

$$J_0\left(h\sqrt{\frac{\omega^2}{v_s^2} - \eta\left(\frac{r\pi}{L}\right)^2}\right) = 0 \quad . \qquad (2.22)$$

This frequency equation is only satisfied by particular values of the Bessel function (Eq. 2.22) argument which in turn defines the natural frequencies of vibration. Letting λ_n, n=1,2,3,..., be the roots of the frequency equation, then the natural frequencies of vibration, for the case where G is constant, are given by

$$\omega_{n,r} = \frac{v_s}{h}\sqrt{\lambda_n^2 + \eta\left(\frac{r\pi h}{L}\right)^2} \quad , \qquad n,r=1,2,3,... \qquad (2.23)$$

where $\omega_{n,r}$ is the frequency of the $(n,r)^{th}$ mode, and the mode shapes of vibration in the y-direction are defined by the function

$$Y_n(y) = J_0\left(\lambda_n \frac{y}{h}\right) \quad , \qquad n=1,2,3,... \quad . \qquad (2.24)$$

For the ordinary differential equation (Eq. 2.16) representing the case: $G(y) = G_0\left(\frac{y}{h}\right)^{\ell/m}$, a change of the independent variable, y, is used to obtain an equation for which solution in series by the method of Frobenius is utilized. The transformation is in the form

$$u = y^{\ell/m} \quad , \qquad \frac{\ell}{m} = 1, \frac{1}{2}, \frac{1}{3}, \frac{2}{5} \quad . \tag{2.25}$$

Then Eq. 2.16 becomes

$$u^2 \frac{d^2Y}{du^2} + 2u \frac{dY}{du} + \left[\left(\frac{m}{\ell}\right)^2 \frac{h^{\ell/m}}{v_{s0}^2} \omega^2 u^{\left(\frac{2m}{\ell} - 1\right)} - \eta\alpha^2\left(\frac{m}{\ell}\right)^2 u^{\frac{2m}{\ell}}\right] Y = 0, \quad \left(\frac{\ell}{m} = 1, \frac{1}{2}, \frac{1}{3}, \frac{2}{5}\right) \tag{2.26}$$

where $\left(\frac{2m}{\ell} - 1\right)$ and $\frac{2m}{\ell}$ are integers for the cases $\frac{\ell}{m} = 1, \frac{1}{2}, \frac{1}{3}, \frac{2}{5}$. Note that the point $y = 0$ (or $u = 0$) is a regular singular point; i.e., the general solution of a linear combination of convergent series exists. This solution is of the type

$$Y(u) = \sum_{k=0}^{\infty} a_k u^{k+s} \tag{2.27}$$

which satisfies the differential equation (Eq. 2.16). That is, the number s and the coefficients $a_0, a_1, a_2, \ldots$ have to be evaluated (by substituting into Eq. 2.26 and equating to zero the coefficient of each power of u) so that the series (Eq. 2.27) does in fact satisfy Eq. 2.16.

The coefficient of the lowest power of u, which is u^s, gives the indicial equation

$$s(s + 1) = 0 \quad \text{or} \quad s_1 = 0 \quad \text{and} \quad s_2 = -1 \ (\text{assuming } a_0 \neq 0) \ . \tag{2.28}$$

For the root $s_1 = 0$ the recurrence relations (which determine successively the coefficients $a_1, a_2, \ldots$ in terms of a_0) are given by

$$\left.\begin{aligned}
&a_0 \neq 0 \qquad \text{(valid for all cases)} \\
&a_1 = 0 \\
&a_2 = 0 \\
&a_{\left(\frac{2m}{\ell}-2\right)} = 0 \\
&a_{\left(\frac{2m}{\ell}-1\right)} = -\frac{1}{\frac{2m}{\ell}\left(\frac{2m}{\ell}-1\right)}\left(\frac{m}{\ell}\right)^2 \frac{h^{\ell/m}}{v_{s0}^2}\omega^2 a_0 \\
&a_{\left(k \geq \frac{2m}{\ell}\right)} = -\frac{1}{k(k+1)}\left(\frac{m}{\ell}\right)^2\left[\frac{h^{\ell/m}}{v_{s0}^2}\omega^2 a_{\left(k-\frac{2m}{\ell}+1\right)} - \eta\alpha^2 a_{\left(k-\frac{2m}{\ell}\right)}\right]
\end{aligned}\right\} \quad (2.29)$$

Note that $a_0 \neq 0$, $a_1 \neq 0$, and $a_2 \neq 0$ for the case of $\ell/m = 1$

And this case (where $s_1 = 0$) yields the solution

$$Y^{(1)}(u) = a_0 + a_{\left(\frac{2m}{\ell}-1\right)} u^{\left(\frac{2m}{\ell}-1\right)} + a_{\left(\frac{2m}{\ell}\right)} u^{\left(\frac{2m}{\ell}\right)} + \ldots + a_k u^k + \ldots\ldots, \quad \left(k > \frac{2m}{\ell}\right) \quad (2.30)$$

or

$$Y^{(1)}(y) = a_0 + a_{\left(\frac{2m}{\ell}-1\right)} y^{\left(2-\frac{\ell}{m}\right)} + a_{\left(\frac{2m}{\ell}\right)} y^2 + \ldots + a_k y^{\left(\frac{k\ell}{m}\right)} + \ldots, \quad \left(k > \frac{2m}{\ell}\right) \quad (2.31)$$

or

$$Y_n(y) = Y^{(1)}\left(\frac{y}{h}\right) = a_0\left[1 - \frac{1}{\frac{2m}{\ell}\left(\frac{2m}{\ell}-1\right)}\left(\frac{m}{\ell}\right)^2\left(\frac{\omega h}{v_{s0}}\right)^2\left(\frac{y}{h}\right)^{\left(2-\frac{\ell}{m}\right)} + \frac{1}{\frac{2m}{\ell}\left(\frac{2m}{\ell}+1\right)}\left(\frac{m}{\ell}\right)^2 \eta\left(\frac{\pi r h}{L}\right)^2\left(\frac{y}{h}\right)^2 + \ldots\right] \quad (2.32)$$

For the root $s_2 = -1$ the solution is given by

$$Y^{(2)}(u) = \left[\sum_{k=0}^{\infty}(s - s_2)a_k(s)u^{k+s}\right]_{s=s_2} \log u + \sum_{k=0}^{\infty}\left\{\frac{d}{ds}\left[(s - s_2)a_k(s)\right]\right\}_{s=s_2} u^{k+s_2} \qquad (2.33)$$

This solution provides infinite displacement at $y = 0$ (or $u = 0$) and therefore should be discarded.

The frequency equation, for the case where $G = G_0\left(\frac{y}{h}\right)^{\ell/m}$, is obtained by satisfying boundary condition (2.18-b) ($Y(y=h) = 0$ of Eq. 2.32); thus the natural frequencies are defined through the roots of

$$F\left(\frac{\omega^2 h^2}{v_{s0}^2},\ \eta\frac{\pi^2 r^2 h^2}{L^2}\right) = 0 \quad \text{or} \quad F\left(\overset{*}{\omega}, \beta_r\right) = 0 \quad , \qquad (2.34)$$

where the dimensionless frequency $\overset{*}{\omega}$ equals $\left(\frac{\omega h}{v_{s0}}\right)^2$, and the coefficient β_r is defined as $\eta\left(\frac{\pi r h}{L}\right)^2$; this coefficient depends on the Poisson's ratio ν of the dam material, the geometric dimension ratio $\left(\frac{h}{L}\right)$ and the order, r, of the modal configuration along the crest ($\beta_r \simeq 0$ implies a very long dam while higher values of β_r indicate a short, high dam or higher modes along the crest). For a wide class of earth dams the practical ranges of both ν and $\frac{h}{L}$ are 0.3 - 0.45 and 0.02 - 0.5, respectively (these give a value of η = 2.60 to 2.90). And for, say, four modal-wave forms ($r = 4$) along the crest the value of β_r ranges between 0.01 and 100. The roots $\overset{*}{\omega}$ for different values of β_r for the various cases of $G = G_0\left(\frac{y}{h}\right)^{\ell/m}$ are determined from the plots of the frequency equation (Eq. 2.34) in Figs. 2.3-a through 2.3-d; the roots are also shown in Table 2.2.

To estimate the natural frequencies and modes of longitudinal vibrations of any earth dam (for earthquake response analysis) it is strongly recommended that field wave-velocity measurements be carried out (using seismic techniques)

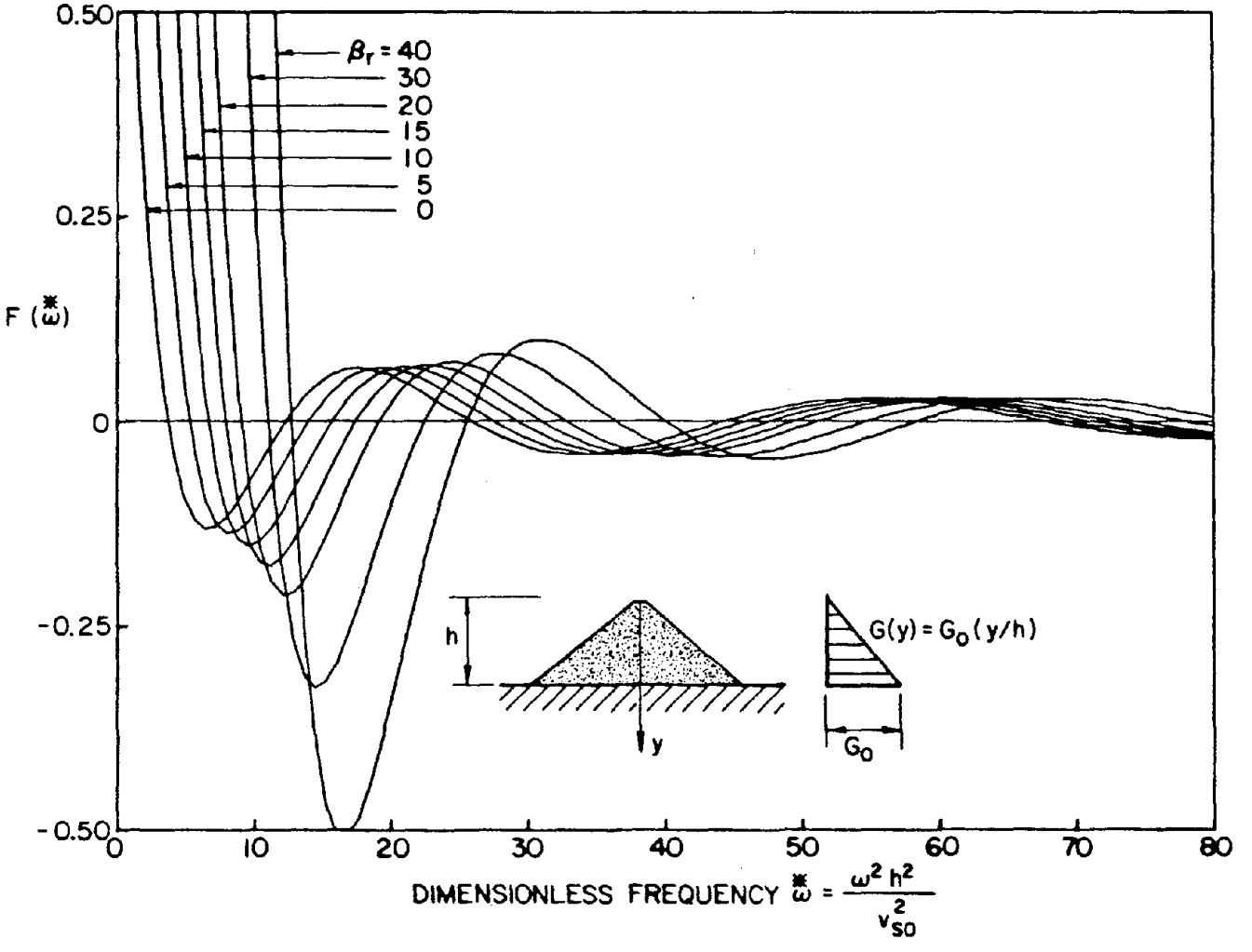

Fig. 2.3-a Plots of the frequency equations for the case where $\ell/m = 1$.

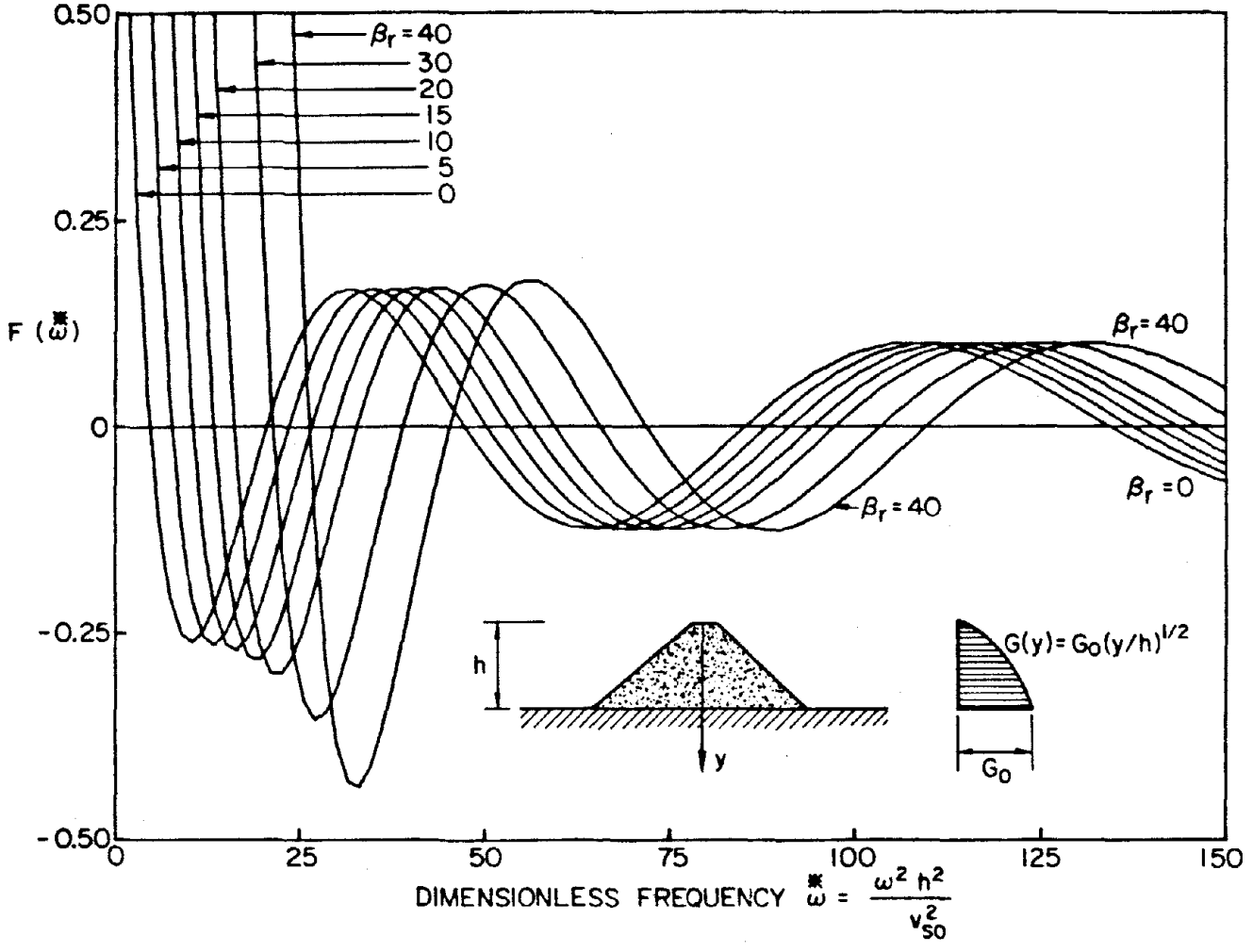

Fig. 2.3-b Plots of the frequency equations for the case where $\ell/m = 1/2$.

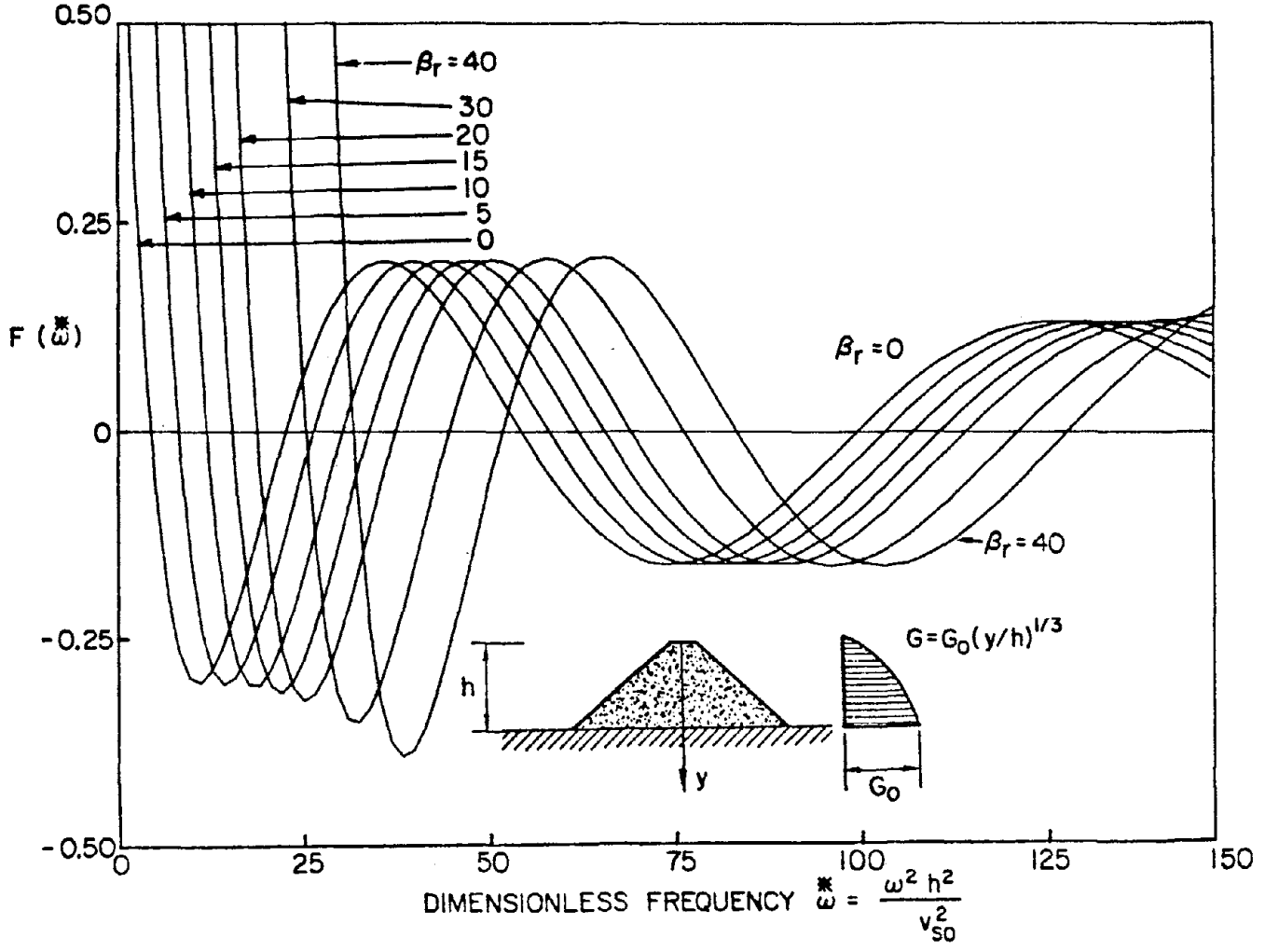

Fig. 2.3-c Plots of the frequency equations for the case where $\ell/m = 1/3$.

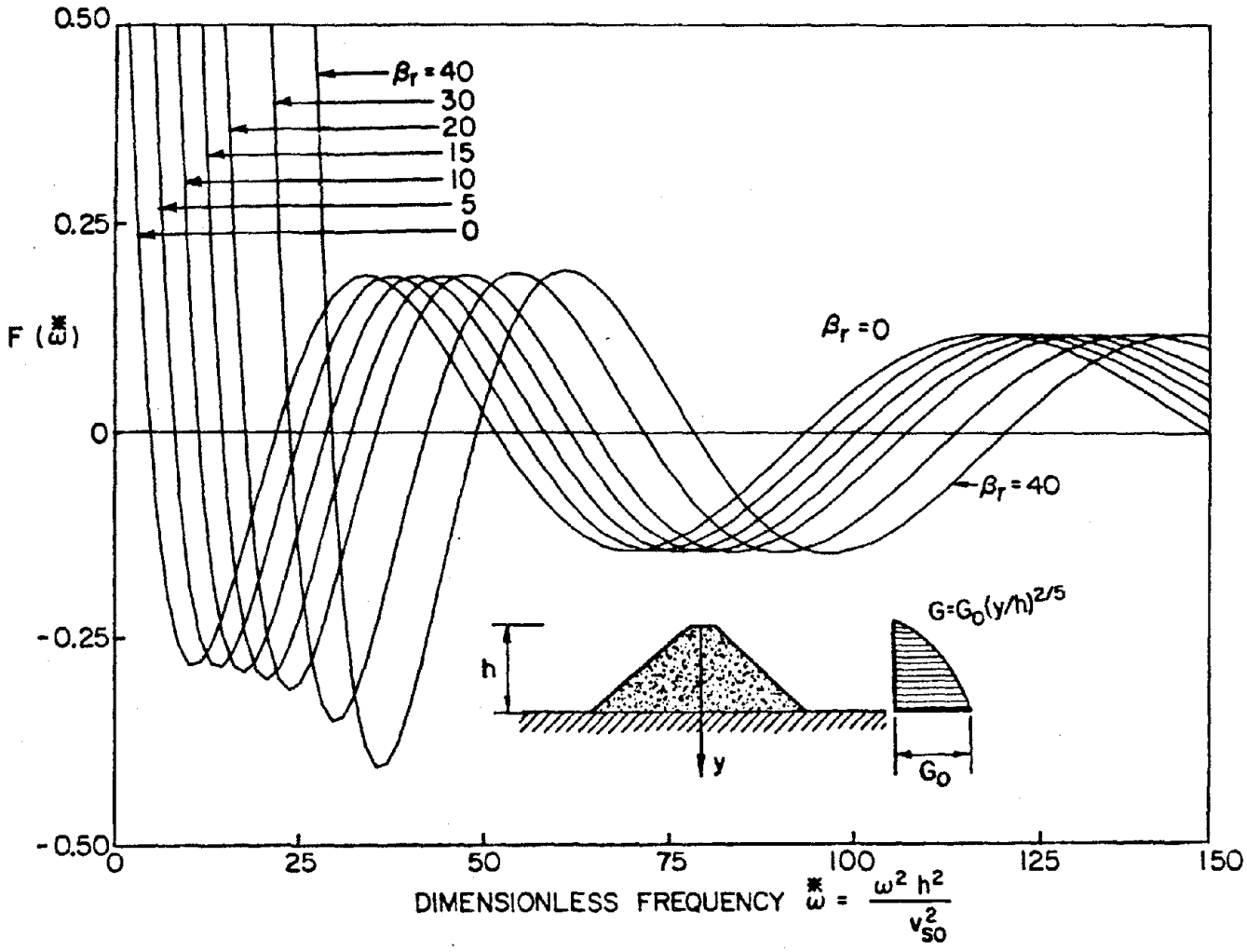

Fig. 2.3-d Plots of the frequency equations for the case where $\ell/m = 2/5$.

Table 2.2 Roots of Frequency Equations

$\beta_r = \eta\left(\frac{r\pi h}{L}\right)^2$	Mode Order (n,r)	Roots $\overset{*}{\omega}\left(=\frac{\omega^2 h^2}{v_{s0}^2}\right)$ of the Frequency Equation				
		G=Constant[a]	$G=G_0\left(\frac{y}{h}\right)$	$G=G_0\left(\frac{y}{h}\right)^{\frac{1}{2}}$	$G=G_0\left(\frac{y}{h}\right)^{\frac{2}{5}}$	$G=G_0\left(\frac{y}{h}\right)^{\frac{1}{3}}$
0	(1,r)	5.859	3.670	4.739	4.949	5.089
	(2,r)	30.472	12.305	20.472	22.325	23.601
	(3,r)	74.887	25.875	47.305	52.329	55.816
	(4,r)	139.039	44.380	85.242	94.966	101.737
5	(1,r)	10.859	5.244	7.697	8.253	8.638
	(2,r)	35.472	13.922	23.485	25.668	27.180
	(3,r)	79.887	27.558	50.313	55.668	59.391
	(4,r)	144.039	46.058	88.246	98.303	105.311
10	(1,r)	15.859	6.642	10.571	11.495	12.141
	(2,r)	40.472	15.708	26.524	29.030	30.773
	(3,r)	84.887	29.273	53.335	59.018	62.975
	(4,r)	149.039	47.757	91.260	101.646	108.890
15	(1,r)	20.859	7.891	13.363	14.677	15.598
	(2,r)	45.472	17.431	29.588	32.411	34.381
	(3,r)	89.887	31.018	56.373	62.378	66.566
	(4,r)	154.039	49.478	94.282	104.996	112.473
20	(1,r)	25.859	9.014	16.073	17.799	19.010
	(2,r)	50.472	13.138	32.676	35.811	38.003
	(3,r)	94.887	32.789	59.425	65.749	70.166
	(4,r)	159.039	51.221	97.314	108.351	116.062
30	(1,r)	35.859	10.973	21.268	23.869	25.698
	(2,r)	60.472	22.437	38.906	42.662	45.291
	(3,r)	104.887	36.399	65.573	72.522	77.389
	(4,r)	169.039	54.771	103.404	115.082	123.253
40	(1,r)	45.859	12.654	26.189	29.720	32.212
	(2,r)	70.472	28.525	45.181	49.568	52.629
	(3,r)	114.887	40.024	71.773	79.338	84.645
	(4,r)	179.039	58.399	109.529	121.839	130.463

[a] From Eq. 2.23:

$$\overset{*}{\omega} = \frac{\omega^2 h^2}{v_s^2} = \lambda_n^2 + \beta_r$$

(where $\lambda_1 = 2.4048$, $\lambda_2 = 5.5201$, $\lambda_3 = 8.6537$, $\lambda_4 = 11.7915$)

to determine the variation of shear wave velocity at various depths below the crest of the dam. Otherwise, the value of the shear wave velocity v_{s0} at the base of the dam has to be assumed and so may be inaccurate. The following table (Table 2.3) contains a guide (based on information in Refs. 1,2,3,15,16,17,21,23) for making such an assumption for specific types of dams.

Table 2.3

Type of Dam	Description	Values of v_{s0} (ft/sec)
Homogeneous Dams	*Hydraulic fill dams	200 - 600
	*Dams constructed of compacted silty clays	200 - 600
	*Dams constructed of compacted sandy clays	400 - 900
	*Dams constructed of compacted well-graded material	600 -1200
Zoned Dams	Dams consisting of zones of both pervious material such as rock gravel, and impervious well-graded alluvial material (compacted gravelly clays).	700 -1400

The mode shapes of vibration in the y-direction, for any value of β_r are defined by Eq. 2.32 after substituting the corresponding frequency $\overset{*}{\omega}$. It is important to indicate that for the general case where $G(y) = G_0\left(\frac{y}{h}\right)^{\ell/m}$ all the boundary conditions, Eq. 2.18, (including free shear stresses on the crest) are satisfied by the mode shape functions of Eqs. 2.20 and 2.32. Furthermore, the frequencies (eigenvalues) $\overset{*}{\omega}_{n,r}$ are distinct, and the mode shapes, $Y_n(y)Z_r(z)$, satisfy the orthogonality condition

$$\int_0^h \int_0^L \rho\left(\frac{2b}{h}\right) y Y_n(y) Y_m(y) Z_r(z) Z_j(z)\, dy dz = 0 \qquad m \neq n,\ r \neq j \quad . \tag{2.35}$$

Therefore, modal superposition can be used successfully to analyze the earthquake response of earth dams of the type defined above (B.1., B.2., B.3. and B.4.). The mode shapes in the y-direction for different values of β_r for the various cases of $G(y)$ are shown in Fig. 2.4 through Fig. 2.7.

Another power series solution for Eq. (2.17) can be obtained by assuming

$$Y(y) = \sum_{k=0}^{\infty} a_k y^{k+s} \tag{2.36}$$

In this case the indicial equation $s^2 = 0$ $(a_0 \neq 0)$ has the repeated roots $s_1 = s_2 = 0$, yielding only one solution, and the resulting recurrence relations are

$$\left.\begin{aligned} a_1 &= 0 \\ a_2 &= -\frac{1}{4\varepsilon h^2}\left[\left(\frac{\omega h}{v_{s0}}\right)^2 - \eta\varepsilon\alpha^2 h^2\right] a_0 \\ a_k &= -\frac{1}{k^2\varepsilon h^2}\left\{\left[k(k-1)(1-\varepsilon)h\right] a_{k-1} + \left[\left(\frac{\omega h}{v_{s0}}\right)^2 - \eta\varepsilon\alpha^2 h^2\right] a_{k-2} - \left[\eta(1-\varepsilon)\alpha^2 h\right] a_{k-3}\right\} \end{aligned}\right\} \tag{2.37}$$

(for $k \geq 2$)

Like the case where G is constant, the solution of this trapezoidal case (Eqs. 2.36 and 2.37) provides finite normal stress condition on the crest, $\sigma_z \neq 0$. The roots $\overset{*}{\omega}$ for different values of β_r for the trapezoidal case are determined from the plots of the frequency equation in Figs. 2.8-a and 2.8-b. The mode shapes in the y-direction for this trapezoidal case are shown in Fig. 2.9.

The frequency equation which defines the natural frequencies of vibration can be written as

$$F(\overset{*}{\omega}, \beta_r, \varepsilon) = 0 \quad . \tag{2.38}$$

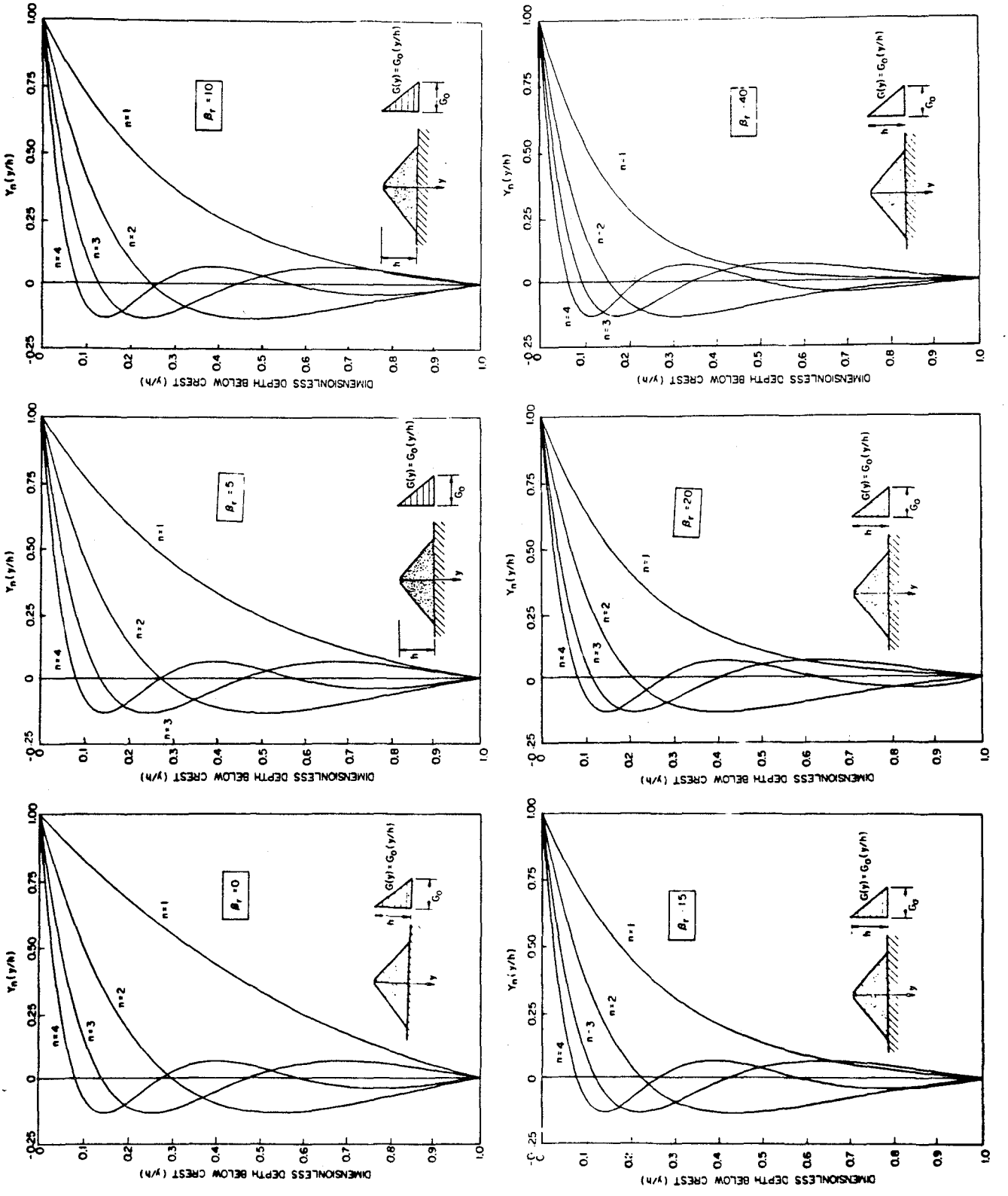

Fig. 2.4 Mode shapes of longitudinal vibration in the y-direction for different values of β_r for the case $G = G_0(y/h)$.

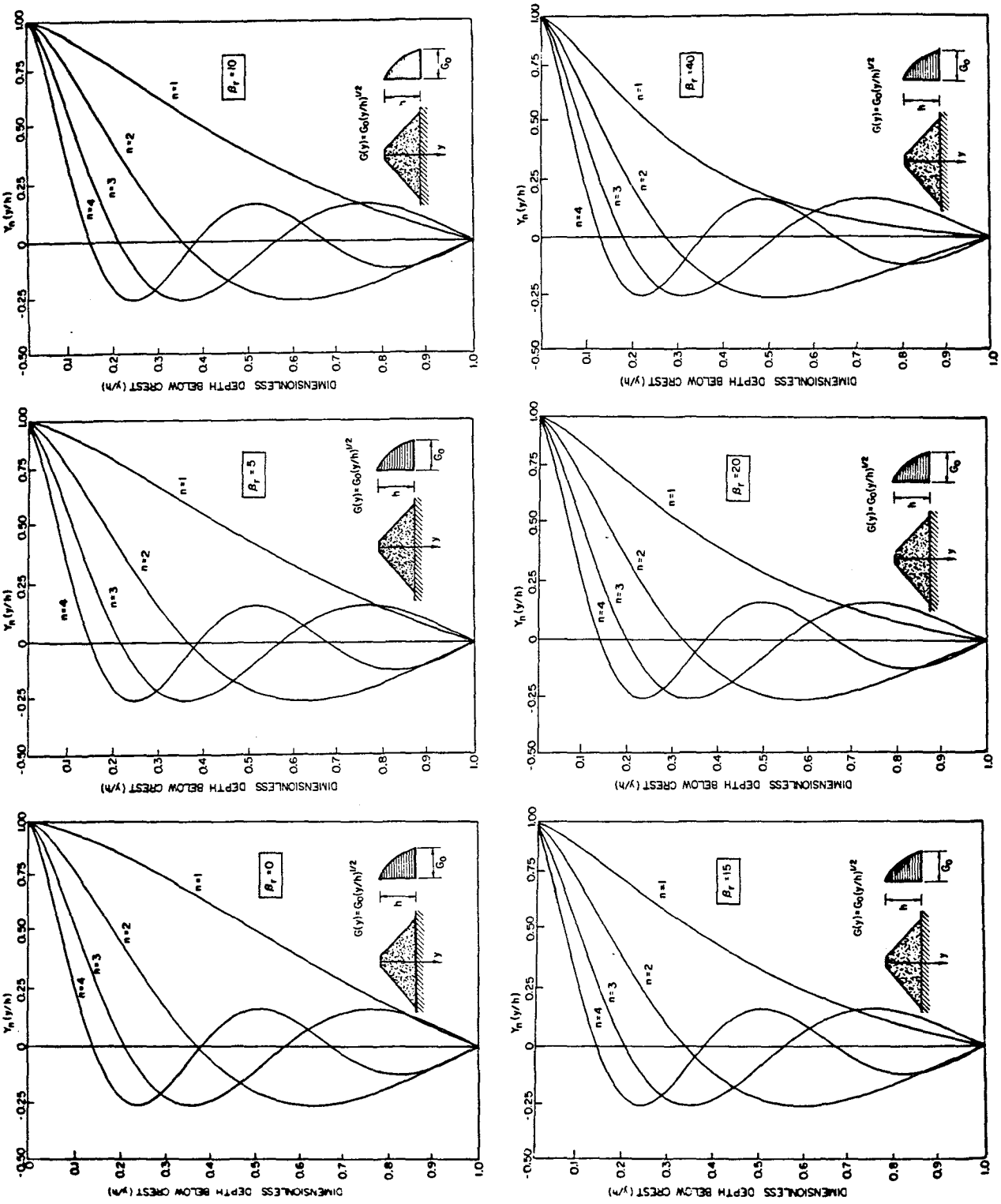

Fig. 2.5 Mode shapes of longitudinal vibration in the y-direction for different values of β_r for the case $G = G_0(y/h)^{1/2}$.

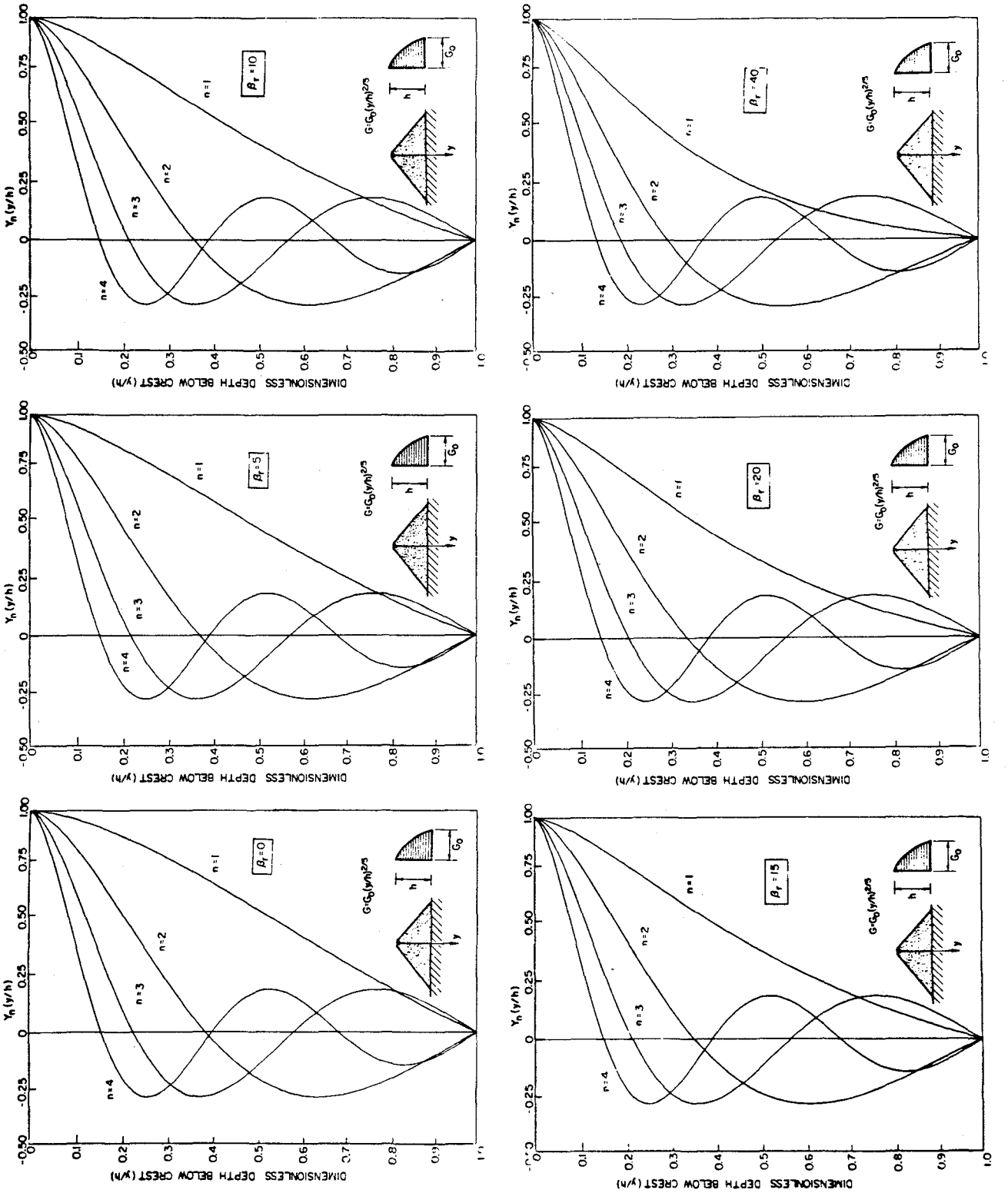

Fig. 2.6 Mode shapes of longitudinal vibration in the y-direction for different values of β_r for the case $G = G_0(y/h)^{2/5}$.

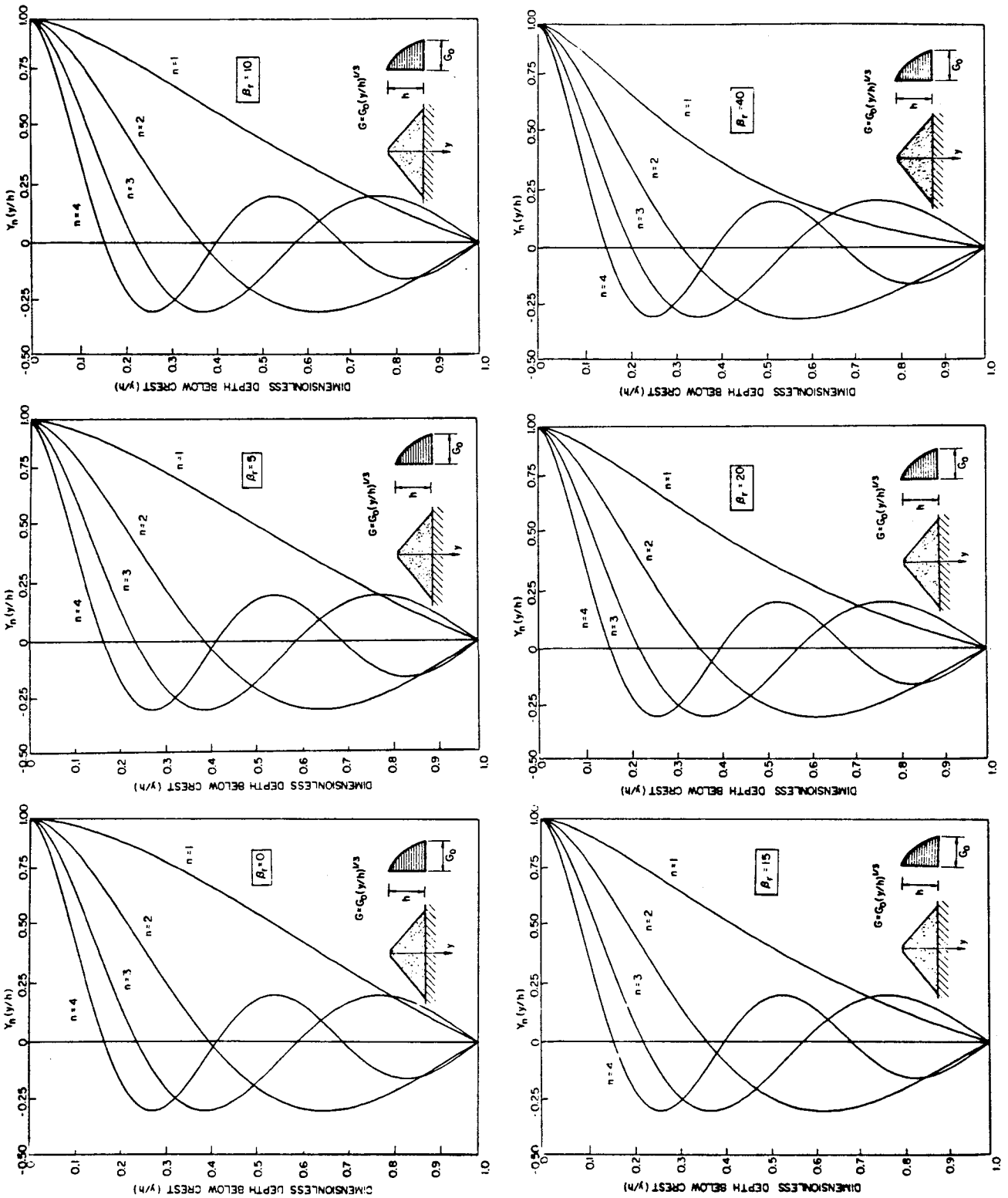

Fig. 2.7 Mode shapes of longitudinal vibration in the y-direction for different values of β_r for the case $G = G_0 (y/h)^{1/3}$.

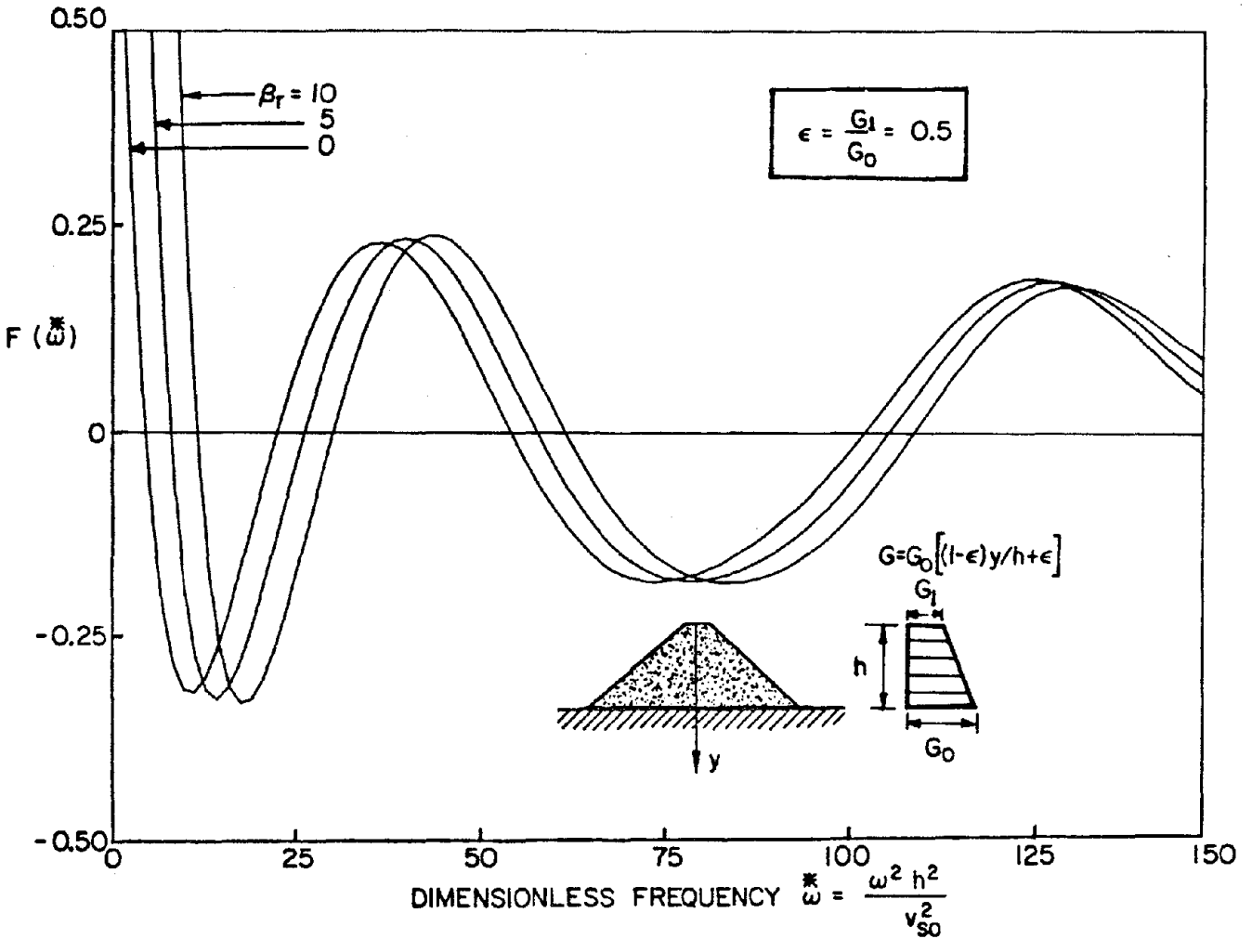

Fig. 2.8-a Plots of the frequency equations for the case where $\varepsilon = 0.5$.

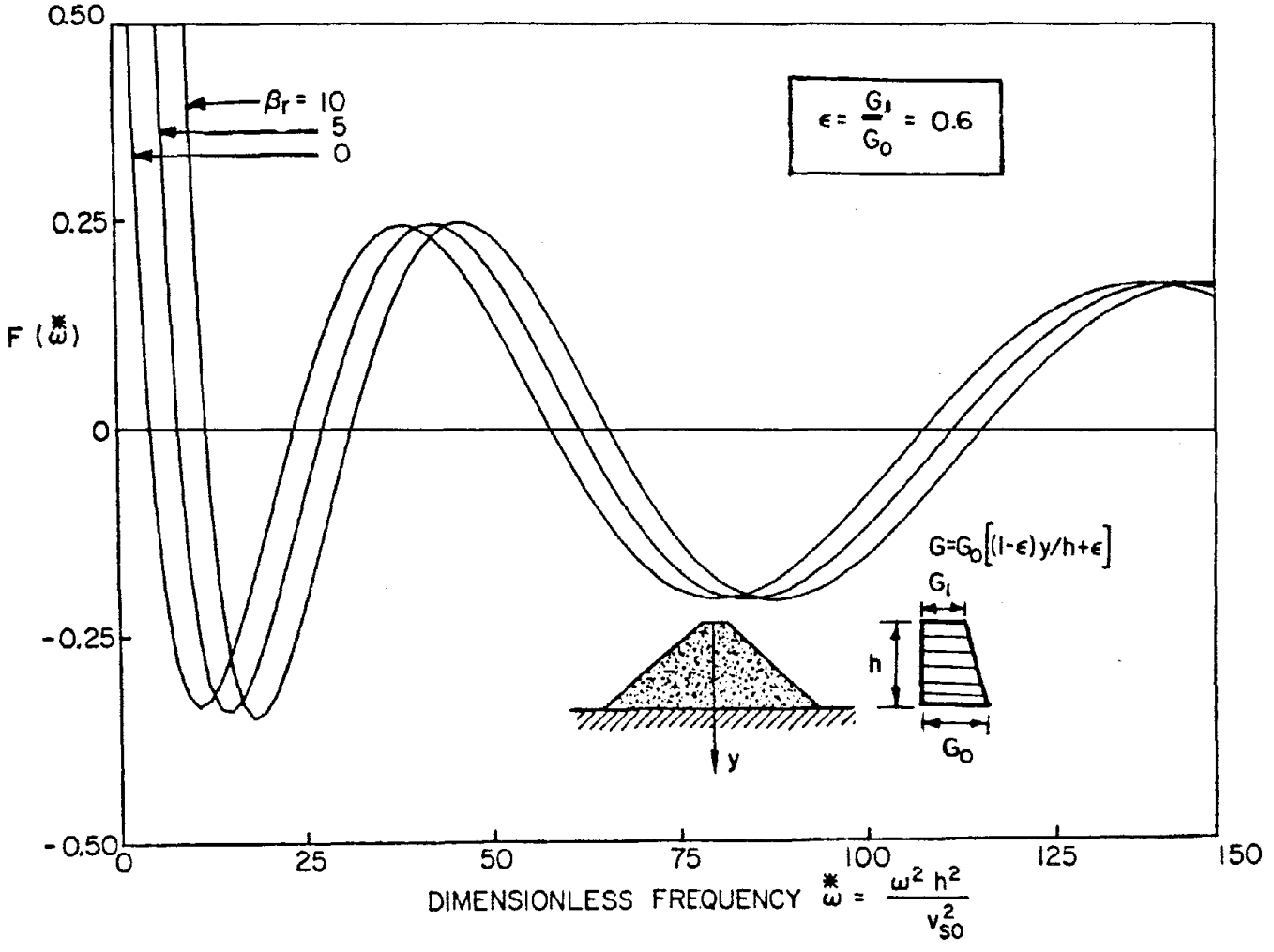

Fig. 2.8-b Plots of the frequency equations for the case where $\varepsilon = 0.6$.

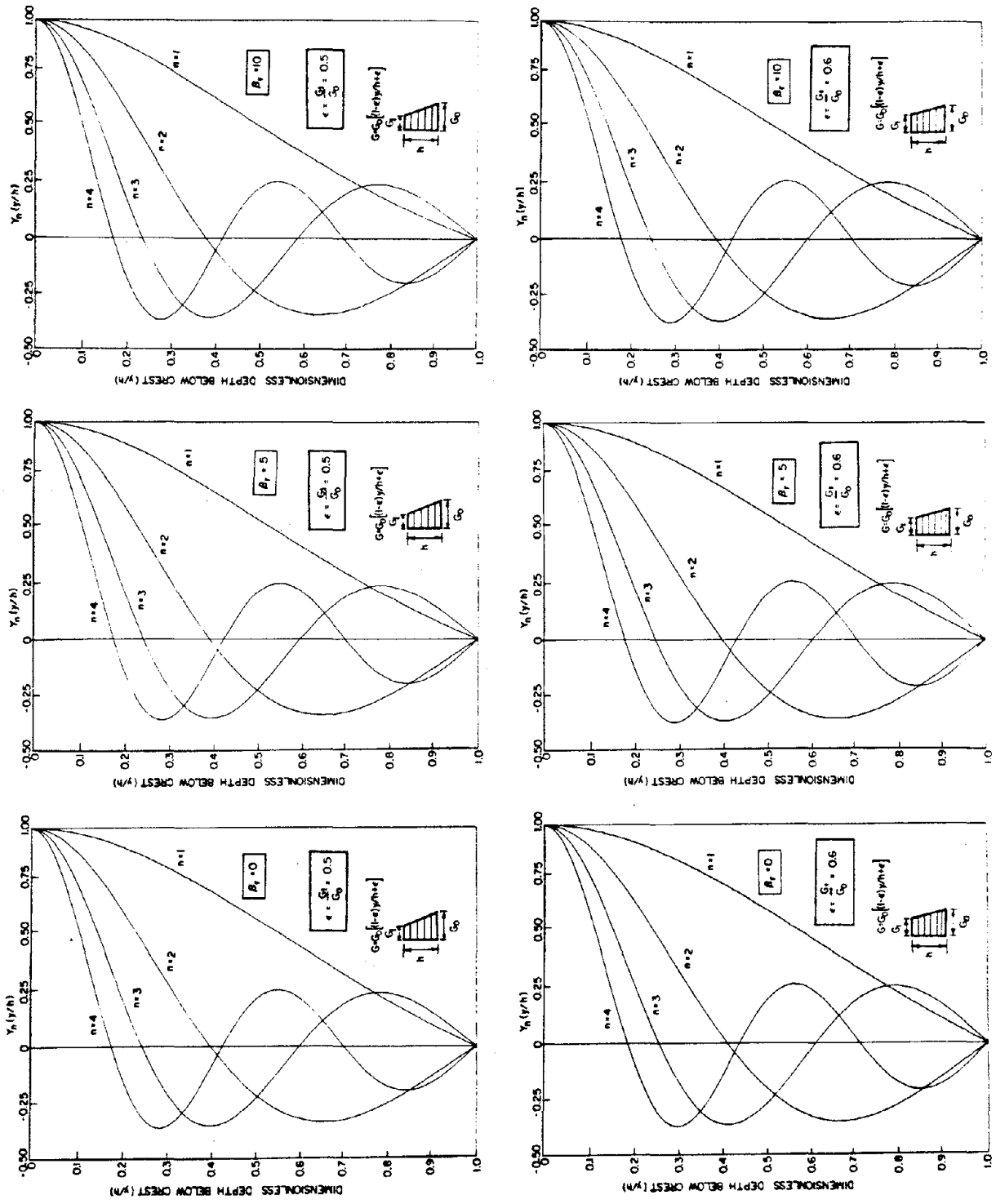

Fig. 2.9 Mode shapes of longitudinal vibration in the y-direction for different values of β_r for the trapezoidal case.

CHAPTER III

COMPARISON BETWEEN THE RESULTS OF THE PROPOSED MODELS AND REAL OBSERVATIONS

III-1. Earthquake Response Records

Resonant frequencies (in the longitudinal direction) of three earth dams (Figs. 3.1, 3.2, and 3.3) in a seismically active area (Southern California) are estimated from their earthquake records. Amplification spectra of the dams' earthquake records were computed (see Refs. 1, 2, and 4) by dividing Fourier amplitudes of acceleration of the crest records by those of the abutment records (input ground motion) to indicate the resonant frequencies and to estimate the relative contribution of different modes (see Figs. 3.1-c to 3.3-c). Then the two-dimensional models presented here were used to establish from the observed fundamental frequency a value for the shear wave velocity, v_s or v_{s0}, which was then used to calculate other frequencies higher than the fundamental. Each trapezoidal canyon of the three dams is represented by an equivalent rectangle of length L equal to the average of the crest length and the length of the base, e.g., for Brea Dam $L = 0.5\ (800 + 400) = 600$ ft; for Carbon Canyon Dam $L = 0.5\ (1{,}925 + 1{,}000) = 1462.5$ ft and for Santa Felicia Dam $L = 0.5\ (1{,}275 + 450) = 912.5$ ft. Tables 3.1, 3.2, and 3.3 show comparisons between the observed resonant frequencies and estimated values computed from the proposed analytical models; they also show the estimated shear-wave velocities from the earthquake records.

From the comparison, the following observations can be made:

1. Observed resonant frequencies of Brea and Carbon Canyon Dams are in good agreement with the symmetric modes' computed frequencies (from the models in which the shear and elastic moduli of the dam material vary along the depth, e.g., $\frac{\ell}{m} = \frac{1}{2}$ or $\frac{1}{3}$ or $\frac{2}{5}$) but not as good with the antisymmetric modes' frequencies because the crest accelerograph was located at the crest mid-point of the two dams.

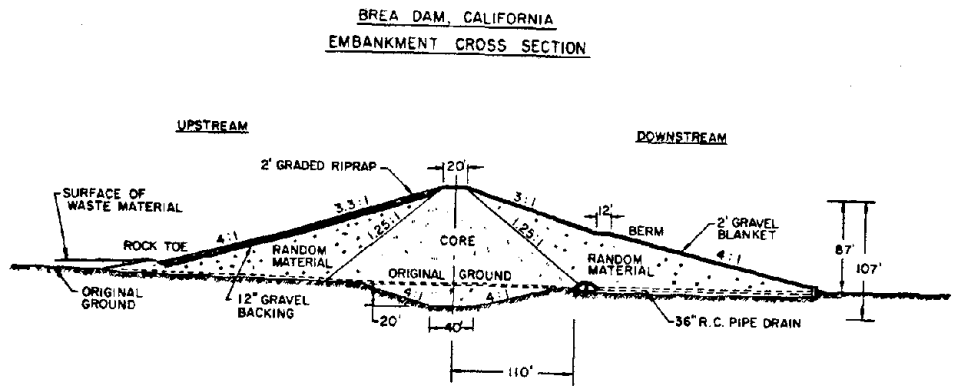

(a) Cross-section of the dam.

(b) Plan view showing location of accelero-graphs.

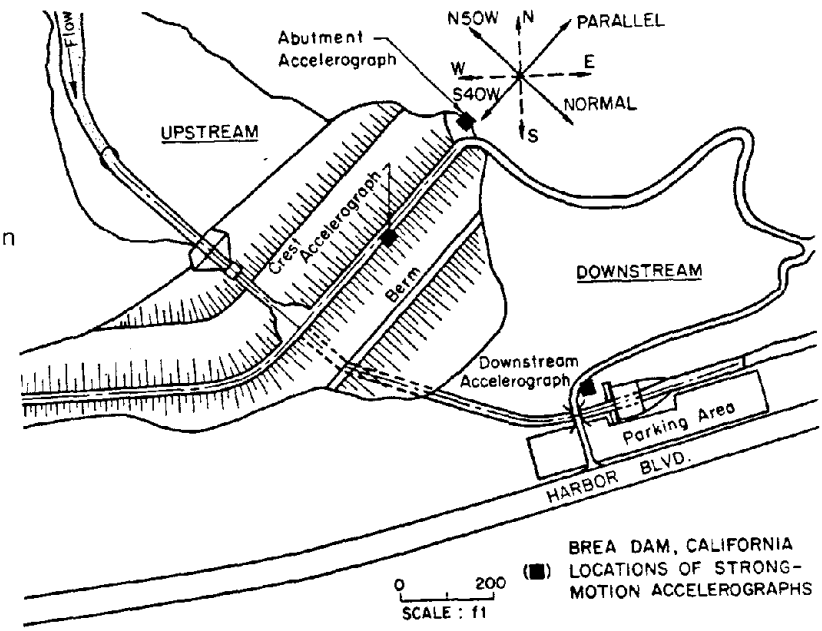

(c) Computed amplification spectrum from the 1976 earthquake (M_L = 4.2) records.

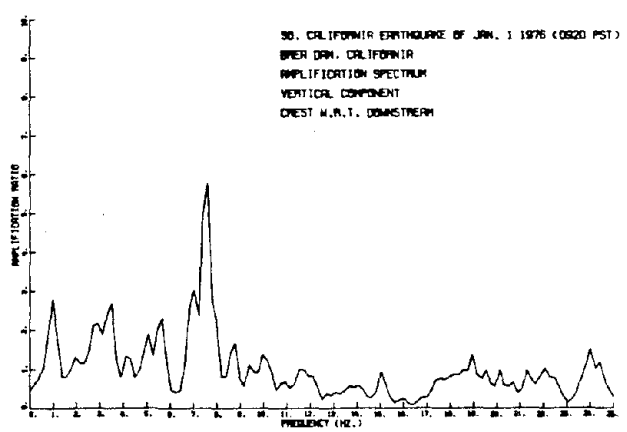

Fig. 3.1 Brea Earth Dam.

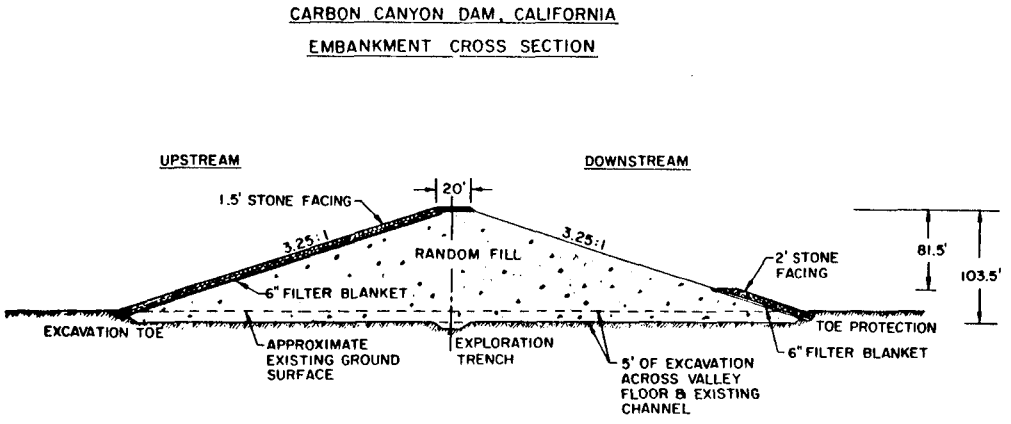

(a) Cross-section of the dam.

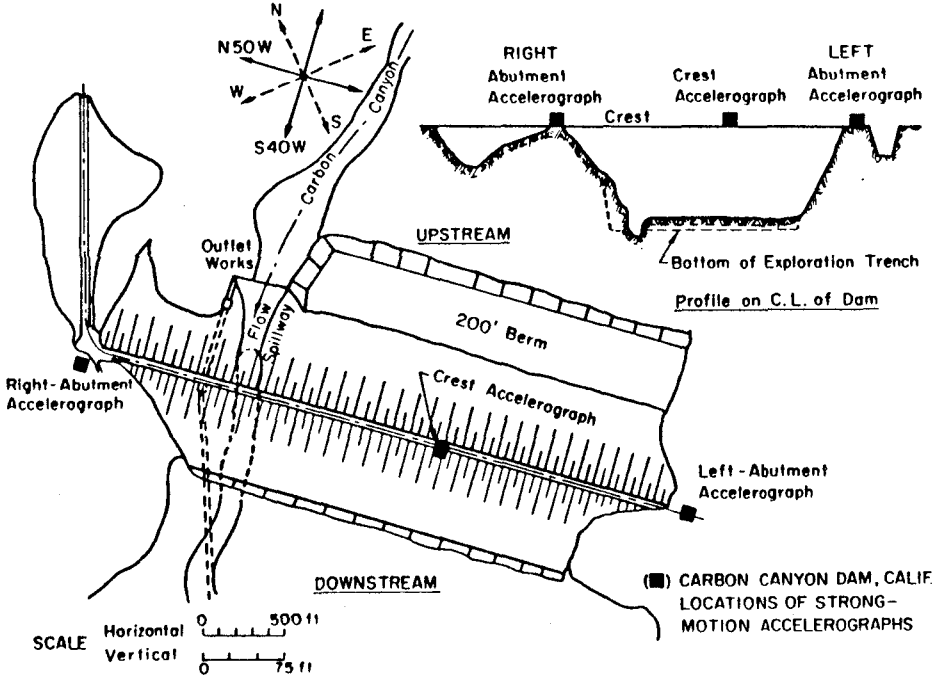

(b) Plan view showing location of accelerographs.

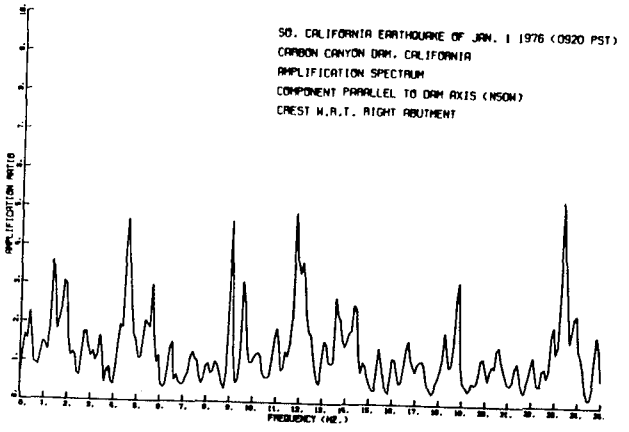

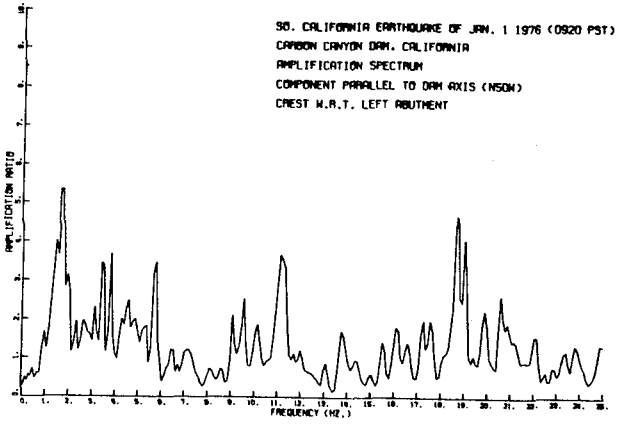

(c) Computed amplification spectra from the 1976 earthquake (M_L = 4.2) records.

Fig. 3.2 Carbon Canyon Earth Dam.

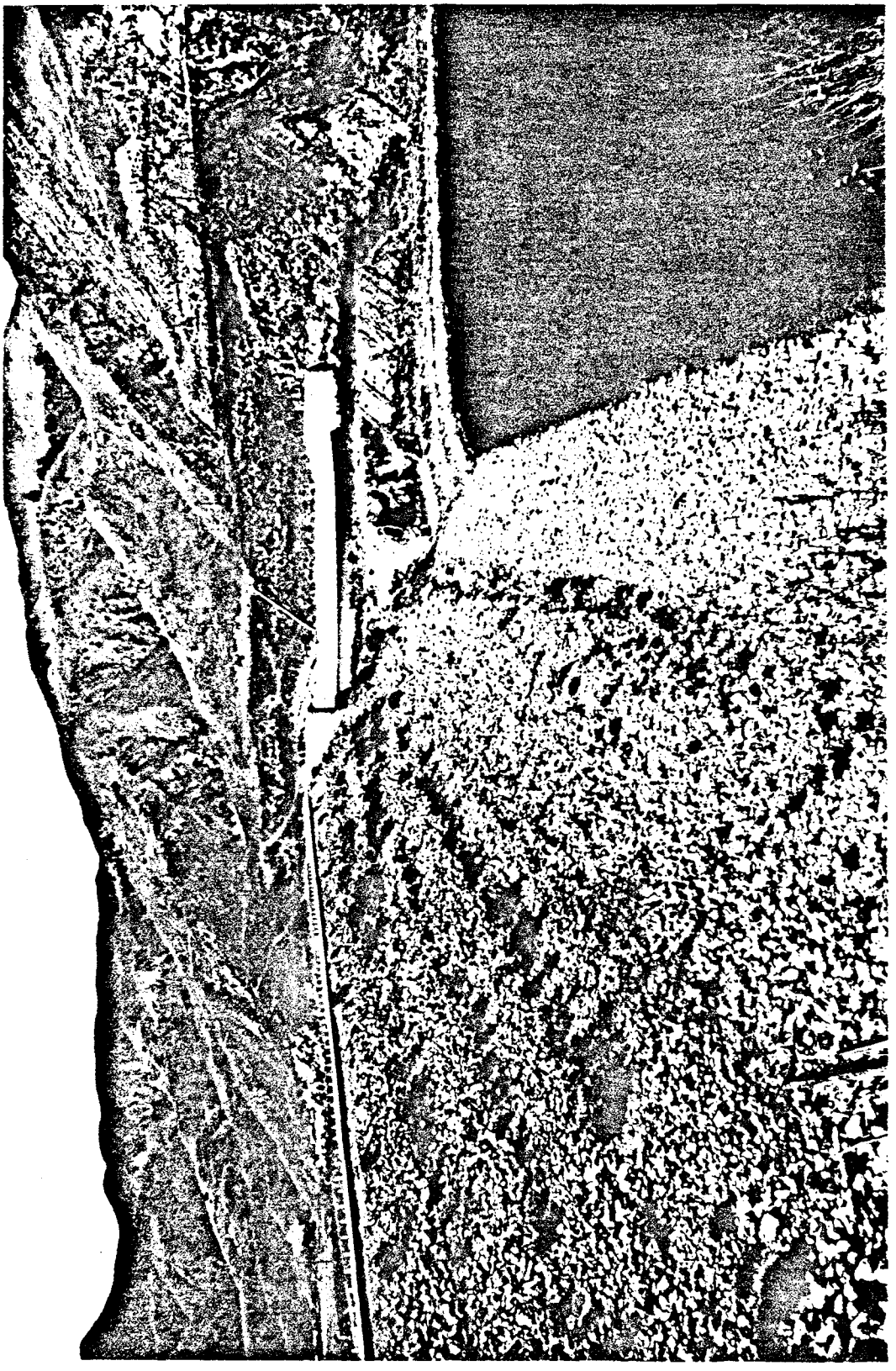

Fig. 3.3 General view showing the upstream side of Santa Felicia Dam and part of the spillway at the right (western) abutment.

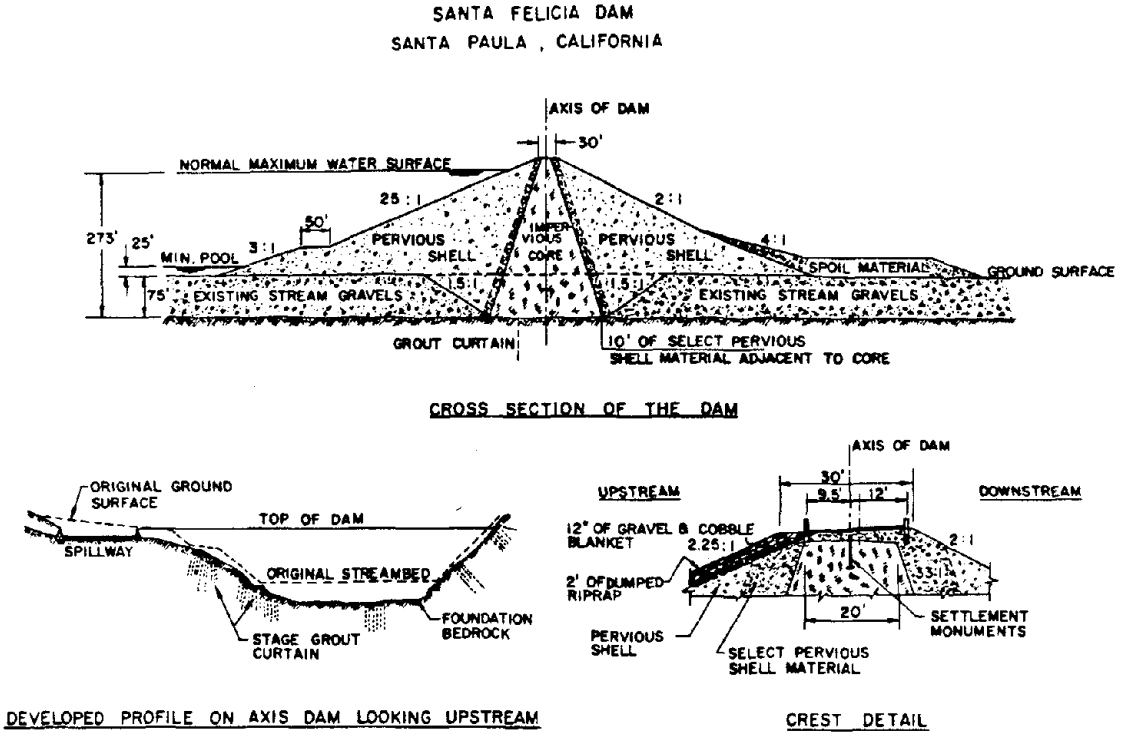

Fig. 3.3-a Structural details of Santa Felicia Dam.

SANTA FELICIA DAM , CALIFORNIA
LOCATIONS OF THE STRONG-MOTION INSTRUMENTS
DURING THE SAN FERNANDO EARTHQUAKE OF FEB. 9 , 1971

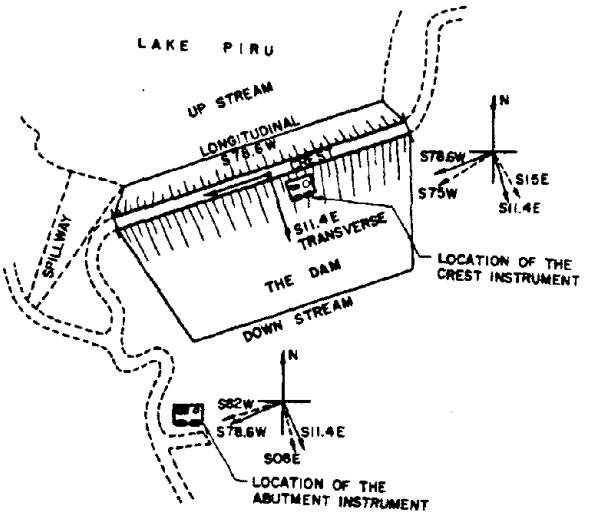

GENERAL VIEW

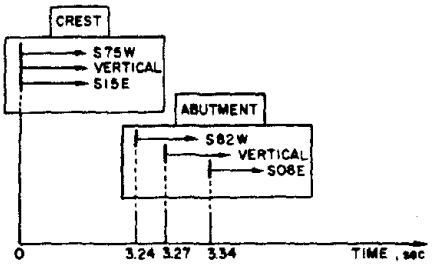

TIME DIFFERENCES BETWEEN THE RECORDS

Fig. 3.3-b

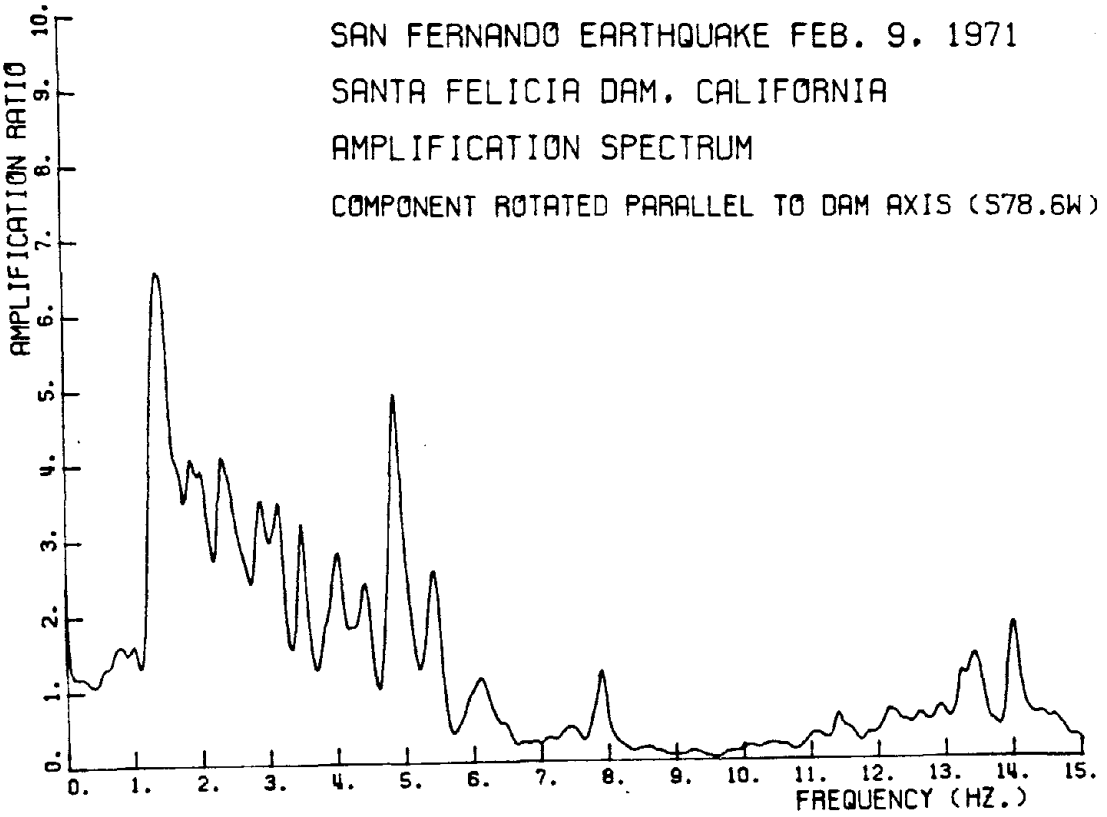

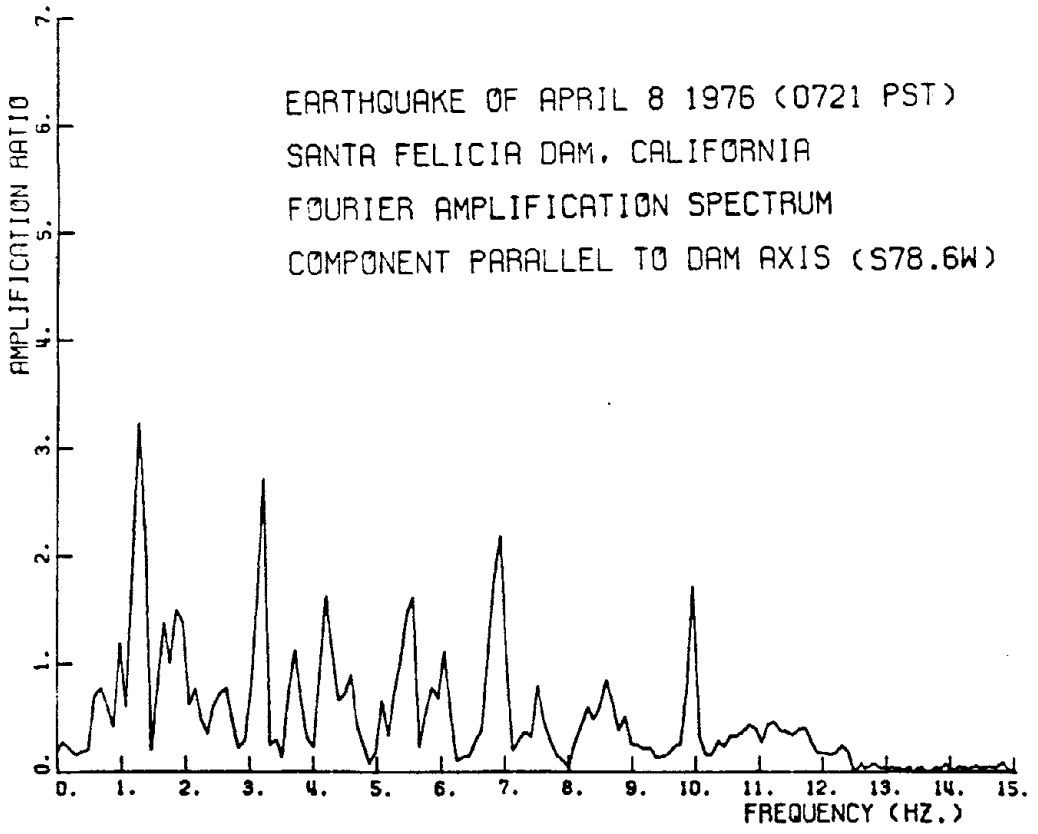

Fig. 3.3-c Amplification spectrum of the 1971 and 1976 earthquakes.

BREA EARTH DAM

Table 3.1 Comparison Between Observed Resonant Frequencies (in Hz) and Those Computed by the Proposed Analytical Models Whittier, California Earthquake of Jan. 1, 1976 (M_L = 4.2) Longitudinal Direction

Obs.Res. Freq. (1976 Earthquake) M_L=4.2	G = constant				$G=G_0(y/h)$		$G=G_0(y/h)^{1/2}$		$G=G_0(y/h)^{2/5}$		$G=G_0(y/h)^{1/3}$	
	Sym.		Antisym.		Sym. Freq.	Antisym. Freq.	Sym. Freq.	Antisym. Freq.	Sym. Freq.	Antisym. Freq.	Sym. Freq.	Antisym. Freq.
	n,r	Freq.	n,r	Freq.								
2.75	1,1	2.75			2.75		2.75		2.75		2.75	
-			1,2	3,17		2.98		3.07		3.09		3.11
3.55	1,3	3.78			3.32		3.54		3.59		3.62	
3.91			1,4	4.49		3.69		4.09		4.17		4.22
4.88	1,5	5.26			4.08		4.69		4.81		4.89	
-			1,6	6.07		4.45		5.30		5.47		5.58
5.45	2,1	6.17			4.93		5.53		5.64		5.70	
-			2,2	6.23		5.07		5.70		5.81		5.89
-	2,3	6.55			5.30		5.97		6.10		6.17	
-			2,4	6.99		5.61		6.34		6.50		6.56
7.03	2,5	7.51			5.98		6.78		6.93		7.03	
-			2,6	8.10		6.40		7.30		7.46		7.56
	v_s = 656.9 ft/sec				v_{s0} = 847.7 ft/sec		v_{s0} = 737.0 ft/sec		v_{s0} = 719.2 ft/sec		v_{s0} = 708.0 ft/sec	

NOTE: The Poisson's ratio, ν, of the dam material was taken to be 0.40.

CARBON CANYON EARTH DAM

Table 3.2 Comparison Between Observed Resonant Frequencies (in Hz) During Two Earthquakes and Those Computed by the Proposed Analytical Models Longitudinal Direction

Observed Resonant Frequencies		G = Constant				$G=G_0(y/h)$		$G=G_0(y/h)^{1/2}$		$G=G_0(y/h)^{2/5}$		$G=G_0(y/h)^{1/3}$	
1971SanFer-nando E.Q. M_L=6.3	1976 E.Q. M_L=4.2	Sym.		Antisym.		Sym. Freq.	Antisym. Freq.	Sym. Freq.	Antisym. Freq.	Sym. Freq.	Antisym. Freq.	Sym. Freq.	Antisym. Freq.
		n,r	Freq.	n,r	Freq.								
1.37	1.37	1,1	1.37			1.37		1.37		1.37		1.37	
-	-			1,2	1.38		1.39		1.40		1.40		1.40
1.47	1.47	1,3	1.41			1.42		1.44		1.45		1.45	
-	-			1,4	1.44		1.46		1.50		1.51		1.51
1.75	1.76	1,5	1.48			1.52		1.57		1.58		1.59	
-	-			1,6	1.53		1.57		1.66		1.67		1.69
1.86	1.86	1,7	1.58			1.68		1.78		1.79		1.82	
-	-			1,8	1.64		1.80		1.92		1.94		1.98
-	1.95	1,9	1.70			1.88		2.07		2.10		2.14	
-	-			1,10	1.77		2.05		2.24		2.29		2.34
2.30	2.30	1,11	1.85			2.13		2.43		2.49		2.55	
-	-			1,12	1.93		2.38		2.63		2.71		2.79
2.64	2.80	2,1	3.12			2.50		2.83		2.89		2.93	
-	-			2,2	3.14		2.51		2.85		2.91		2.95
3.15	3.15	2,3	3.15			2.53		2.87		2.93		2.97	
-	-			2,4	3.17		2.56		2.90		2.96		3.00
		v_s=330.1 ft/sec				v_{s0}= 413.6 ft/sec		v_{s0}= 363.3 ft/sec		v_{s0}= 355.4 ft/sec		v_{s0}= 350.3 ft/sec	

NOTE: $\nu = 0.35$

SANTA FELICIA EARTH DAM

Table 3.3 Comparison Between Observed Resonant Frequencies (in Hz) During Two Earthquakes and Those Computed by the Proposed Analytical Models Longitudinal Direction

1971 Earthquake (M_L=6.3)		Mode Order	$G = G_0(y/h)^{\ell/m}$					1976 Earthquake (M_L=4.7)		Mode Order	$G = G_0(y/h)^{\ell/m}$				
Freq.	Part. Fact.[a]	(n,r)	$\frac{\ell}{m}=0$	$\frac{\ell}{m}=1$	$\frac{\ell}{m}=\frac{1}{2}$	$\frac{\ell}{m}=\frac{2}{5}$	$\frac{\ell}{m}=\frac{1}{3}$	Freq.	Part. Fact.[a]	(n,r)	$\frac{\ell}{m}=0$	$\frac{\ell}{m}=1$	$\frac{\ell}{m}=\frac{1}{2}$	$\frac{\ell}{m}=\frac{2}{5}$	$\frac{\ell}{m}=\frac{1}{3}$
1.35	1.00	1,1	1.35	1.35	1.35	1.35	1.35	1.27	1.00	1,1	1.27	1.27	1.27	1.27	1.27
1.70	0.61	1,2	1.79	1.60	1.69	1.71	1.72	1.66	0.67	1,2	1.68	1.50	1.59	1.61	1.62
1.86	0.62	1,3	2.34	1.89	2.13	2.17	2.20	1.86	0.73	1,3	2.20	1.78	2.00	2.04	2.07
2.15	0.44	2,1	2.77	2.17	2.58	2.63	2.65	2.15	0.38	2,1	2.60	2.20	2.43	2.47	2.50
2.32	0.62	1,4	2.94	2.34	2.59	2.67	2.72	2.64	0.38	1,4	2.77	2.04	2.44	2.51	2.57
2.91	0.53	2,2	3.00	2.43	2.79	2.84	2.87			2,2	2.83	2.28	2.62	2.67	2.70
3.15	0.53	2,3	3.36	2.51	3.05	3.15	3.19			2,3	3.16	2.37	2.87	2.97	3.00
3.49	0.49	1,5	3.57	2.78	3.10	3.17	3.24	3.22	0.91	1,5	3.36	2.52	2.91	2.98	3.05
		2,4	3.81	3.10	3.49	3.55	3.59			2,4	3.58	2.91	3.28	3.34	3.38
3.85	0.34	1,6	4.21	3.20	3.50	3.66	3.77			1,6	3.96	2.56	3.29	3.44	3.54
		3,1	4.26	3.35	3.87	3.96	4.02	3.71	0.55	3,1	4.01	3.16	3.65	3.73	3.78
4.03	0.43	2,5	4.31	3.44	3.94	4.02	4.06			2,5	4.05	3.23	3.71	3.78	3.82
		3,2	4.42	3.48	4.01	4.10	4.16			3,2	4.16	3.27	3.77	3.86	3.91
4.42	0.36	3,3	4.63	3.68	4.23	4.33	4.39	4.20	0.79	3,3	4.39	3.46	3.98	4.07	4.13
		2,6	4.86	3.76	4.43	4.52	4.58			2,6	4.57	3.53	4.17	4.25	4.30
4.88	0.75	3,4	5.00	3.94	4.52	4.62	4.69	4.59	0.44	3,4	4.70	3.71	4.25	4.35	4.41
v_{s0} (in ft/sec.) =			722.8	967.8	827.0	804.0	789.5	v_{s0} (in ft/sec.) =			680.0	910.5	778.0	756.4	742.7

[a]Participation factor was obtained by dividing the value of the amplitude corresponding to a given resonant frequency by the largest amplitude that corresponds to the fundamental frequency.

NOTE: Based on the in-situ wave-velocity measurements, the Poisson's ratio was taken to be 0.45.

2. Similarly, the comparison for the Santa Felicia Dam (Table 3.3) suggests that the cases where $\frac{\ell}{m} = \frac{1}{2}, \frac{1}{3}$ and $\frac{2}{5}$ are the most appropriate representations for predicting the dynamic characteristics. Actually, from the soil-stiffness determination (through the low-strain field-wave velocity measurements on the dam (1,4) it was found that the 2/5-power variation law is best resembling the measurements.

3. Average values of the shear-wave velocity for each of the three dams were estimated by using their upstream-downstream earthquake responses (Refs. 1, 2, and 4) and existing shear-beam models (Refs. 9, 16, and 23) in that direction. These values were: v_s = 677.0 ft/sec. for Brea Dam (a zoned earthfill embankment constructed with a central impervious core composed of graded material and two shells constructed of random material). v_s = 375.7 ft/sec. for Carbon Canyon Dam (a random earthfill resting on 100 ft of recent silt, sand and gravel), and v_s = 850.0 ft/sec. for Santa Felicia Dam (a random rolled-fill earth dam constructed from well-graded alluvial materials consisting of clay, sands, gravel, and boulders).

   These values are consistent with those which resulted from the longitudinal models (Tables 3.1, 3.2, and 3.3) in which both shear and axial deformation were considered.

4. The nonuniform distribution of ground acceleration along the length of the dam (as illustrated by the Fourier amplitude spectra of Carbon Canyon Dam (Fig. 3.2-c and Ref. 2)) would considerably influence the nature of the dynamic response of an earth dam to an earthquake. For instance, an oblique angle of approach of traveling seismic waves raises the possibility of phase differences along the boundaries and the strong coupling

between longitudinal and transverse vibrations. Obviously more precise detailed evaluation of the seismic response of earth dams (e.g., via a three-dimensional finite element or finite difference techniques) is needed.

III-2. Full Scale Dynamic Test Results

Results of full-scale dynamic tests on Santa Felicia Dam, involving longitudinal forced vibration tests, Fig. 3.4-a,b,c (using only one shaker at station E2 of Fig. 3.4-a) as well as ambient vibration tests, Fig. 3.5-a,b (for more details see Ref. 3), were compared with those computed from the suggested models. Table 3.4 summarizes these comparisons, while Fig.3.4-c shows estimations of the measured modes along the crest (obtained during the frequency sweeps); because only eight seismometers were used during the longitudinal shaking, it was difficult to completely determine several modes corresponding to the resonant frequencies of Table 3.4. The solid lines connecting the data points of Fig. 3.4-c are estimates of the modal configurations, while the dashed lines represent possible extrapolations; the local magnification effect of the soil surrounding the shaker block is also shown. It was found that some resonant longitudinal frequencies are very close (even identical) to some of the upstream-downstream frequencies. This proximity may suggest a strong coupling between these two horizontal directions, or it may suggest that due to both the eccentricity of the single shaker (it was not located on the longitudinal axis of the dam) and the fact that the dam is not symmetrical, the upstream-downstream modes containing significant longitudinal motions were excited. Again, the comparison suggests that models with $\frac{\ell}{m} = \frac{1}{2}$ or $\frac{1}{3}$ or $\frac{2}{5}$ are most appropriate to estimate the dynamic characteristics of the dam in the longitudinal direction. Furthermore,

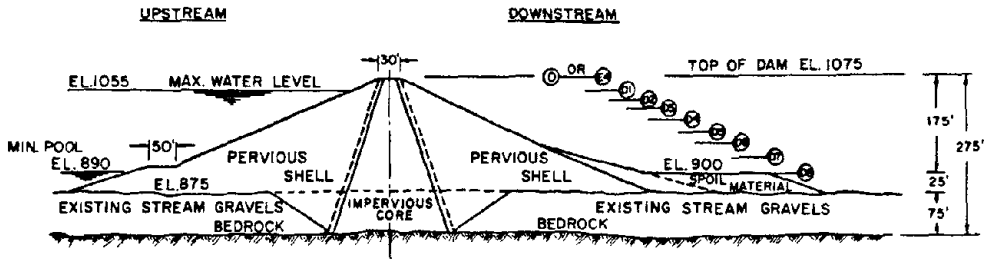

CROSS-SECTION

PLAN VIEW

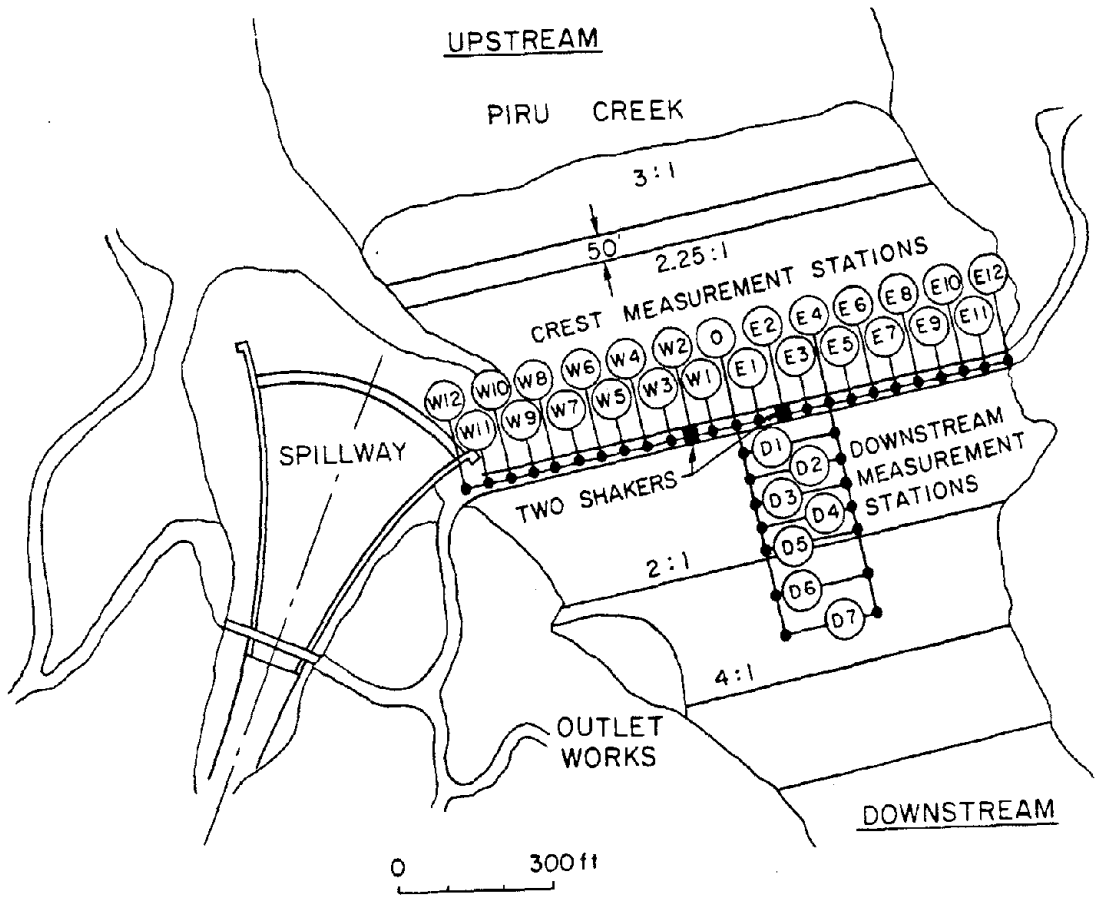

Fig. 3.4-a Cross-section, plan view showing the measurement stations of the full-scale dynamic tests on Santa Felicia Earth Dam.

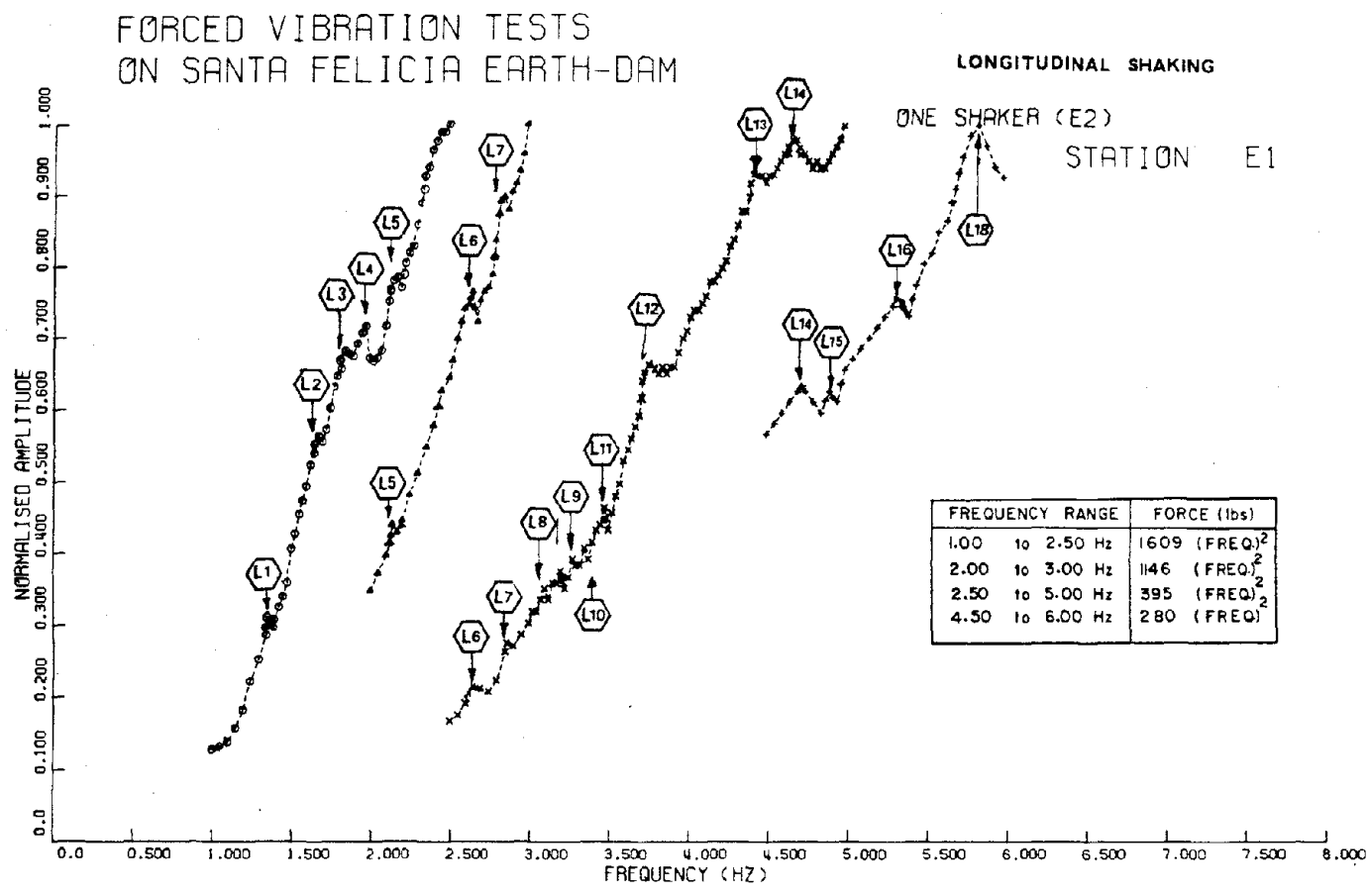

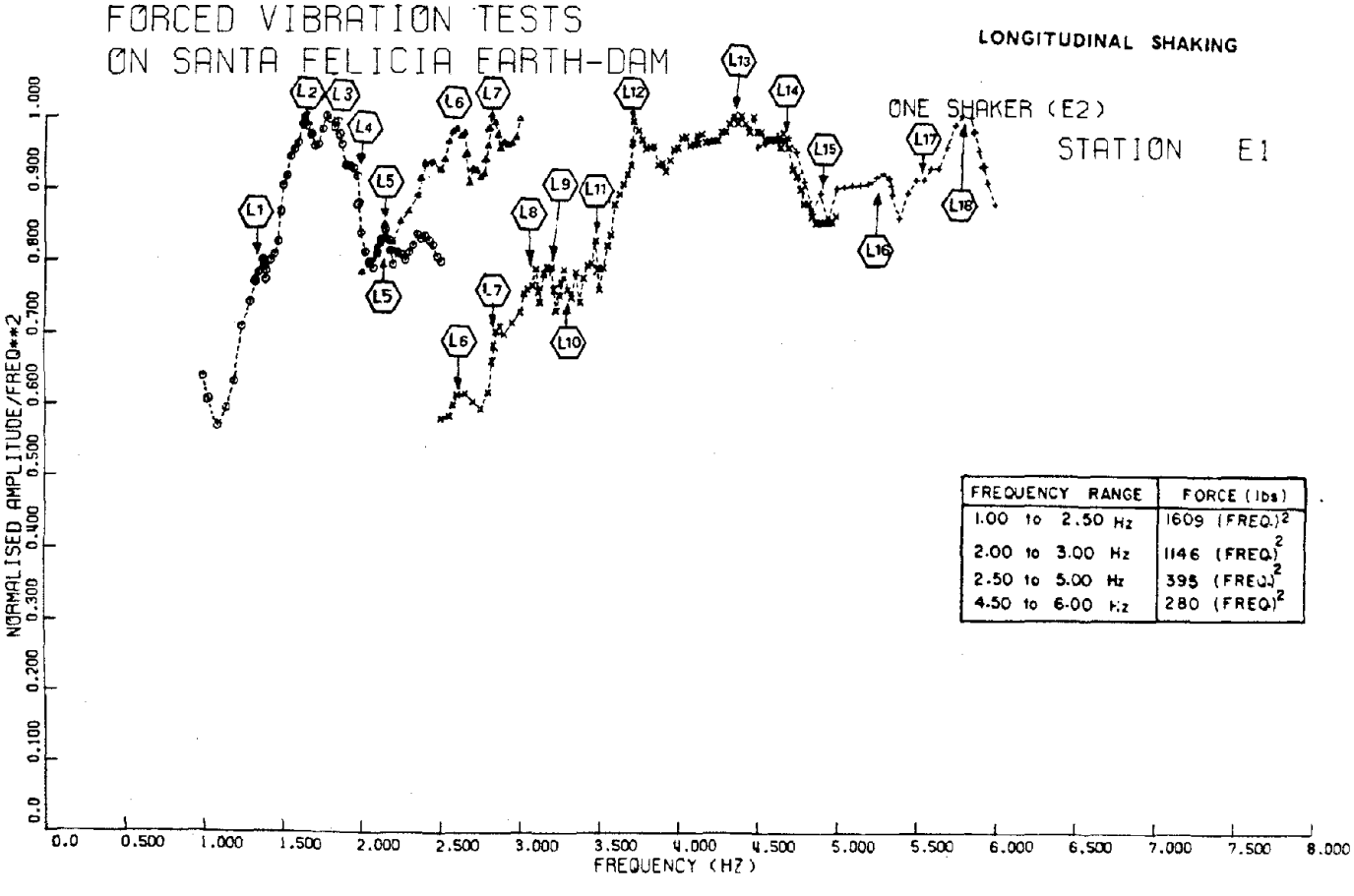

Fig. 3.4-b Response curves of longitudinal shaking.

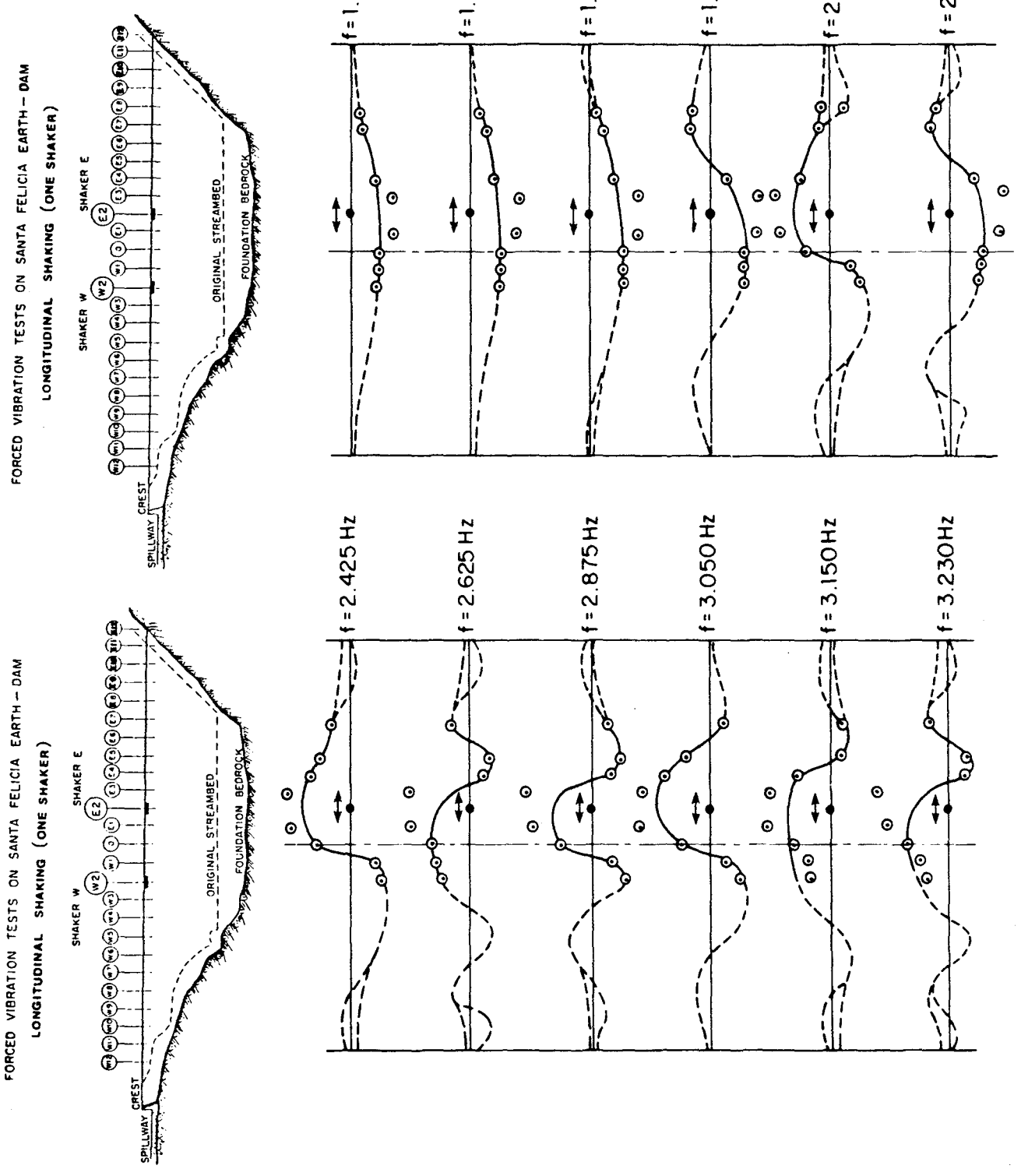

Fig. 3.4-c Estimation of the resonating modes obtained during the longitudinal frequency sweeps on Santa Felicia Dam (only one shaker was used).

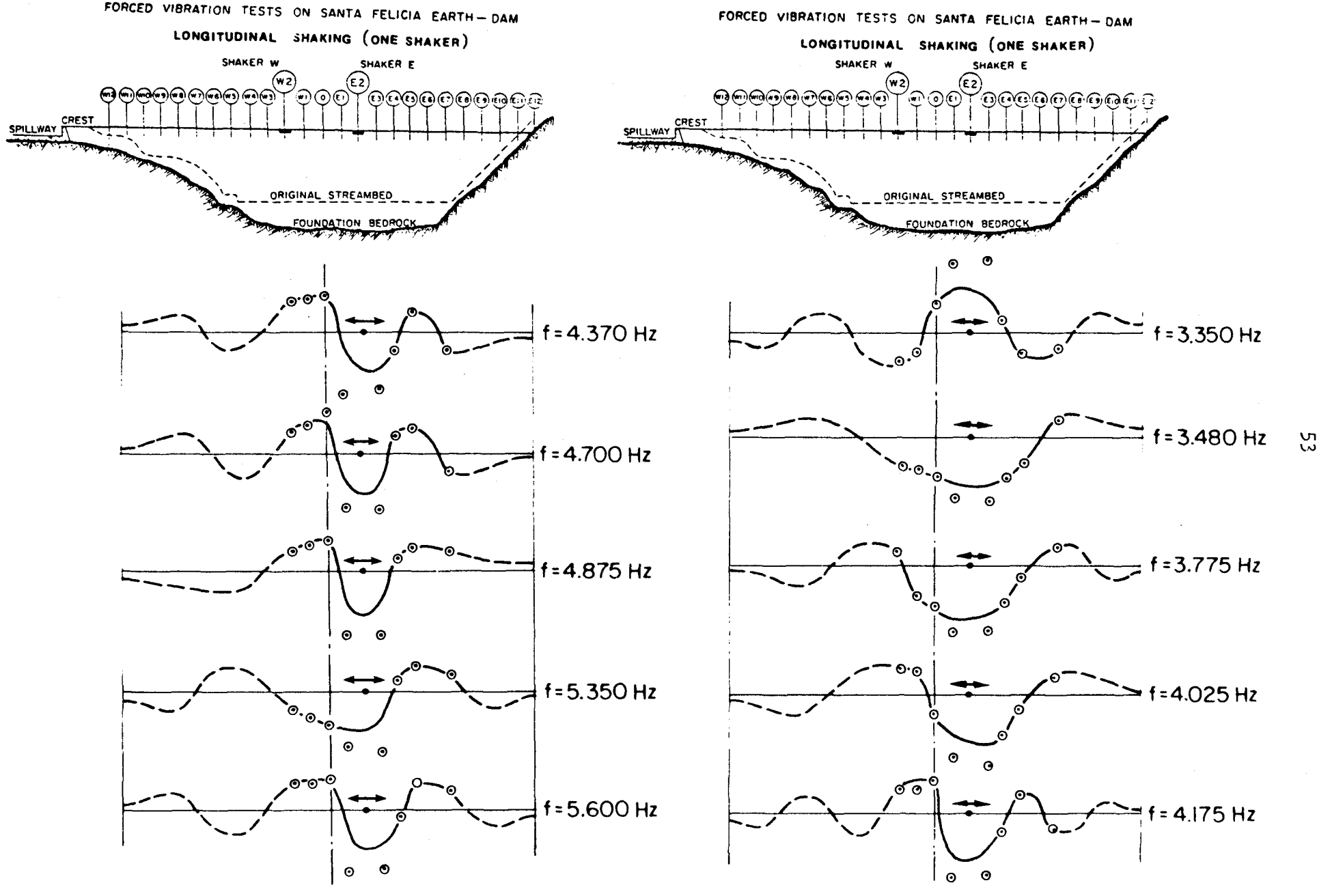

Fig. 3.4-c (cont'd) -- Estimation of the resonating modes obtained during the longitudinal frequency sweeps on Santa Felicia Dam

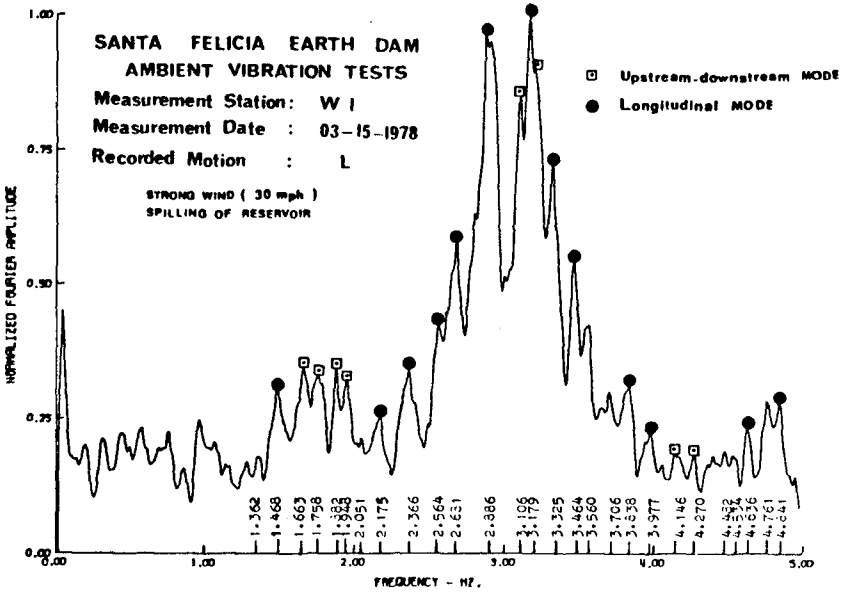

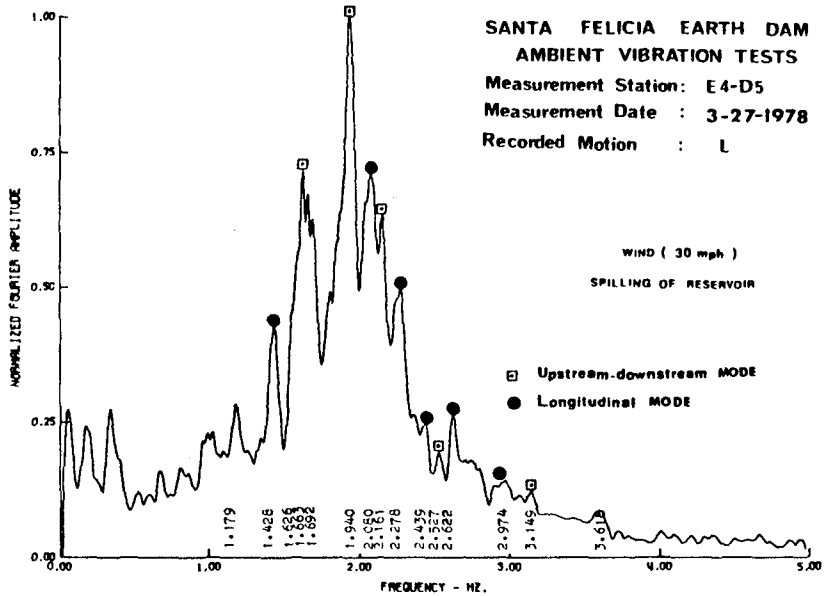

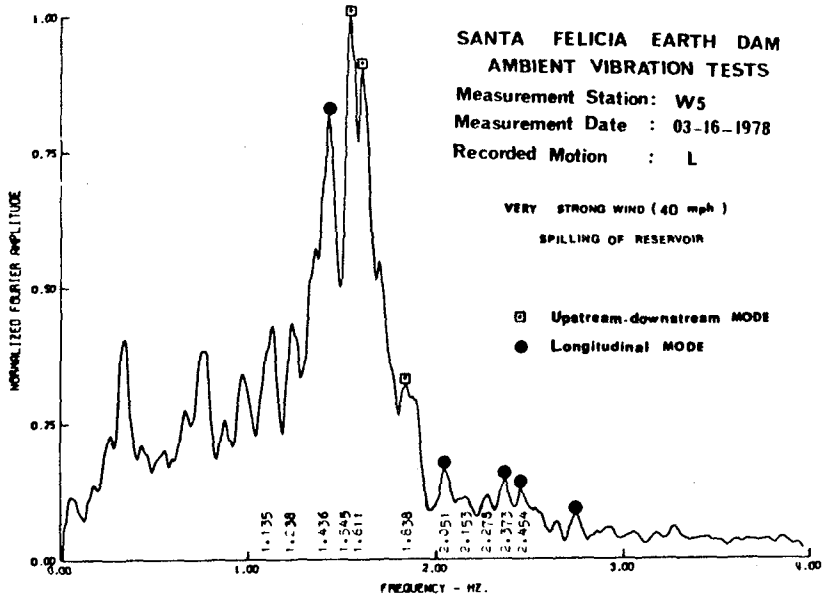

Fig. 3.5-a Fourier amplitude spectra of the longitudinal motion recorded at different stations on different days (the frequency resolution is 0.0073 Hz).

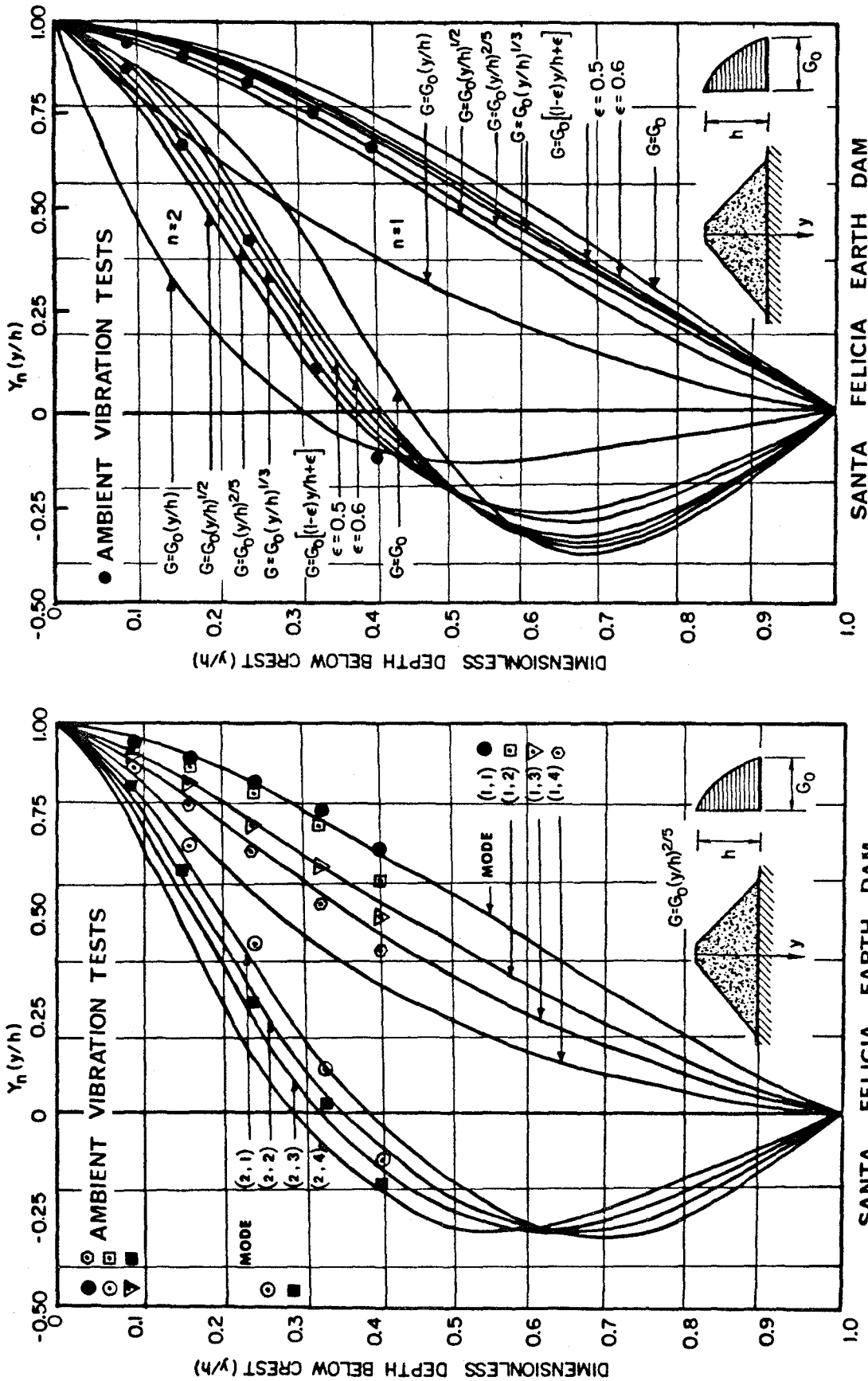

Fig. 3.5-b Comparison between the results of ambient vibration tests and those of the analytical models.

SANTA FELICIA EARTH DAM

Table 3.4 Comparison Between Resonant Frequencies (in Hz) From Full-Scale Dynamic Tests and Those Computed by the Proposed Analytical Models
Longitudinal Direction

Forced Vibration Tests		Ambient Vibration Tests	Mode Order	$G = G_0(y/h)^{\ell/m}$				
Measured Frequency	Mode Designation and Remarks	Average Measured Frequency	n,r	$\frac{\ell}{m}=0$	$\frac{\ell}{m}=1$	$\frac{\ell}{m}=\frac{1}{2}$	$\frac{\ell}{m}=\frac{2}{5}$	$\frac{\ell}{m}=\frac{1}{3}$
1.425	L1	1.446	1,1	1.446	1.446	1.446	1.446	1.446
1.675	L2: Identical to U-D[a] Mode S1.[b]	1.638	-	-	-	-	-	-
1.850	L3: " " " " R1.	1.849	-	-	-	-	-	-
1.950	L4: " " " " S2.	1.986	-	-	-	-	-	-
2.155	L5	2.175	1,2	1.912	1.711	1.813	1.833	1.846
2.275	L	2.317	1,3	2.502	2.025	2.278	2.326	2.357
2.425	L	2.452	2,2	3.218	2.694	2.987	3.037	3.069
2.625	L6: " " " " R3.	2.638	-	-	-	-	-	-
2.875	L7	2.880	1,4	3.148	2.325	2.772	2.857	2.911
3.050	L8: " " " " AS3.	3.033	-	-	-	-	-	-
3.150	L9: " " " " R4.	3.150	-	-	-	-	-	-
3.230	L	3.229	1,5	3.821	2.598	3.263	3.392	3.476
3.350	L10	3.323	1,6	4.509	2.846	3.737	3.918	4.036
3.480	L11	3.487	2,3	3.600	2.978	3.319	3.377	3.416
3.775	L12	3.775	2,5	4.615	3.681	4.224	4.303	4.353
4.025	L	4.051	2,4	4.076	3.323	3.740	3.807	3.852
4.175	L : " " " " AS5.	4.190	-	-	-	-	-	-
4.370	L13: " " " " AR3.	4.358	-	-	-	-	-	-
4.700	L14	4.667	2,6	5.199	4.026	4.747	4.843	4.901
4.875	L15	4.876	3,4	5.354	4.225	4.843	4.952	5.023
5.350	L	-	3,5	5.776	4.572	5.223	5.337	5.413
5.600	L	-	3,6	5.920	4.949	5.660	5.778	5.857
		v_{s0} (in ft/sec)=		774.2	1037.0	885.8	861.2	845.6

[a] Upstream-Downstream direction.
[b] S and AS correspond to symmetric and antisymmetric shear modes, while R and AR correspond to symmetric and antisymmetric rocking modes (see Ref. 3, 7, and 8).

several modes of longitudinal vibration, along the depth, resulting from the case of $\ell/m = 2/5$ are depicted in Fig. 3.5-b; the modal configurations estimated from the ambient vibration measurements are also shown in the same figure. The ambient-measurement results confirm the prediction by the analytical models that for $n = 1$, the lower modes along the crest (low values of r, e.g., $r = 1,2$) are associated with shear-type modal configuration along the depth, while the higher modes (large values of r, e.g., $r \geq 3$) are associated with bending-type modal configurations. This agreement between theory and observation may also be attributed to the fact that relative to other earth dams in California, the Santa Felicia canyon has one of the best-suited sections for an equivalent rectangle analysis, in the sense that it is closer to a steepsided parallelograph than to a trapezoid. In general, mode shapes (particularly configuration along the crest) of other dams can be quite different from those of models due to irregular geometry and zones of different materials. Finally, the first and second longitudinal modes (1,1) and (2,1) along the depth (where $n = 1$ and 2), resulting from all the proposed analytical models are also shown in Fig. 3.5-b; the modal configurations estimated from the ambient vibration measurements are also shown in the same figure. Again, the comparison suggests that model with $\ell/m = 2/5$ is the most appropriate to estimate the dynamic properties of the dam in the longitudinal direction.

CHAPTER IV

EARTHQUAKE-INDUCED LONGITUDINAL STRAINS AND STRESSES IN NONHOMOGENEOUS EARTH DAMS

IV-1. Earthquake Response Analysis

The two-dimensional model used in Chapter II for finding the natural frequencies and modes of longitudinal vibration of earth dams is utilized for this earthquake response analysis. The model which is a nonhomogeneous elastic wedge of finite length (with symmetric triangular section) in a rectangular canyon, resting on a rigid foundation, is subjected to uniform longitudinal ground motion (acceleration) $\ddot{w}_g(t)$ (Fig. 4.1).

To evaluate the magnitude and distribution of the modal strains and stresses induced by earthquake motion, the equation of motion of the dam can be written as

$$\rho \frac{\partial^2 w}{\partial t^2} + c\frac{\partial w}{\partial t} - \frac{1}{y}\frac{\partial}{\partial y}\left[G(y)\frac{\partial w}{\partial y}\, y\right] - \frac{1}{y}\frac{\partial}{\partial z}\left[\eta G(y)\frac{\partial w}{\partial z}\, y\right] = -\rho\ddot{w}_g(t) \quad , \qquad (4.1)$$

where ρ is the uniform mass density of the dam material, $w(y,z,t)$ is the longitudinal vibrational displacement (relative to the base of the dam), c is the damping coefficient, $G(y)$ is the shear modulus (which varies along the depth), and $\eta[= E(y)/G(y) = 2(1 + \nu)]$ is an elastic constant (where $E(y)$ is the modulus of elasticity and ν is the Poisson's ratio of the dam material).

A wide class of earth dams ranging from ones having constant elastic moduli, linear and trapezoidal variations of elastic moduli, to ones having elastic moduli increasing as the one-half, one-third, two-fifths, and a general $(\ell/m)^{th}$ powers of the depth are studied; i.e., the continuous variation of soil stiffness is represented by the following suggested relationships for both $G(y)$ and $E(y)$: (see Fig. 4.1 and Chapter II)

$$G(y) = G = \text{constant} \quad , \qquad (4.2\text{-a})$$

$$G(y) = G_0\left(\frac{y}{h}\right)^{\ell/m} \quad , \qquad \left(\frac{\ell}{m} = 1, \frac{1}{2}, \frac{1}{3}, \frac{2}{5}\right) \quad , \qquad (4.2\text{-b})$$

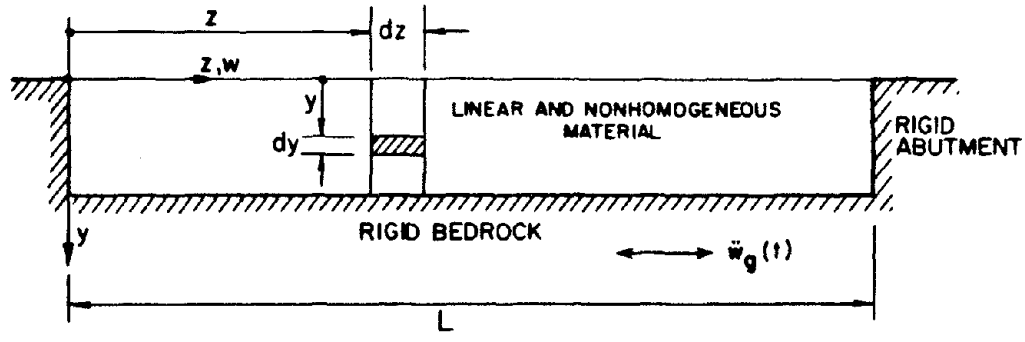

(a) The two-dimensional model with longitudinal ground acceleration

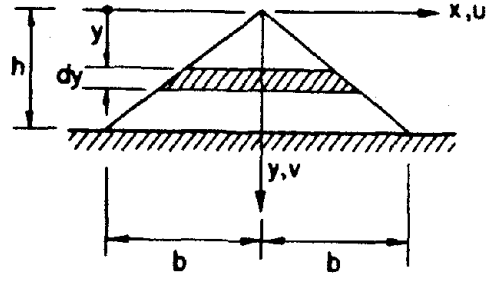

(b) Variation of stiffness properties along the depth of the dam and the results of the in-situ wave velocity measurement on the Santa Felicia Earth Dam.

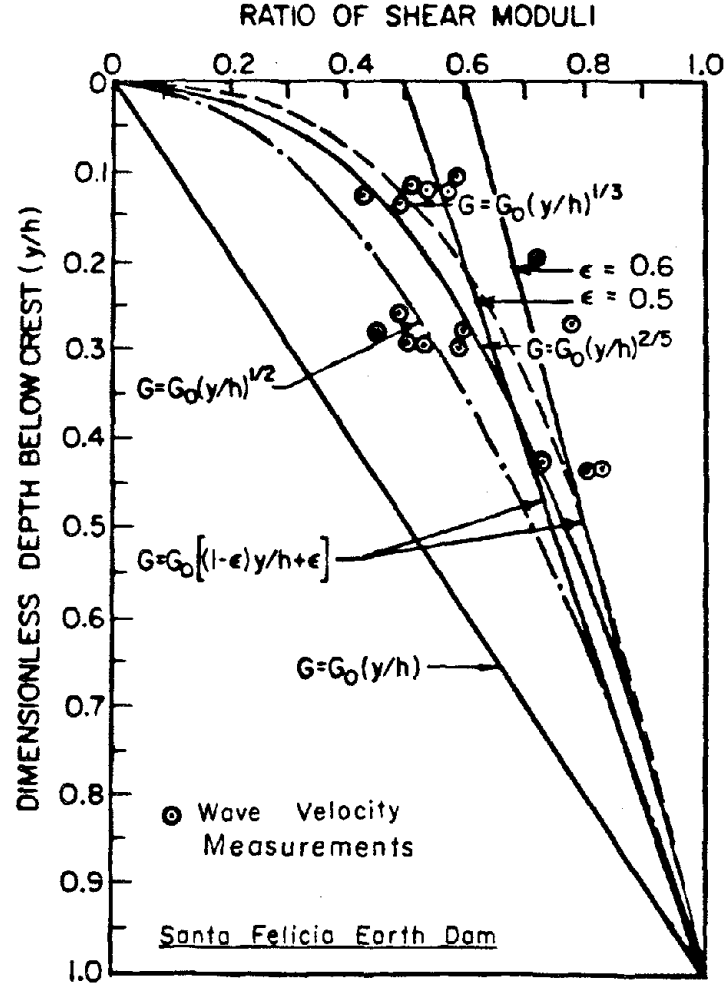

Fig. 4.1 The model and the stiffness variations considered in the earthquake response analysis.

$$G(y) = G_0\left[(1 - \varepsilon)\frac{y}{h} + \varepsilon\right] \quad , \qquad \varepsilon = \frac{G_1}{G_0} \quad , \tag{4.2-c}$$

where G_0 and G_1 are the shear moduli of the dam material at the base and at the crest, respectively, and h is the height of the dam. Note that similar relationships are assumed for the modulus of elasticity $E(y)$ and that values of shear moduli evaluated from in-situ wave-velocity measurements on Santa Felicia Dam (1,4) are shown on Fig. 4.1.

Using the generalized coordinates and the principle of mode superposition, one can write

$$w(y,z,t) = \sum_{n=1}^{\infty} \sum_{r=1}^{\infty} Y_n(y) Z_r(z) T_{n,r}(t) \quad , \tag{4.3}$$

where the subscripts n and r refer to the $(n,r)^{th}$ mode of longitudinal vibration. The modal configuration along the crest, $Z_r(z)$, is given by

$$Z_r(z) = \sin \frac{r\pi}{L} z \quad , \qquad r = 1,2,3,.... \quad , \tag{4.4}$$

while the modal configuration along the depth $Y_n(y)$ is given in Chapter II for the above stiffness variations. In the above equation L is the equivalent (average) length of the crest.

Substituting Eq. 4.3 into 4.1 and using the orthogonality properties of the mode shapes gives

$$\ddot{T}_{n,r}(t) + 2\zeta_{n,r}\omega_{n,r}\dot{T}_{n,r}(t) + \omega_{n,r}^2 T_{n,r}(t) = -P_{n,r}\ddot{w}_g(t) \quad ,$$

$$n,r = 1,2,3,... \quad , \tag{4.5}$$

where $\zeta_{n,r}$ is the modal damping factor, $\omega_{n,r}$ is the $(n,r)^{th}$ natural frequency, and $P_{n,r}$ is the modal participation factor given by

$$P_{n,r} = \left[\int_0^h \int_0^L Y_n(y) Z_r(z)\, y\, dy\, dz\right] \Bigg/ \left[\int_0^h \int_0^L Y_n^2(y) Z_r^2(z)\, y\, dy\, dz\right] \quad ,$$

$$n,r = 1,2,3,... \quad . \tag{4.6}$$

Because only the symmetrical modes can contribute to the response to uniformly distributed ground motion, values of r are limited to odd integers. Thus the participation factor becomes

$$\left.\begin{aligned} P_{n,r} &= \frac{4}{r\pi}\left[\int_0^h yY_n(y)\,dy\right]\Bigg/\left[\int_0^h yY_n^2(y)\,dy\right] \quad , \\ &\qquad\qquad n = 1,2,3,\ldots, \quad r = 1,3,5,\ldots \quad , \\ &= \frac{4}{r\pi}\,\overset{*}{P}_{n,r} \quad , \end{aligned}\right\} \tag{4.7}$$

where $\overset{*}{P}_{n,r}$ is the participation factor resulting from the modal configuration along the depth.

For the case where G is constant $P_{n,r}$ is given by

$$P_{n,r} = \frac{4}{r\pi}\,\frac{2}{\lambda_n J_1(\lambda_n)} \qquad n = 1,2,3,\ldots \quad , \quad r = 1,3,5,\ldots \quad , \tag{4.8}$$

where λ_n is the n^{th} root of the Bessel function of the first kind and zero order; J_1 is the Bessel function of the first kind and first order.

Values of $\overset{*}{P}_{n,r}$ of Eq.4.7 are computed for different values of the coefficient $\beta_r\left[=\eta\left(\frac{\pi rh}{L}\right)^2\right]$ for various cases of the stiffness variations (Eqs. 4.2-b and 4.2-c) and are listed in Table 4.1.

The solution of Eq. 4.5 is obtained as a Duhamel integral in the form

$$T_{n,r}(t) = \frac{P_{n,r}}{\omega_{n,r}\sqrt{1-\zeta_{n,r}^2}}\left[\int_0^t \ddot{w}_g(\tau)e^{-\zeta_{n,r}\omega_{n,r}(t-\tau)}\sin\omega_{n,r}\sqrt{1-\zeta_{n,r}^2}\,(t-\tau)\,d\tau\right]. \tag{4.9}$$

Thus the problem has been reduced to that of the earthquake response of a single-degree-of-freedom system. As the mode shapes and the modal participation factor $P_{n,r}$ are known, the normal stress and normal strain as well as shear

Table 4.1 Participation Factors $\overset{*}{P}_{n,r}$

$\beta_r=\eta\left(\frac{r\pi h}{L}\right)^2$	Mode Order (n,r)	$\overset{*}{P}_{n,r} = \left[\int_0^1 \left(\frac{y}{h}\right) Y_n\left(\frac{y}{h}\right) d\left(\frac{y}{h}\right)\right] \Big/ \left[\int_0^1 \left(\frac{y}{h}\right) Y_n^2\left(\frac{y}{h}\right) d\left(\frac{y}{h}\right)\right]$					
		$G=G_0\left(\frac{y}{h}\right)$	$G=G_0\left(\frac{y}{h}\right)^{\frac{1}{2}}$	$G=G_0\left(\frac{y}{h}\right)^{\frac{2}{5}}$	$G=G_0\left(\frac{y}{h}\right)^{\frac{1}{3}}$	$G=G_0\left[(1-\varepsilon)\frac{y}{h}+\varepsilon\right]$	
						$\varepsilon=0.5$	$\varepsilon=0.6$
0	(1,r)	2.483	1.859	1.791	1.752	1.719	1.687
	(2,r)	-3.332	-1.650	-1.490	-1.398	-1.295	-1.231
	(3,r)	4.005	1.539	1.340	1.230	1.068	1.006
	(4,r)	-4.580	-1.466	-1.244	-1.124	-0.927	-0.870
5	(1,r)	2.867	2.006	1.907	1.847	1.770	1.725
	(2,r)	-3.999	-1.830	-1.623	-1.505	-1.357	-1.276
	(3,r)	4.481	1.598	1.377	1.256	1.086	1.018
	(4,r)	-4.913	-1.502	-1.268	-1.142	-0.936	-0.876
10	(1,r)	3.182	2.146	2.018	1.939	1.819	1.761
	(2,r)	-4.613	-2.006	-1.755	-1.610	-1.417	-1.320
	(3,r)	4.990	1.660	1.416	1.283	1.104	1.031
	(4,r)	-5.272	-1.539	-1.292	-1.160	-0.946	-0.883
15	(1,r)	3.421	2.275	2.122	2.027		
	(2,r)	-5.158	-2.174	-1.882	-1.712		
	(3,r)	5.521	1.726	1.456	1.312		
	(4,r)	-5.656	-1.577	-1.317	-1.178		
20	(1,r)	3.593	2.391	2.220	2.111		
	(2,r)	-5.632	-2.333	-2.003	-1.811		
	(3,r)	6.061	1.795	1.499	1.341		
	(4,r)	-6.064	-1.615	-1.340	-1.196		
30	(1,r)	3.798	2.582	2.390	2.263		
	(2,r)	-6.390	-2.616	-2.227	-1.997		
	(3,r)	7.124	1.943	1.589	1.404		
	(4,r)	-6.943	-1.694	-1.391	-1.231		
40	(1,r)	3.897	2.721	2.526	2.391		
	(2,r)	-6.932	-2.856	-2.424	-2.165		
	(3,r)	8.101	2.100	1.687	1.472		
	(4,r)	-7.885	-1.776	-1.441	-1.260		

stress and shear strain modal participation factors can be computed and plotted; in addition, the response spectrum can be used to evaluate maximum displacement, strain and stress.

Using the modal solution (Eq. 4.3), the response of the dam to the earthquake longitudinal component can be written as

$$w(y,z,t) = \sum_{n=1}^{\infty} \sum_{r=1,3,5}^{\infty} Y_n(y) \sin\left(\frac{r\pi z}{L}\right) \frac{P_{n,r}}{\omega_{n,r}\sqrt{1-\zeta_{n,r}^2}} V_{n,r}(t) \quad , \qquad (4.10)$$

where the function $V_{n,r}(t)$ is equal to the quantity between the two brackets in Eq. 4.9.

VI-2. Dynamic Shear Strains and Stresses

The magnitude and distribution of shear strains in the $(n,r)^{th}$ mode are given by

$$\gamma_{n,r}(y,z,t) = \frac{\partial w}{\partial y} = \frac{P_{n,r}}{\omega_{n,r}\sqrt{1-\zeta_{n,r}^2}} \frac{dY_n(y)}{dy} \sin\left(\frac{r\pi z}{L}\right) \quad V_{n,r}(t) \quad ,$$

$$n = 1,2,3,\ldots \quad , \quad r = 1,3,5,\ldots \quad , \qquad (4.11)$$

or

$$\gamma_{n,r}(y,z,t) = \frac{4\overset{*}{P}_{n,r}}{r\pi h\omega_{n,r}\sqrt{1-\zeta_{n,r}^2}} \Psi_{n,r}\left(\frac{y}{h}\right) \sin\left(\frac{r\pi z}{L}\right) V_{n,r}(t) \quad ,$$

$$n = 1,2,3,\ldots \quad , \quad r = 1,3,5,\ldots \quad , \qquad (4.12)$$

where $\Psi_{n,r}\left(\frac{y}{h}\right)$ is defined as $\frac{dY_n\left(\frac{y}{h}\right)}{d\left(\frac{y}{h}\right)}$; it expresses the modal participation and distribution of shear strain.

For the case where G is constant, the shear strain is given by

$$\gamma_{n,r}(y,z,t) = \frac{8}{r\pi h\, J_1(\lambda_n)\omega_{n,r}\sqrt{1-\zeta_{n,r}^2}} J_1\left(\lambda_n \frac{y}{h}\right) \sin\left(\frac{r\pi z}{L}\right) V_{n,r}(t) \qquad (4.13)$$

For the cases where $G = G_0\left(\frac{y}{h}\right)^{\ell/m}$, $\frac{\ell}{m} = 1, \frac{1}{2}, \frac{1}{3}, \frac{2}{5}$, the function $\Psi_{n,r}\left(\frac{y}{h}\right)$ is given by (see Chapter II)

$$\Psi_{n,r}\left(\frac{y}{h}\right) = a_{\left(\frac{2m}{\ell}-1\right)}\left(\frac{y}{h}\right)^{\left(1-\frac{\ell}{m}\right)} + a_{\left(\frac{2m}{\ell}\right)}\left(\frac{y}{h}\right) + \ldots + a_k\left(\frac{y}{h}\right)^{\left(\frac{k\ell}{m}-1\right)} + \ldots , \quad \left(k > \frac{2m}{\ell}\right), \tag{4.14}$$

where

$$\left.\begin{aligned} a_0 &= 1 \\ a_1 &= 0 \\ a_2 &= 0 \\ &\vdots \\ a_{\left(\frac{2m}{\ell}-2\right)} &= 0 \\ a_{\left(\frac{2m}{\ell}-1\right)} &= -\frac{\left(2-\frac{\ell}{m}\right)}{\frac{2m}{\ell}\left(\frac{2m}{\ell}-1\right)}\left(\frac{m}{\ell}\right)^2\left(\frac{\omega_{n,r}h}{v_{s0}}\right)^2 \\ a_{\left(k\geq\frac{2m}{\ell}\right)} &= -\frac{k\frac{\ell}{m}}{k(k+1)}\left(\frac{m}{\ell}\right)^2\left[\left(\frac{\omega_{n,r}h}{v_{s0}}\right)^2 a_{\left(k-\frac{2m}{\ell}+1\right)} - n\left(\frac{r\pi h}{L}\right)^2 a_{\left(k-\frac{2m}{\ell}\right)}\right] \end{aligned}\right\} \tag{4.15}$$

In the above equations $v_{s0}\left(=\sqrt{G_0/\rho}\right)$ is the shear wave velocity at the base of the dam material; also, $\left(\frac{2m}{\ell}-1\right)$ and $\left(\frac{2m}{\ell}\right)$ are integers.

The shear strain modal participation factors $\Psi_{n,r}$ or Ψ_n (with $n = 1,2,3,4$) in the y-direction for values of $\beta_r\left[=n\left(\frac{r\pi h}{L}\right)^2\right]$ equal to 0, 5, 10, 15, 20, and 40 and for cases of $\frac{\ell}{m} = 1, \frac{1}{2}, \frac{1}{3}$, and $\frac{2}{5}$ are shown in Figs. 4.2 through 4.5. It is important to mention that the linear case $\left(\frac{\ell}{m}=1\right)$ gave reasonable results for the natural frequencies and modes of vibration (Chapter III) but gave erroneous results for the shear strain as indicated by the relatively large finite values at the shear-strain-free crest and by the very low values inside the dam (Fig. 4.2). The occurrence of maximum values for shear strain at the region near the crest is expected as the lower shear modulus near the top of the dam would result in correspondingly higher shear strains for the same assumed

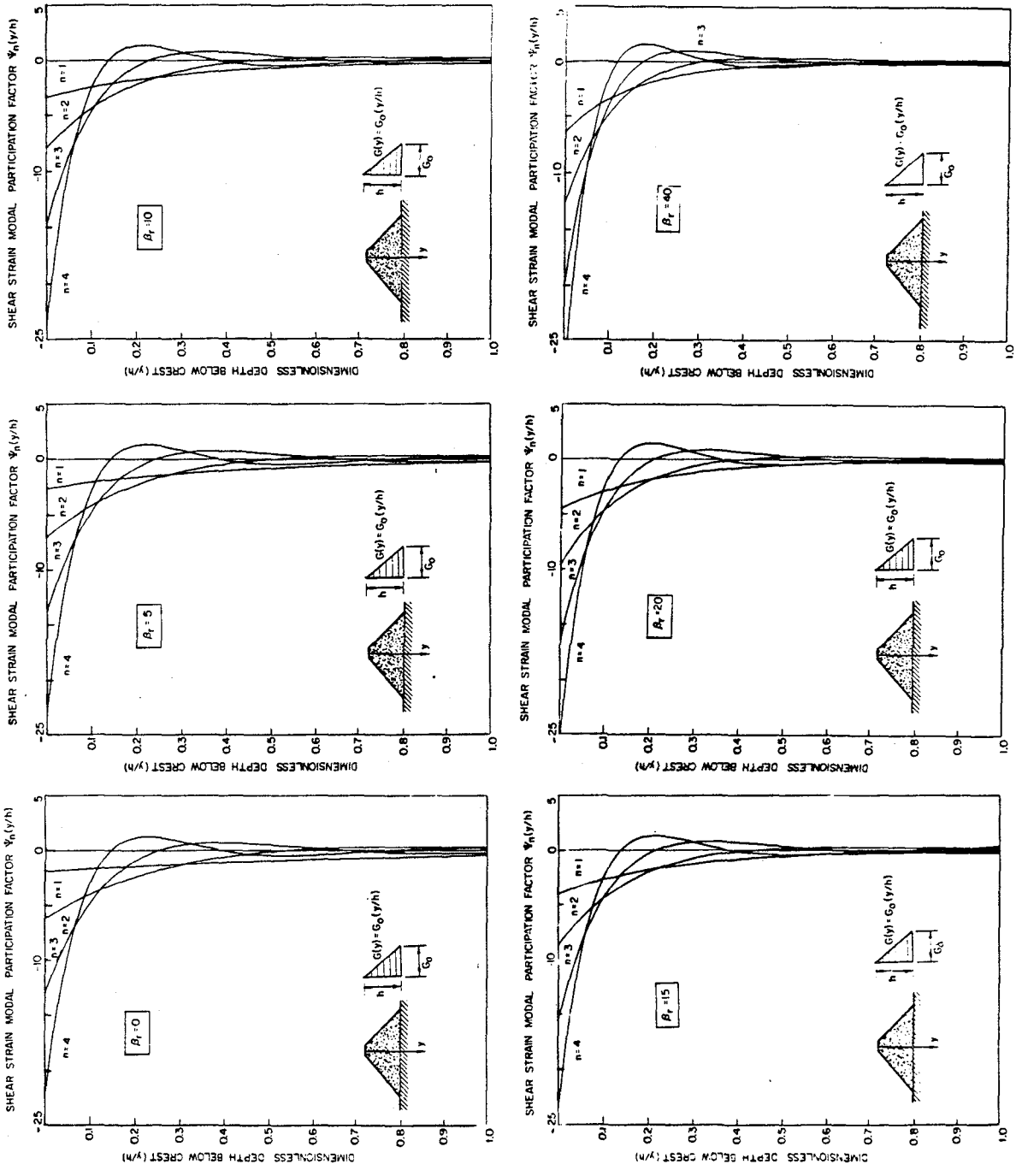

Fig. 4.2 Shear strain modal participation factors for the linear case.

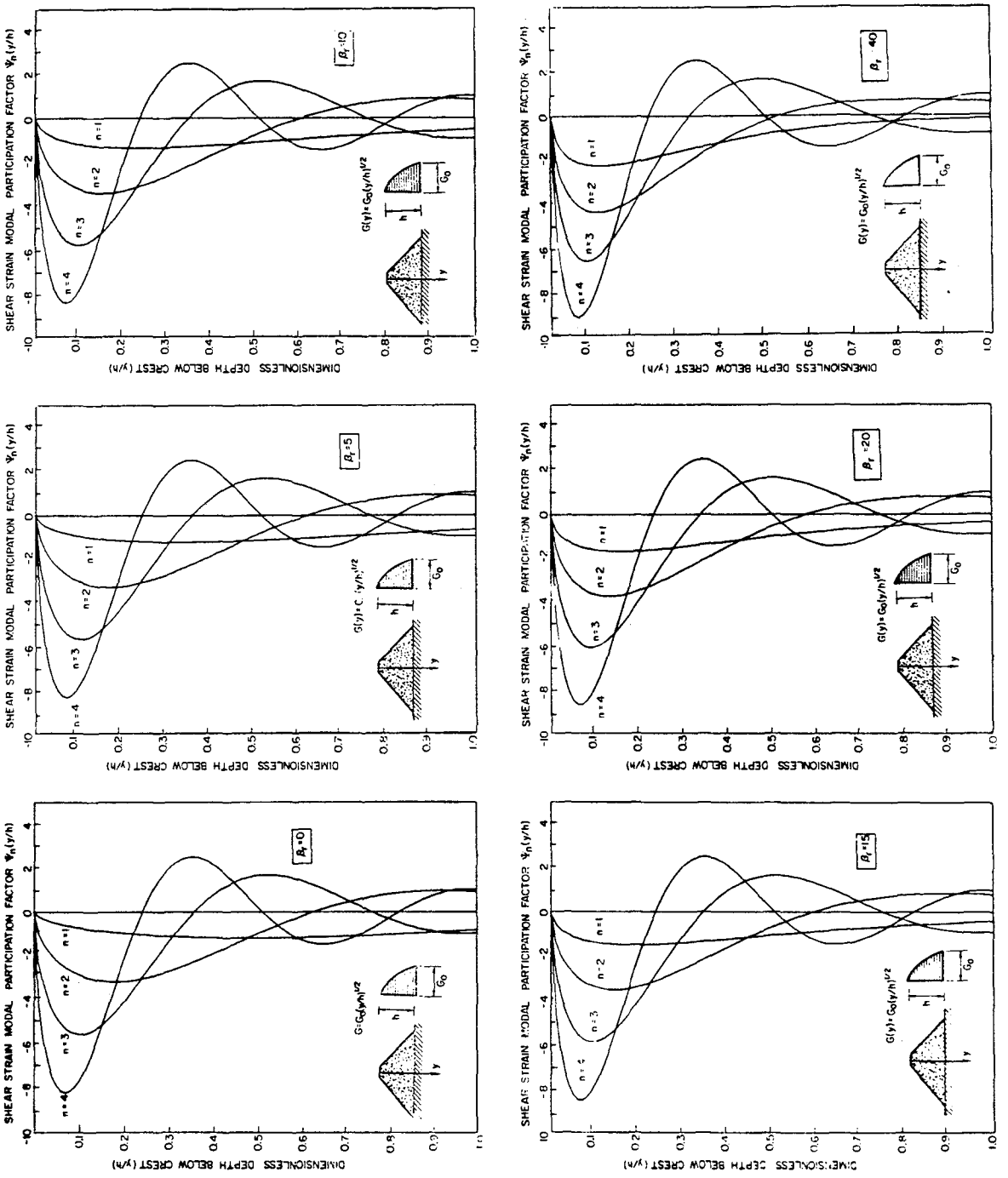

Fig. 4.3 Shear strain modal participation factors for the square root case.

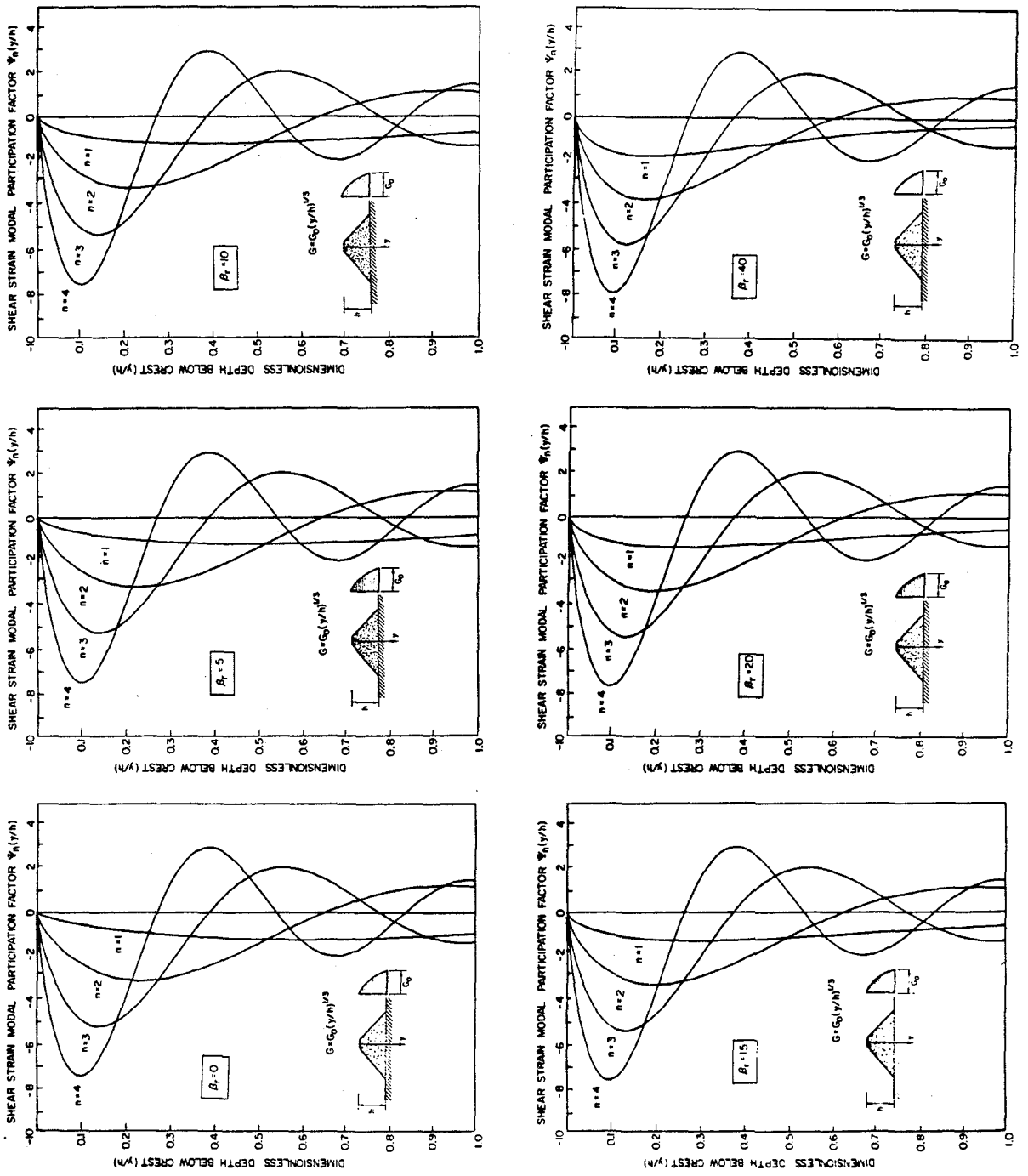

Fig. 4.4 Shear strain modal participation factors for the one-third case.

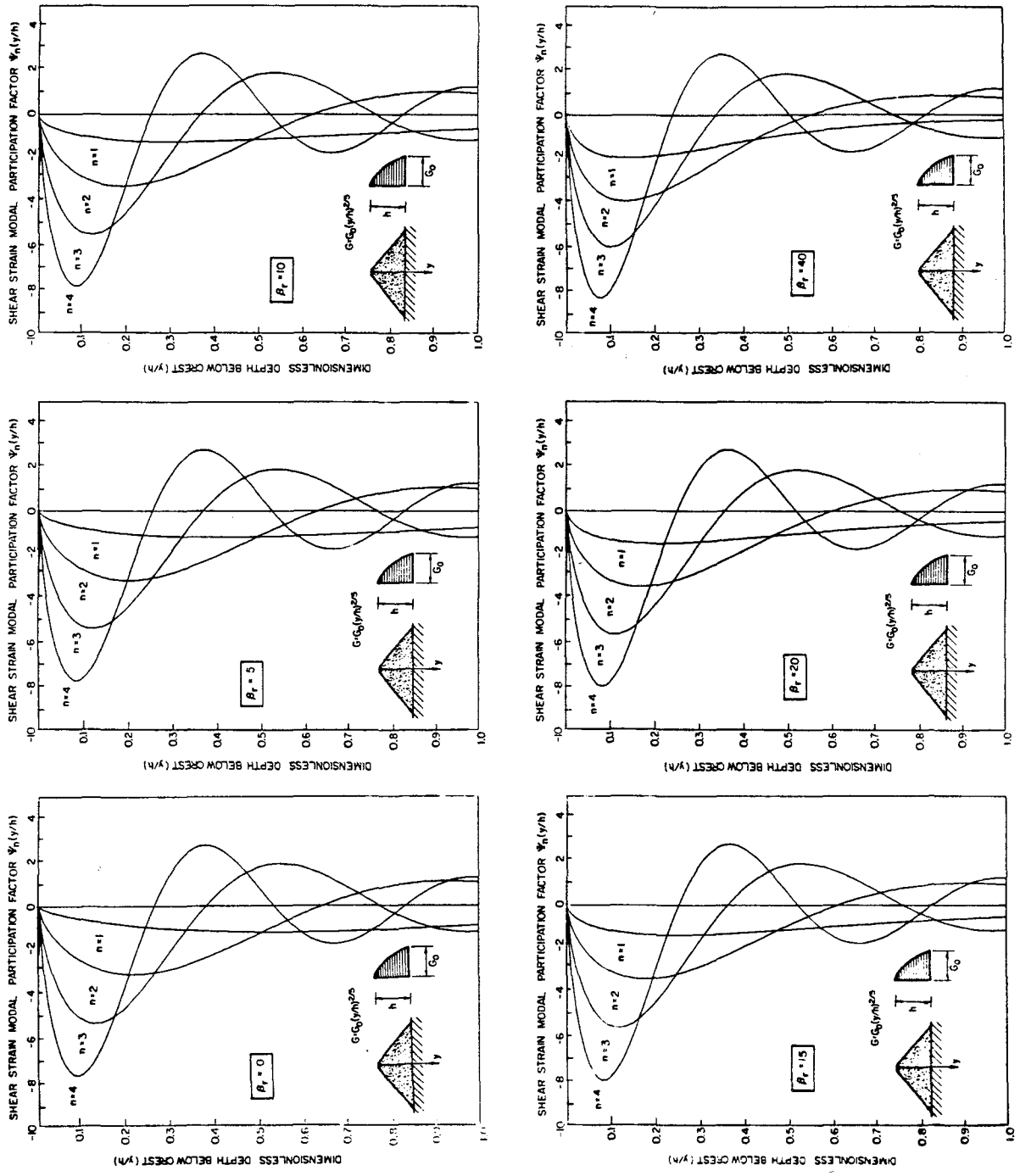

Fig. 4.5 Shear strain modal participation factors for the two-fifths case.

shear stress. Cases of $\frac{\ell}{m} = \frac{1}{2}, \frac{1}{3}$, and $\frac{2}{5}$ gave similar results for the distribution of shear strains within the dam. The coefficient β_r depends on the Poisson's ratio ν of the dam material, the dam's depth-to-length ratio (h/L), and the order, r, of the modal configuration along the longitudinal axis of the dam (low $\beta_r (= 0,5)$ implies low modal order (r = 1 to 3) or a very long dam, while higher values of $\beta_r (> 5)$ indicate a short, high dam or higher modes along the crest). The basic characteristics of the shear strain modal participation functions, Ψ_n, (i.e., the maximum values and their locations and the relative modal contributions) can be easily extracted for various types of dams from Figs. 4.2, 4.3, 4.4, and 4.5.

For the case where $G = G_0\left[(1 - \varepsilon)\left(\frac{y}{h}\right) + \varepsilon\right]$, the function $\Psi_{n,r}\left(\frac{y}{h}\right)$ is given by

$$\Psi_{n,r}\left(\frac{y}{h}\right) = 2a_2\left(\frac{y}{h}\right) + 3a_3\left(\frac{y}{h}\right)^2 + \ldots + ka_k\left(\frac{y}{h}\right)^{(k-1)} + \ldots \qquad k > 3 , \tag{4.16}$$

where

$$\left.\begin{aligned} a_0 &= 1 \\ a_1 &= 0 \\ a_2 &= -\frac{1}{4\varepsilon}\left[\left(\frac{\omega_{n,r}h}{v_{s0}}\right)^2 - \eta\varepsilon\left(\frac{r\pi h}{L}\right)^2\right] \\ &\vdots \\ a_k &= -\frac{1}{k^2\varepsilon}\left\{[k(k-1)(1-\varepsilon)]a_{k-1} + \left[\left(\frac{\omega_{n,r}h}{v_{s0}}\right)^2 - \eta\varepsilon\left(\frac{r\pi h}{L}\right)^2\right]a_{k-2} \right. \\ &\qquad \left. - \left[\eta(1-\varepsilon)\left(\frac{r\pi h}{L}\right)^2\right]a_{k-3}\right\} , \qquad k \geq 3 \end{aligned}\right\} \tag{4.17}$$

This function is shown in Fig. 4.6 for the two cases $\varepsilon = 0.5$ and 0.6 and the different values of $\beta_r = 0$, 5, and 10.

In general, Figs. 4.2 through 4.6 show significant contributions from higher modes along the depth ($n \geq 2$).

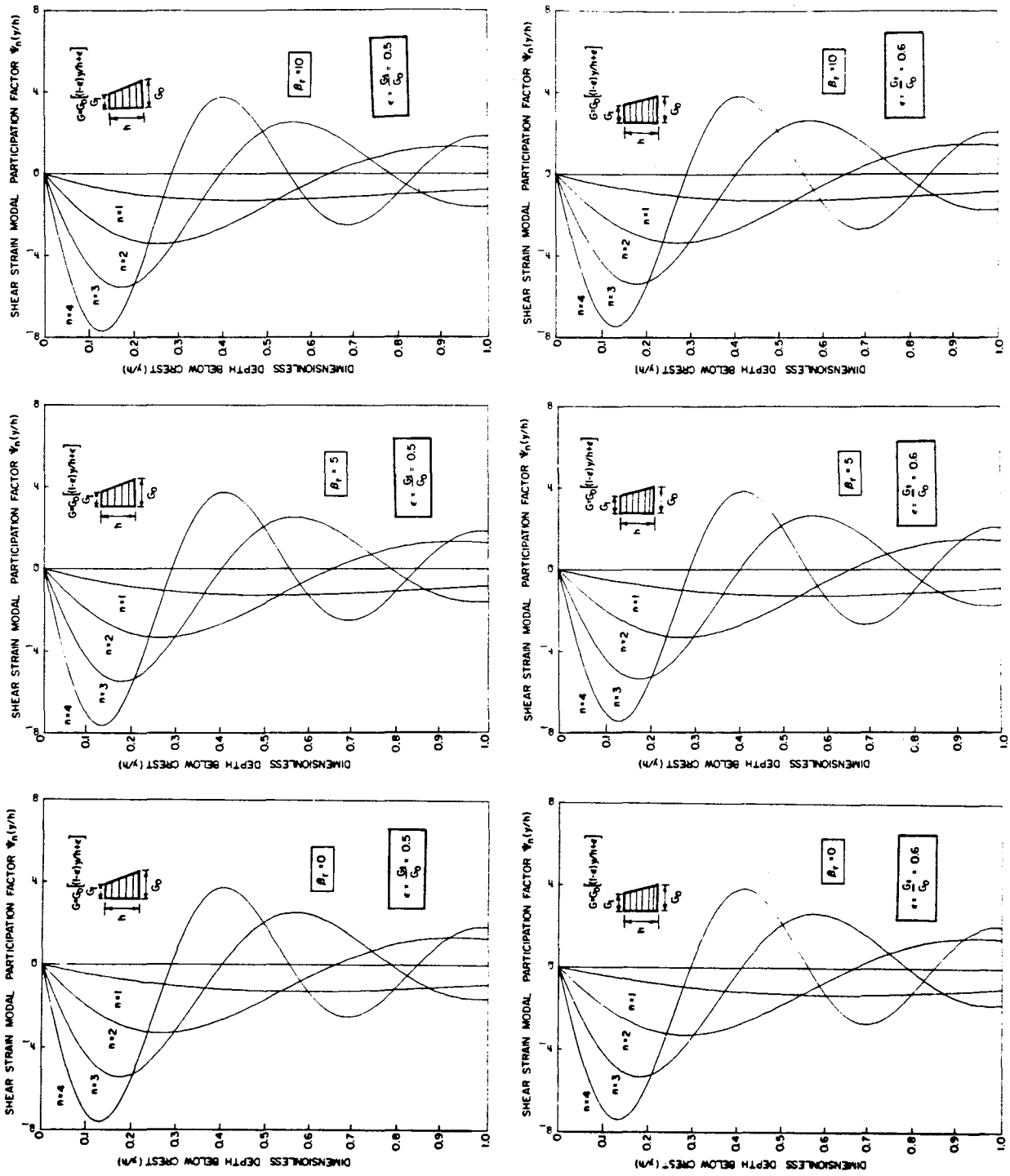

Fig. 4.6 Shear strain modal participation factors for the truncated case (with ϵ = 0.5 and 0.6).

Now, the modal shear stresses are given by

$$\tau_{n,r}(y,z,t) = G(y)\gamma_{n,r}(y,z,t). \tag{4.18}$$

For the case where G is constant, multiply the numerator and denominator of Eq. 4.13 by $\omega_{n,r}$ which is given by (Chapter II)

$$\omega_{n,r}^2 = \frac{v_s^2}{h^2}\left[\lambda_n^2 + \eta\left(\frac{r\pi h}{L}\right)^2\right] \quad , \tag{4.19}$$

and then Eq. 4.18 becomes

$$\tau_{n,r}(y,z,t) = \frac{8h\rho\omega_{n,r}}{r\pi\left[\lambda_n^2 + \eta\left(\frac{r\pi h}{L}\right)^2\right]J_1(\lambda_n)\sqrt{1-\zeta_{n,r}^2}} J_1\left(\lambda_n \frac{y}{h}\right)\sin\left(\frac{r\pi z}{L}\right)V_{n,r}(t) \, . \tag{4.20}$$

In Eq. 4.19 $v_s = \sqrt{G/\rho}$ is the shear wave velocity.

It follows that the modal participation and distribution functions for the shear stress are expressed by the function $J_1\left(\lambda_n \frac{y}{h}\right)$ as in the case of the shear strain (Eq. 4.13).

The modal shear stresses for the case where $G(y) = G_0\left(\frac{y}{h}\right)^{\ell/m}$ are given (using Eqs. 4.11, 4.12, and 4.18) by

$$\tau_{n,r}(y,z,t) = \frac{4G_0\overset{*}{P}_{n,r}}{r\pi h\omega_{n,r}\sqrt{1-\zeta_{n,r}^2}} \Phi_{n,r}\left(\frac{y}{h}\right)\sin\left(\frac{r\pi z}{L}\right)V_{n,r}(t) \quad , \tag{4.21}$$

where $\Phi_{n,r}\left(\frac{y}{h}\right)$ is defined by $\left(\frac{y}{h}\right)^{\ell/m} \cdot \left[\frac{dY_n\left(\frac{y}{h}\right)}{d\left(\frac{y}{h}\right)}\right]$; it expresses the modal participation and distribution of shear stress, and it is given by

$$\Phi_{n,r}\left(\frac{y}{h}\right) = a_{\left(\frac{2m}{\ell}-1\right)}\left(\frac{y}{h}\right) + a_{\left(\frac{2m}{\ell}\right)}\left(\frac{y}{h}\right)^{\left(\frac{\ell}{m}+1\right)} + \ldots + a_k\left(\frac{y}{h}\right)^{\left[\frac{\ell}{m}(k+1)-1\right]} + \ldots \quad ,$$

$$\left(k > \frac{2m}{\ell}\right) \quad , \tag{4.22}$$

where the a's coefficients are defined through Eq. 4.15.

The shear stress modal participation factors $\Phi_{n,r}$ or $\phi_n\left(\frac{y}{h}\right)$ (with $n = 1,2,3,4$) for $\frac{\ell}{m} = 1, \frac{1}{2}, \frac{1}{3}$ and $\frac{2}{5}$ are shown in Figs. 4.7 through 4.10.

For the linear case $\left(\frac{\ell}{m} = 1\right)$ the shear stress distribution (Fig. 4.7) seems physically more reasonable than the shear strain distribution shown in Fig. 4.2. Like the shear strain case, great similarity exists among the cases of $\frac{\ell}{m} = \frac{1}{2}, \frac{1}{3}$ and $\frac{2}{5}$ of the shear stress distributions.

The function $\Phi_{n,r}\left(\frac{y}{h}\right)$ for the linear truncated stiffness case (Eq. 4.2-c) can be expressed, in terms of $\Psi_{n,r}$ of Eq. 4.16, as

$$\Phi_{n,r}\left(\frac{y}{h}\right) = \left[(1 - \varepsilon)\left(\frac{y}{h}\right) + \varepsilon\right]\Psi_{n,r}\left(\frac{y}{h}\right) \quad . \tag{4.23}$$

The shear stress modal participation function ($\Phi_{n,r}$ or Φ_n) is plotted in Fig. 4.11 for the two cases where $\varepsilon = 0.5$ and 0.6; for each case four modes ($n = 1,2,3,4$) are shown for the values of $\beta_r = 0$, 5 and 10. Again, the basic features and differences of all the above-mentioned stiffness variations for the shear stress case can be easily deduced from Figs. 4.7, 4.8, 4.9, 4.10, and 4.11.

IV-3 Dynamic Axial (Mornal) Strains and Stresses

Analogous to the development of the previous equations expressing dynamic shear strains and stresses, the magnitude and distribution of normal (axial) strains and stresses in the $(n,r)^{th}$ mode can be given by

$$\varepsilon_{n,r}(y,z,t) = \frac{\partial w}{\partial z} = \frac{4\overset{*}{P}_{n,r}}{L\omega_{n,r}\sqrt{1 - \zeta_{n,r}^2}}\, Y_n\left(\frac{y}{h}\right)\cos\left(\frac{r\pi z}{L}\right)V_{n,r}(t) \quad , \tag{4.24}$$

and

$$\sigma_{n,r}(y,z,t) = E(y)\varepsilon_{n,r}(y,z,t) = \eta G(y)\frac{\partial w}{\partial z} \quad . \tag{4.25}$$

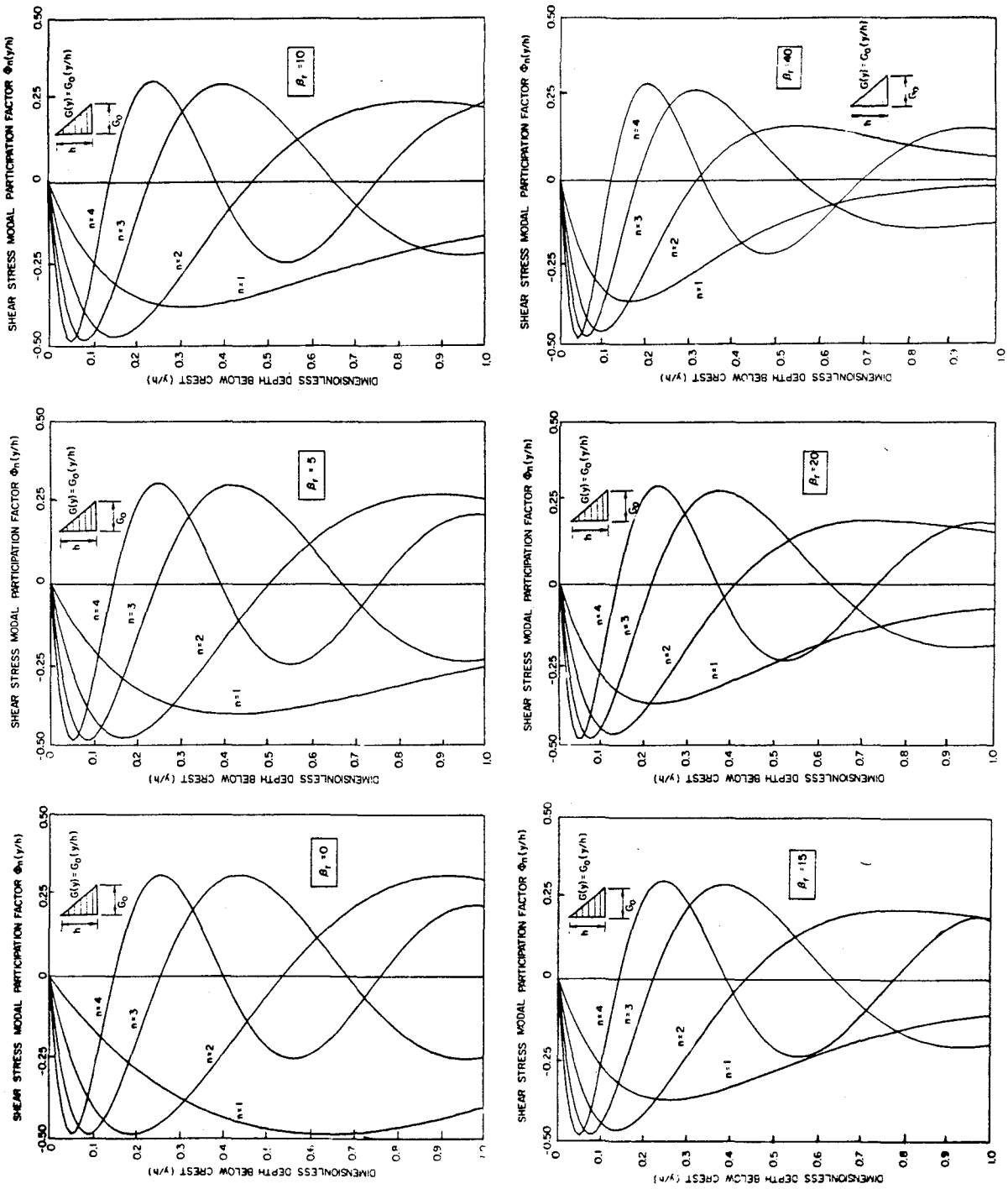

Fig. 4.7 Shear stress modal participation factors for the linear case.

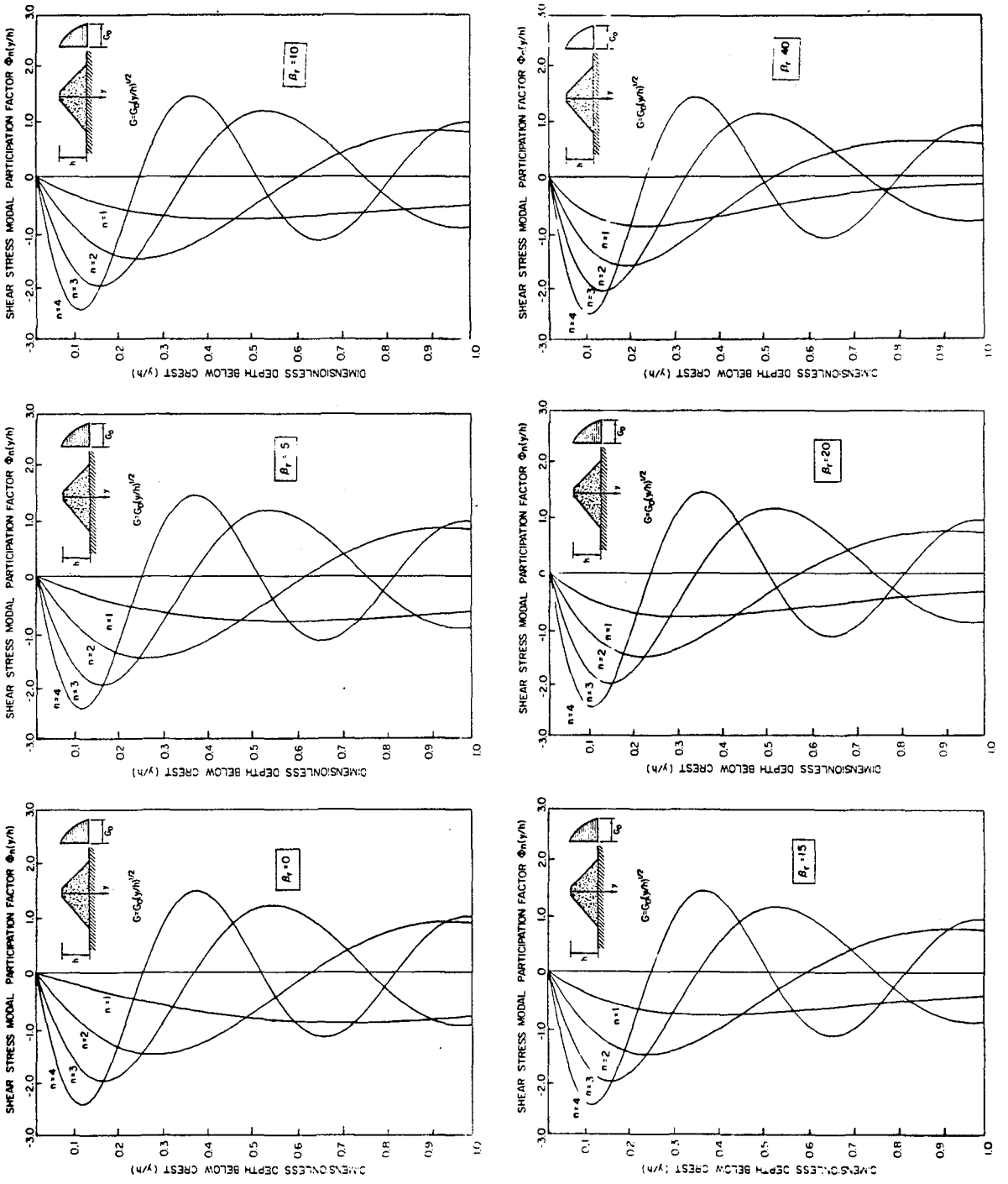

Fig. 4.8 Shear stress modal participation factors for the square-root case.

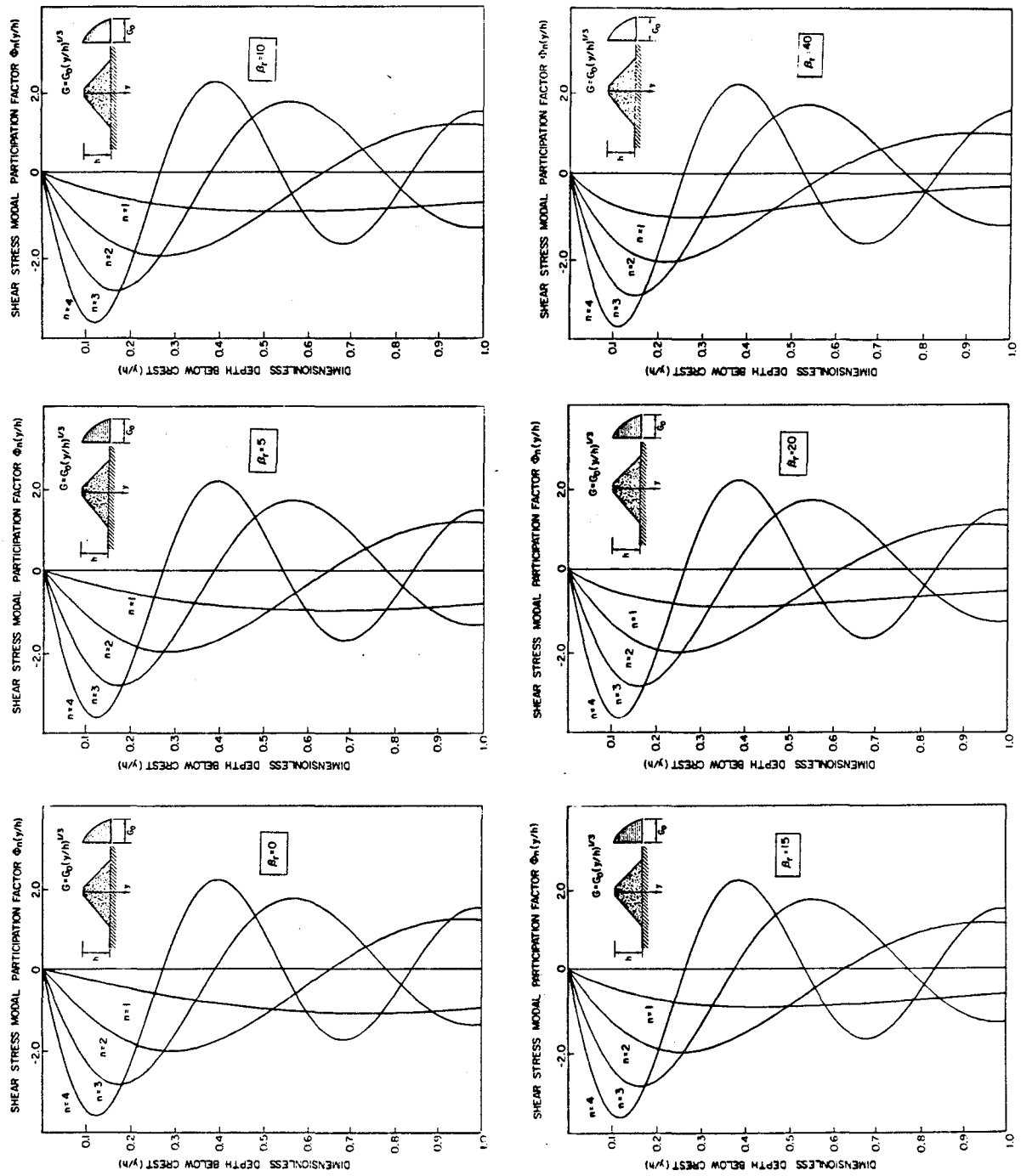

Fig. 4.9 Shear stress modal participation factors for the one-third case.

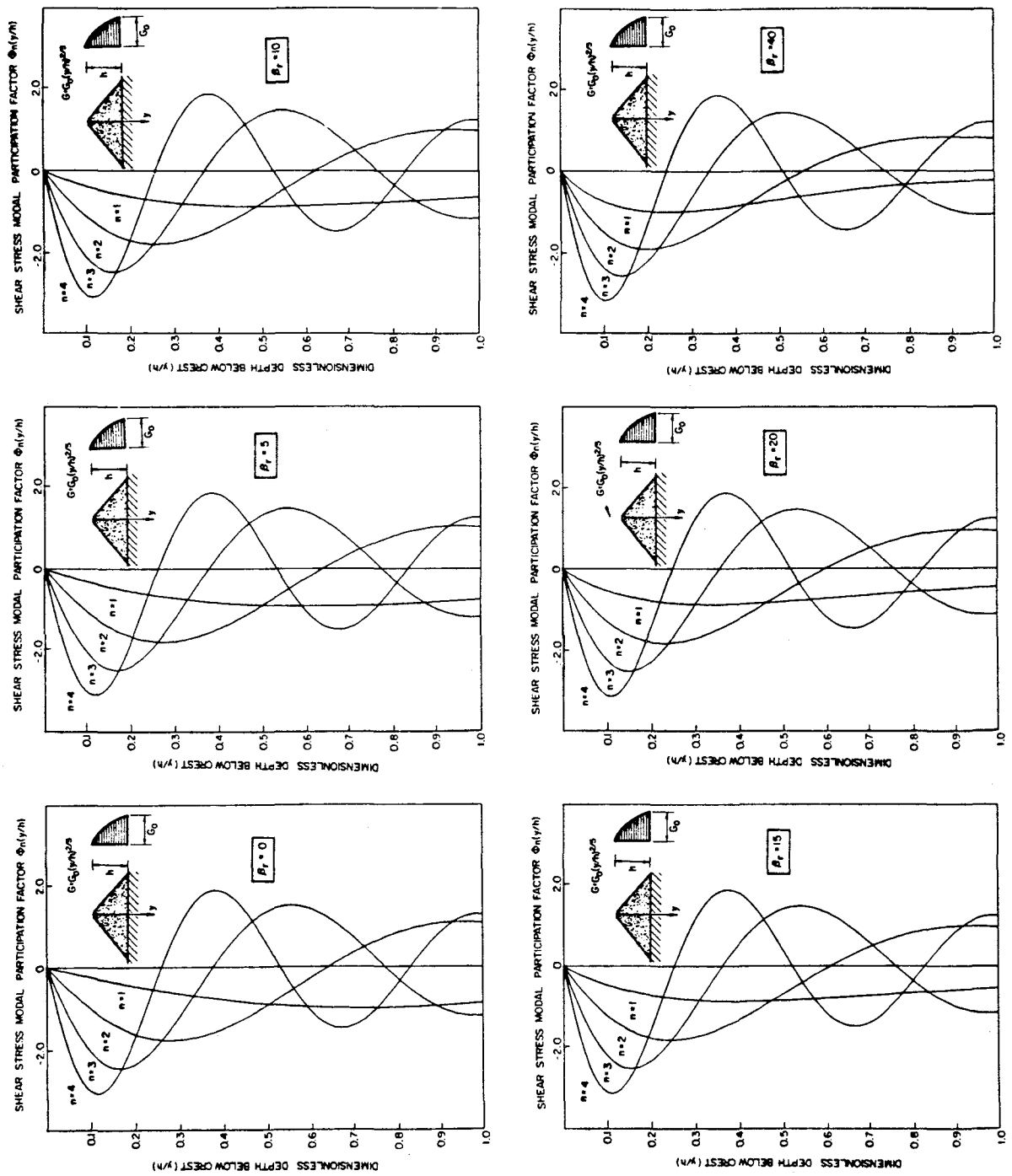

Fig. 4.10 Shear stress modal participation factors for the two-fifths case.

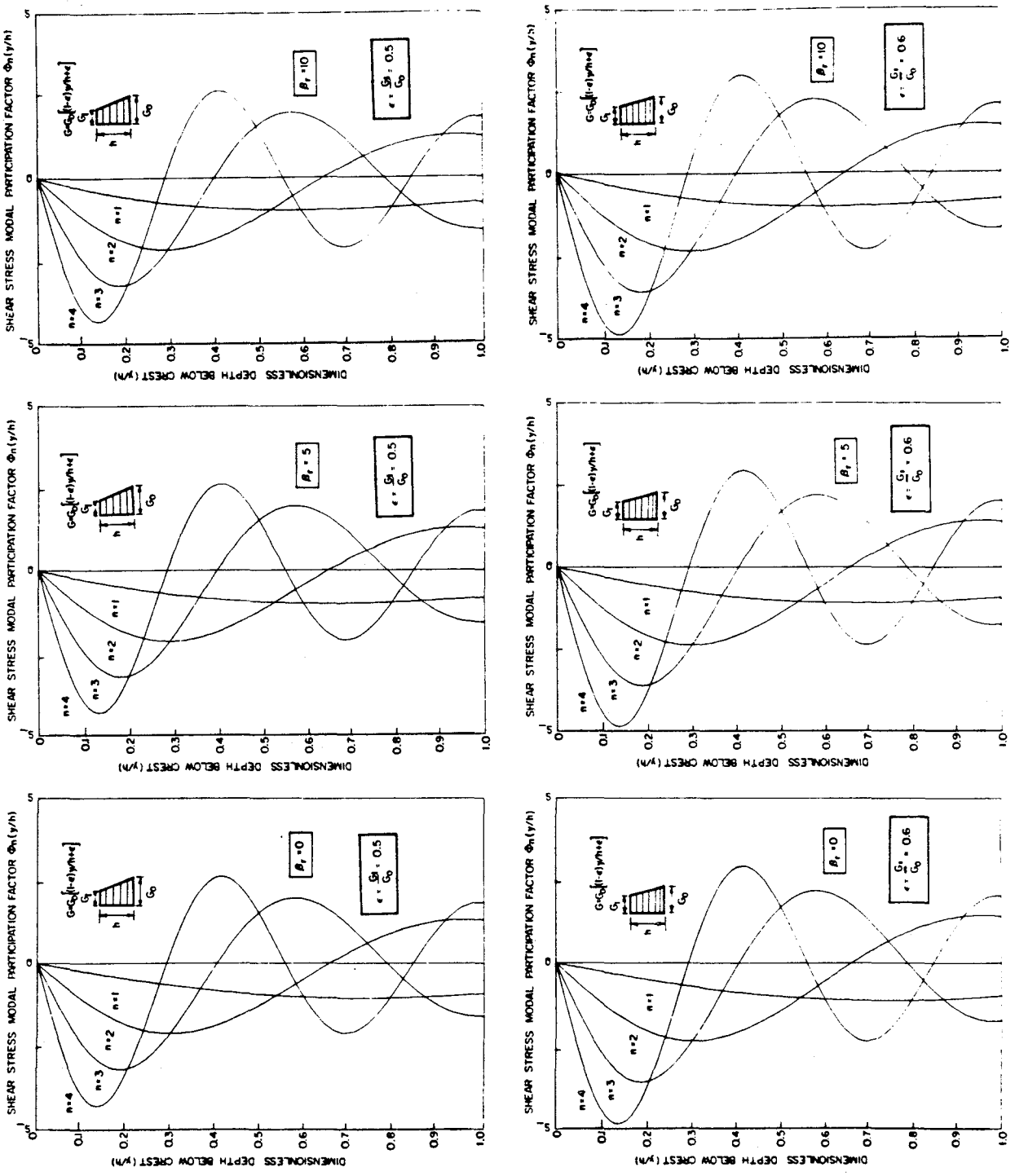

Fig. 4.11 Shear stress modal participation factors for the truncated case (with $\epsilon = 0.5$ and 0.6).

For the case where G is constant, the above two equations can be expressed as

$$\varepsilon_{n,r}(y,z,t) = \frac{8}{L\lambda_n J_1(\lambda_n)\omega_{n,r}\sqrt{1-\zeta_{n,r}^2}} J_0\left(\lambda_n \frac{y}{h}\right)\cos\left(\frac{r\pi z}{L}\right)V_{n,r}(t) \quad , \tag{4.26}$$

$$\sigma_{n,r}(y,z,t) = \frac{8\left(\frac{h}{L}\right)\eta h\rho\omega_{n,r}}{\lambda_n\left[\lambda_n^2 + \eta\left(\frac{r\pi h}{L}\right)^2\right]J_1(\lambda_n)\sqrt{1-\zeta_{n,r}^2}} J_0\left(\lambda_n \frac{y}{h}\right)\cos\left(\frac{r\pi z}{L}\right)V_{n,r}(t), \tag{4.27}$$

where J_0 is the Bessel function of first kind and zero order.

It follows from Eq. 4.24 that the modal participation and distribution functions for the normal (axial) strain, of the general $(\ell/m)^{th}$ case, are expressed by the modal configuration $Y_n\left(\frac{y}{h}\right)$ which is expressed by (Chapter II)

$$Y_n\left(\frac{y}{h}\right) = a_0 + \frac{1}{\left(2-\frac{\ell}{m}\right)} a_{\left(\frac{2m}{\ell}-1\right)}\left(\frac{y}{h}\right)^{\left(2-\frac{\ell}{m}\right)} + \frac{1}{2} a_{\left(\frac{2m}{\ell}\right)}\left(\frac{y}{h}\right)^2 + \ldots. +$$

$$\frac{1}{k\left(\frac{\ell}{m}\right)} a_k\left(\frac{y}{h}\right)^{k\left(\frac{\ell}{m}\right)} + \ldots. \quad , \quad k > \frac{2m}{\ell} \quad , \tag{4.28}$$

where the a's coefficients are defined through Eq. 4.15.

The modal normal stresses are given (using Eqs. 4.24 and 4.25) by

$$\sigma_{n,r}(y,z,t) = \frac{4\eta G_0 \ddot{\bar{P}}_{n,r}}{L\omega_{n,r}\sqrt{1-\zeta_{n,r}^2}} \Gamma_{n,r}\left(\frac{y}{h}\right)\cos\left(\frac{r\pi z}{L}\right)V_{n,r}(t) \quad , \tag{4.29}$$

where the normal stress modal participation function $\Gamma_{n,r}\left(\frac{y}{h}\right)\left[= \left(\frac{y}{h}\right)^{\ell/m} Y_n\left(\frac{y}{h}\right)\right]$ is given by

$$\Gamma_{n,r}\left(\frac{y}{h}\right) = a_0\left(\frac{y}{h}\right)^{\ell/m} + \frac{1}{\left(2 - \frac{\ell}{m}\right)} a\left(\frac{2m}{\ell} - 1\right)\left(\frac{y}{h}\right)^2 + \frac{1}{2} a\left(\frac{2m}{\ell}\right)\left(\frac{y}{h}\right)^{\left(2 + \frac{\ell}{m}\right)} + \ldots. +$$

$$\frac{1}{k\left(\frac{\ell}{m}\right)} a_k\left(\frac{y}{h}\right)^{\frac{\ell}{m}(k+1)} + \ldots. \quad , \quad k > \frac{2m}{\ell} \quad , \qquad (4.30)$$

where, again, the a's coefficients are defined by Eq. 4.15.

Figures 4.12 through 4.15 show the normal stress modal participation factors $\Gamma_{n,r}$ or $\Gamma_n\left(\frac{y}{h}\right)$ for the various cases mentioned previously.

The normal stress modal participation function, for the truncated linear stiffness case (Eq. 4.2-c), is given by

$$\Gamma_{n,r}\left(\frac{y}{h}\right) = \left[(1 - \varepsilon)\left(\frac{y}{h}\right) + \varepsilon\right]\left\{a_0 + a_2\left(\frac{y}{h}\right)^2 + \ldots. + a_k\left(\frac{y}{h}\right)^k + \ldots.\right\} \quad , k \geq 3 \qquad (4.31)$$

The coefficients a_0, a_2, ... and a_k are defined through Eq. 4.17; the quantity in braces is equal to the mode shapes $Y_n(y/h)$ or the normal strain modal participation function. Figure 4.16 depicts the function $\Gamma_{n,r}$ or $\Gamma_n (n = 1,2,3,4)$ for the two cases mentioned before (i.e., for $\varepsilon = 0.5$ and 0.6).

It can be seen from Figs. 4.12 through 4.16 and Eqs. 4.24 and 4.25 that the maximum dynamic normal strains and stresses occur near the top region of the dam at the end abutments (where $\cos\left(\frac{r\pi z}{L}\right) \simeq 1$); this may explain the Santa Felicia Dam crack mentioned previously and shown in Fig. 1.2 (Chapter 1).

IV-4. Utilization of Response Spectra

Based on the above formulation, the response spectra technique can be utilized for estimating maximum earthquake-induced longitudinal strains and stresses. The maximum value of the quantity $V_{n,r}(t)$ of Eqs. 4.12, 4.13, 4.20, 4.21, 4.24, 4.26, 4.27, and 4.29 is equal to the ordinate of the velocity spectrum S_v of the ground motion, corresponding to the natural frequency $\omega_{n,r}$ and the damping factor $\zeta_{n,r}$ of the $(n,r)^{th}$ mode, i.e.,

$$V_{n,r}(t)\big|_{max} = S_v(\omega_{n,r}, \zeta_{n,r}) \quad . \qquad (4.32)$$

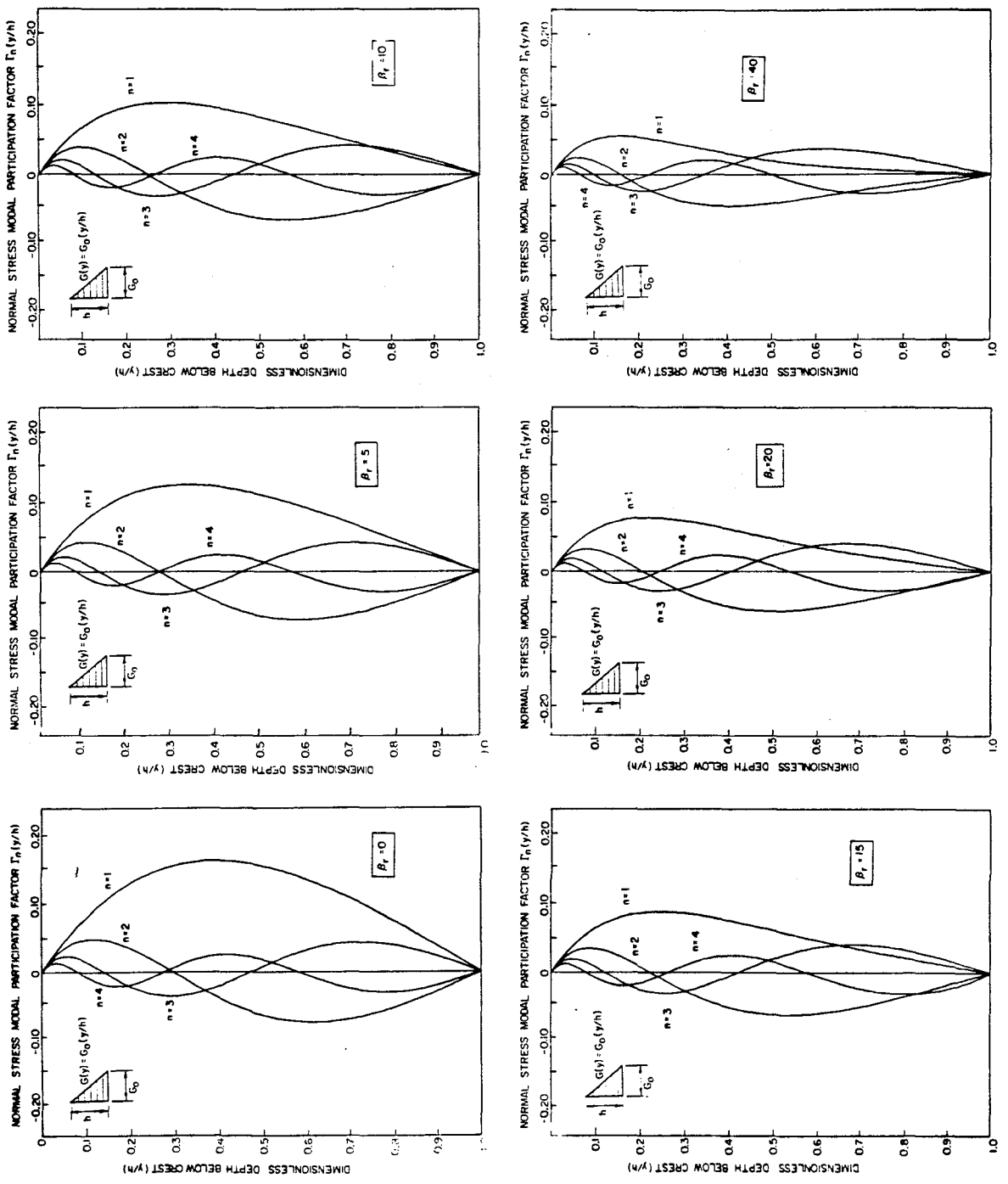

Fig. 4.12 Normal stress modal participation factors for the linear case.

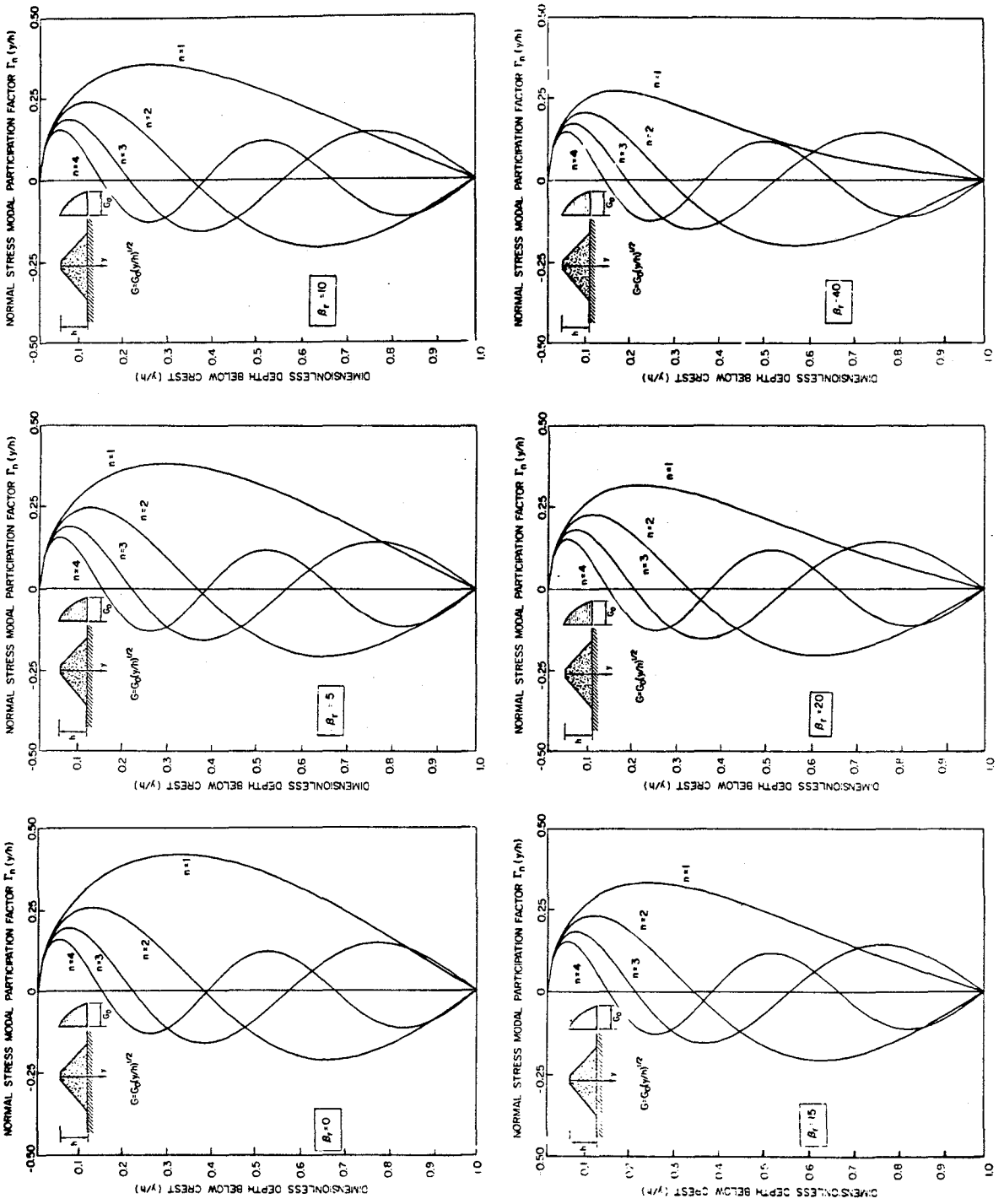

Fig. 4.13 Normal stress modal participation factors for the square-root case.

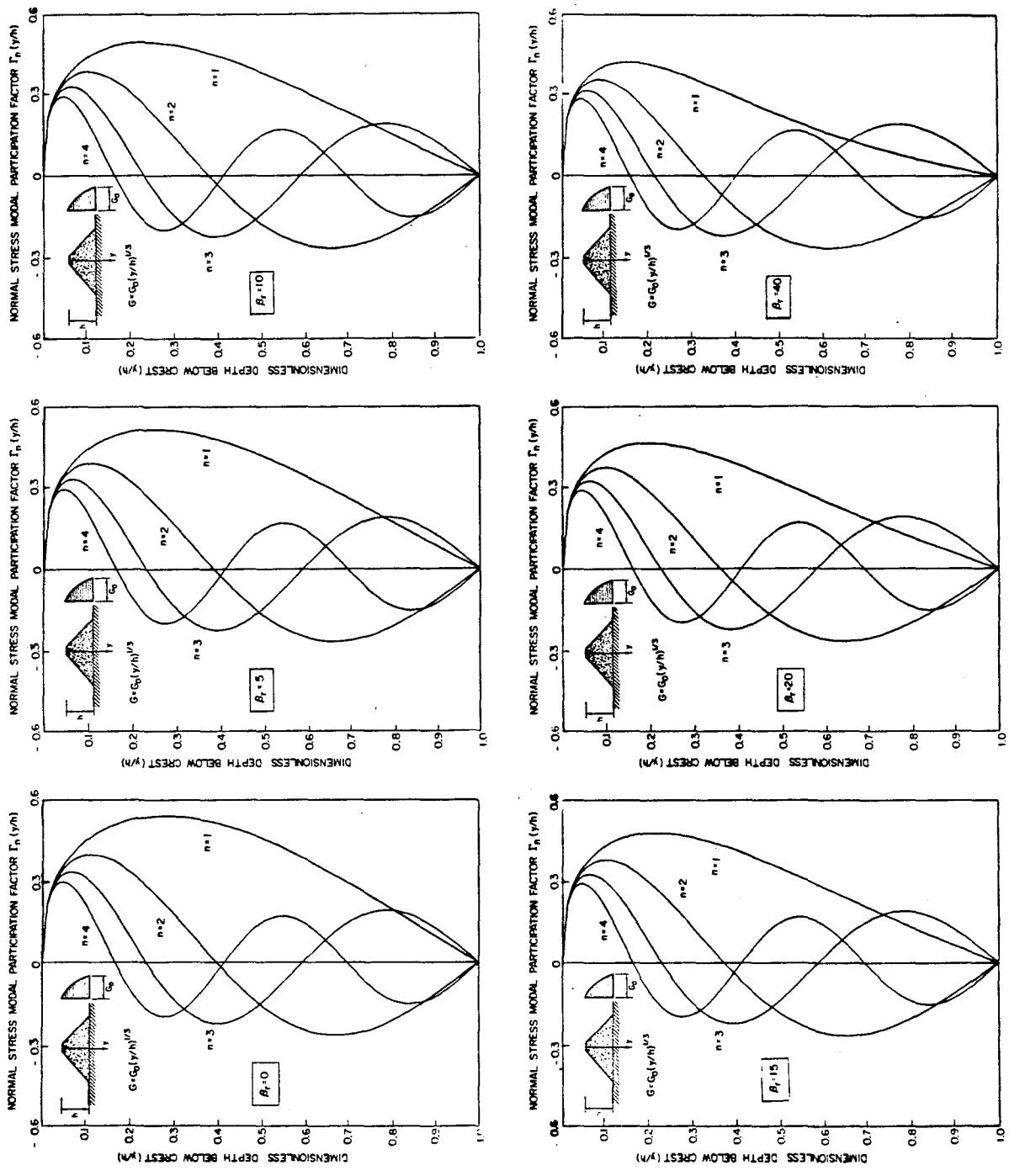

Fig. 4.14 Normal stress modal participation factors for the one-third case.

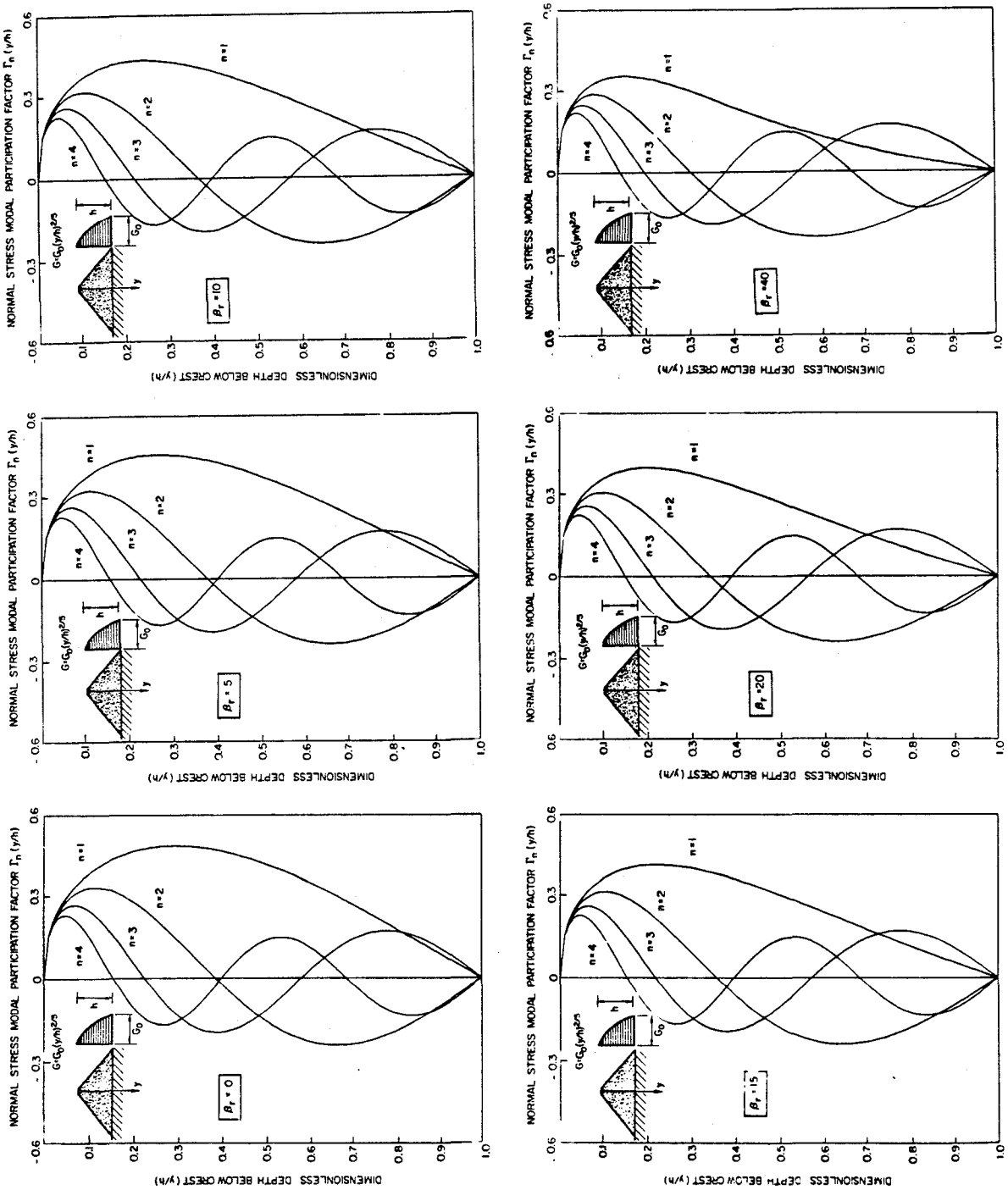

Fig. 4.15 Normal stress modal participation factors for the two-fifths case.

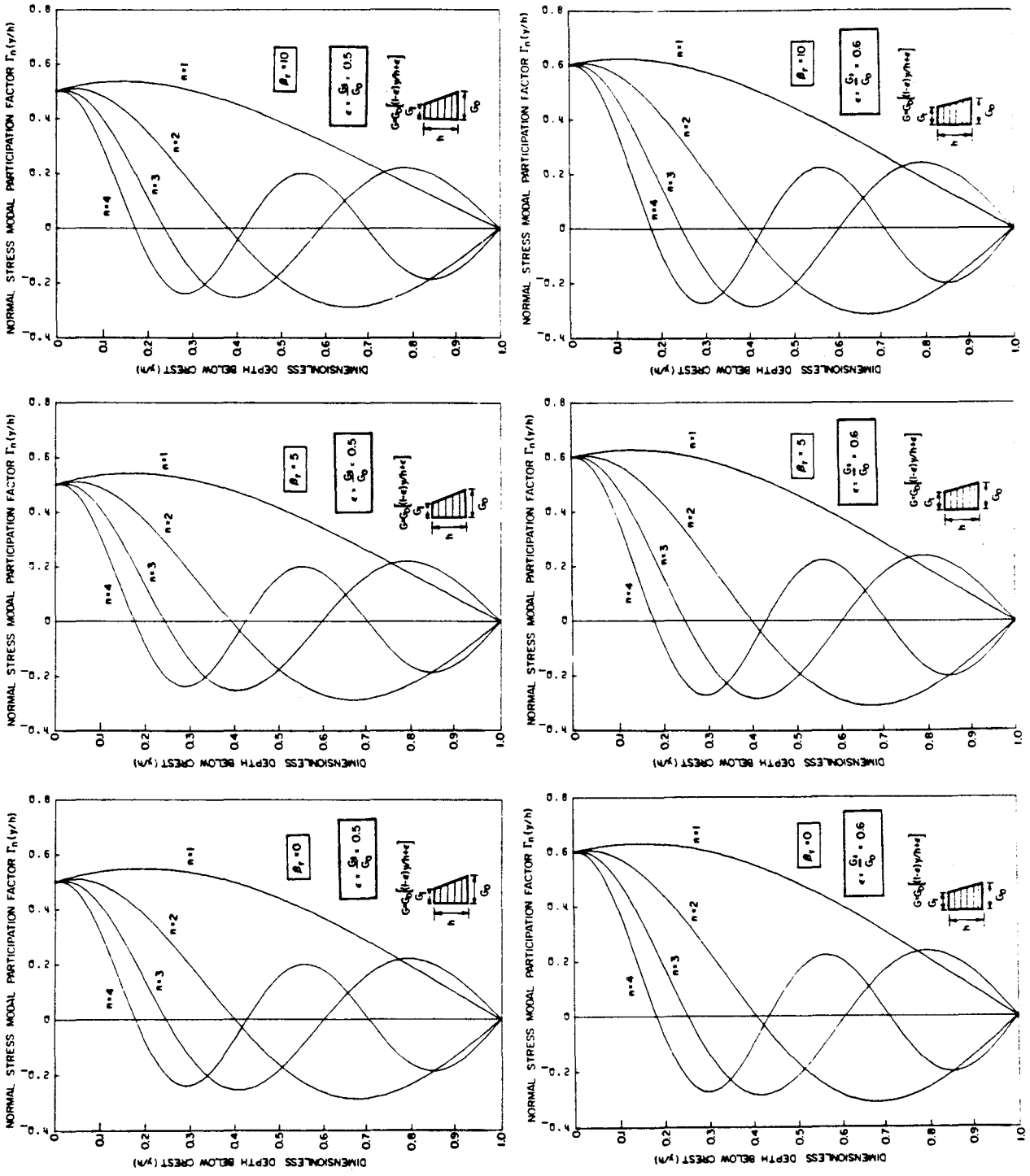

Fig. 4.16 Normal stress modal participation factors for the truncated case (with $\epsilon = 0.5$ and 0.6).

For earthquake-like excitations where little error is involved for $\zeta_{n,r} < 20\%$, it can be shown that

$$S_a = \omega_{n,r}^2 S_d = \omega_{n,r} S_v \quad , \tag{4.33}$$

where S_d and S_a are the ordinates of the calculated acceleration and displacement spectra, respectively. Then, finally, for the maximum value of Eq. 10, one can get

$$T_{n,r}(t)\big|_{max} = \frac{4}{r\pi} \frac{\overset{*}{P}_{n,r}}{\omega_{n,r}\sqrt{1 - \zeta_{n,r}^2}} S_v \quad . \tag{4.34}$$

The maximum shear strains and stresses in the first mode (n = 1, r = 1), which occur in the central region of the dam ($z \simeq L/2$), along the y-axis (the depth axis) of Fig. 4.1, can be written as (with the aid of Eqs. 4.11, 4.20, 4.21, and 4.34)

$$\gamma_{1,1}\big|_{max} = \left[\frac{4\overset{*}{P}_{1,1}}{\pi h} \Psi_{1,1}\big|_{max}\right] S_d \quad , \tag{4.35}$$

and

$$\tau_{1,1}\big|_{max} = \left[\frac{4G_0\overset{*}{P}_{1,1}}{\pi h\omega_{1,1}^2} \Phi_{1,1}\big|_{max}\right] S_a \quad . \tag{4.36}$$

Similarly, the maximum tensile or compressive strains, and stresses in the first mode, occurring in the top region near the crest at its ends (where $z \simeq L$ or $\cos(r\pi z/L) \simeq 1$), are given (with the aid of Eqs. 4.24, 4.25, 4.26, and 4.27) by

$$\varepsilon_{1,1}\big|_{max} = \left[\frac{4\overset{*}{P}_{1,1}}{L} Y_{1\ max}\right] S_d \quad , \tag{4.37}$$

and

$$\sigma_{1,1}\big|_{max} = \left[\frac{4\eta G_0\overset{*}{P}_{1,1}}{L\omega_{1,1}^2} \Gamma_{1,1}\big|_{max}\right] S_a \quad . \tag{4.38}$$

It is important to note that the use of the response spectra technique may lead to inaccuracies in ascertaining the true influence of material nonlinearity on the dam response since the technique provides only single-valued estimates of stresses and strains induced by earthquakes. The manner in which

the amplitudes of an earth dam's motion vary with time have a major role in the dam's earthquake response characteristics. In the next chapter a rational method is presented which takes into account this variation, also using the elastic analytical models.

CHAPTER V

IDENTIFICATION OF CONSTITUTIVE RELATIONS, ELASTIC MODULI, AND DAMPING FACTORS OF EARTH DAMS FROM THEIR EARTHQUAKE RECORDS

V-1. Basis of the Analysis

The dynamic soil properties which exert the greatest influence on an earth dam's dynamic responses are those related to the stress-strain relations. Like all soils, materials of earth dams develop nonlinear inelastic stress-strain relationships when subjected to earthquake loading conditions. By using earthquake response records of the crest and the base (structural and input ground motions), together with the results of the analytical models (presented here), these stress-strain relationships can be estimated for the dam's materials. The strain-dependent elastic moduli and damping factors have already been determined in this manner for the upstream-downstream recorded motion of a modern earth dam (see Refs. 1, 4, and 6), using existing analytical shear-beam models (9, 22, 23).

One of the purposes of this report is to present a similar procedure (like the one developed by Abdel-Ghaffar and Scott, Ref. 6) to estimate longitudinal dynamic stresses and strains and corresponding elastic moduli and damping factors for earth dams from their hysteretic responses to real earthquakes, utilizing the hysteresis loops from crest and base records and the above-mentioned longitudinal elastic analytical models.

The idea is illustrated in Fig. 5.1 and can be summarized in the following steps:

(1) By using the earthquake records, the experimental results and the analytical models (of Chapters II and IV), the fundamental frequency in longitudinal direction can be identified.

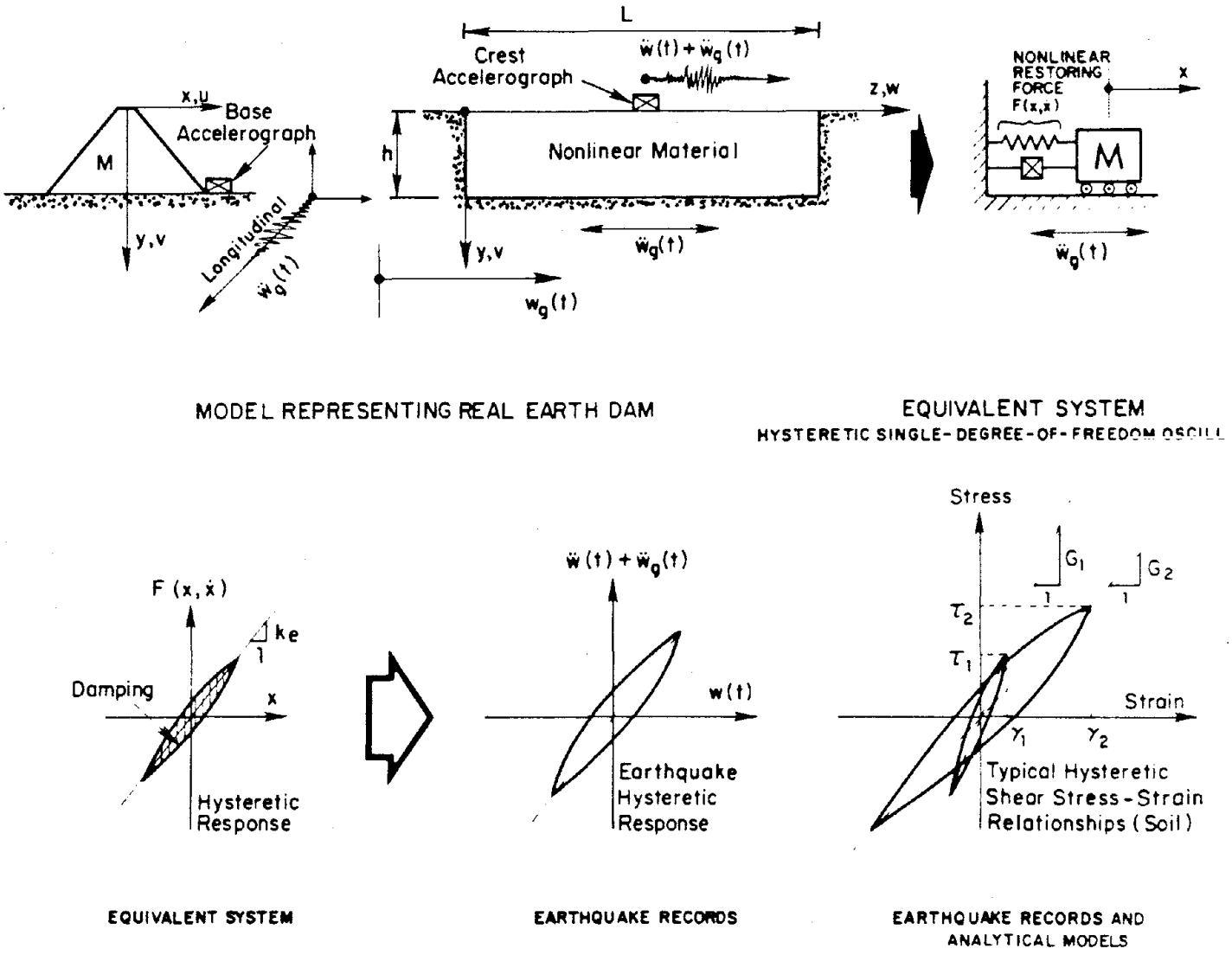

Fig. 5.1 IDENTIFICATION OF ELASTIC MODULI AND DAMPING FACTORS FROM EARTHQUAKE RECORDS

(2) By using very narrow band-pass digital filtering around the fundamental frequency (usually the primary) of the crest and base records, the pure fundamental mode response can be obtained.

(3) By treating the filtered modal response as that of a single-degree-of-freedom (SDOF) hysteretic structure (with nonlinear restoring force $F(x,\dot{x})$ equal to $-M(\ddot{x} + \ddot{w}_g(t))$; x, $\dot{x}$, and $\ddot{x}$ are the relative displacement, velocity, and acceleration, respectively, and M is the mass) the hysteresis loops, which show the relationship between the relative displacement of the crest with respect to the base and the absolute acceleration of the dam, can be obtained.

(4) By using the elastic longitudinal analytical models, the shear stresses and shear strains (Eqs. 4.35, 4.36) can be determined as functions of the maximum absolute acceleration and maximum relative displacement, respectively, for each hysteresis loop, and consequently, equivalent (secant) shear moduli and damping factors can be determined from the slope and the area, respectively, of the loop. Since it was assumed that each hysteresis loop is a response of an SDOF oscillator, and in order to get a qualitative picture of the dynamic shear strain and stress from the hysteretic response, the value of S_d and of S_a in Eqs. 4.37 and 4.38 are assumed to be the maximum relative displacement, $(w(t))_{max}$, and the maximum absolute acceleration, $(\ddot{w}(t) + \ddot{w}_g(t))_{max}$, respectively, for each hysteresis loop.

(5) Finally, the data so obtained permit development of typical stress-strain curves which are then approximated by the Ramberg-Osgood analytical models and/or the hyperbolic curves. The data can also be compared with those previously available from soil-dynamic laboratory investigations and can be combined with those obtained

from the analysis of the upstream-downstream vibrations (Ref. 6) to give informative materials to both earthquake and the geotechnical engineers.

V-2. Application of the Analysis

V-2.1. Longitudinal Dynamic Shear Stress-Strain Relations for Santa Felicia Earth Dam

The Santa Felicia Dam (1, 3, 4, 6) is equipped with two accelerographs (one on the central region of the crest and the other at the base) that yielded data on how it responded to two earthquakes (1,4).

Amplification spectra of the dam's two earthquake records which were (presented in Chapter III) computed by dividing Fourier amplitudes of acceleration of the crest records by those of the base records (to indicate the resonant frequencies and to estimate the relative contribution of different modes in the longitudinal direction) revealed that the values of the resonant frequencies vary slightly from one earthquake to the other. In addition, amplification spectra of the upstream-downstream direction showed that the dam responded primarily in its fundamental mode in that direction, but the spectra of the longitudinal component are lacking pronounced single peaks.

For Santa Felicia Dam, the first longitudinal frequency determined from the amplification spectra of the 1971 earthquake is 1.35 Hz (1.27 Hz for the 1976 earthquake), $\rho = 4.02$ lb-sec^2/ft^4, $\nu = 0.45$ (3), and $h/L = 236.5/912.5 = 0.26$; this gives $\beta_r = 1.92\ r^2$, $r = 1,2,3,\ldots$ (or $\beta_1 = 1.92$ for the first mode). The calculated shear stress and shear strain modal participation factors, along the depth of the dam, $\Phi_{n,r}$ (or Φ_n, n = 1 and 2) and $\Psi_{n,r}$ (or Ψ_n, n =1,2, and 3), as well as the normal stress modal participation factor $\Gamma_{n,r}$ (or Γ_n, n = 1) for various stiffness variations are

shown in Figs. 5.2a, b, c, and d. The first-mode maximum shear strains for the analytical models of various stiffness variations occur at about 0.4 - 0.7 of the dam height (except for the linear case, where $\ell/m = 1$, in which the maximum occurs at the crest). The maximum shear stress occurs at about 0.7 - 0.8 of the dam height. Values of the participation factors $\overset{*}{P}_{1,1}$, $\Psi_1|_{max}$, $\Phi_1|_{max}$, $\Gamma_1|_{max}$ resulting from the modal configuration along the depth and the corresponding maximum strains and stresses (Eqs. 4.35,4.36,4.37, and 4.38) are given in Table 5.1; also shown in the tables are values of v_{s0} (and G_0) estimated from the 1971 earthquake records and the various analytical models of Chapters II and IV.

In general, it was found that the higher modes make a considerable contribution to the overall earthquake response of the dam (displacements, stresses, etc.); this is consistent with the earthquake amplification spectra of Fig. 3.3-c.

The average maximum shear strain (percent) for each hysteresis loop, of the 1971 earthquake, (Eq. 4.35) can be given by

$$\gamma_{1,1}|_{max} = 0.04078\ w(t)|_{max} \qquad (w_{max} \text{ in cm}) \tag{5.1}$$

and the associated average maximum shear stress (in psf) of Eq. 4.36 is given by

$$\tau_{1,1}|_{max} = 11.78\ (\ddot{w}(t) + \ddot{w}_g(t))_{max} \tag{5.2}$$

(accelerations are in cm/sec^2) .

The maximum (average) values of axial stresses and strains (from Eqs. 4.37 and 4.38) are:

$$\varepsilon_{1,1}|_{max} = 0.02773\ w(t)|_{max} \quad , (w_{max} \text{ in cm}) \tag{5.3}$$

and

$$\sigma_{1,1}|_{max} = 14.35\ (\ddot{w}(t) + \ddot{w}_g(t))_{max} \tag{5.4}$$

(accelerations are in cm/sec^2).

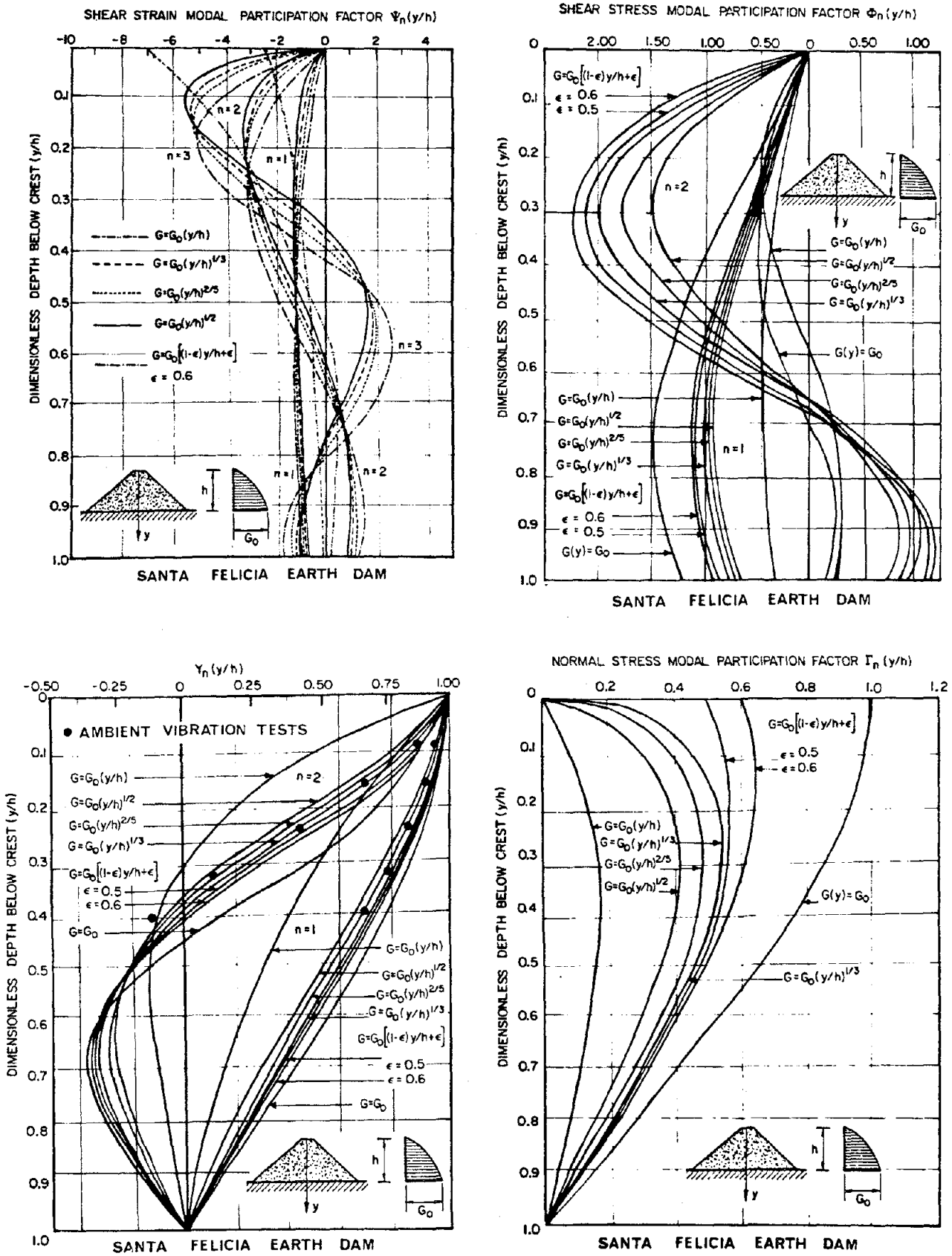

Fig. 5.2 Modal participation factors, of Santa Felicia Earth Dam, resulting from various stiffness variations.

TABLE 5.1

Key Parameters of the Stress and Strain Calculations
(Santa Felicia Dam)

PARAMETER \ CASE	$\frac{\ell}{m} = 0$	$\frac{\ell}{m} = 1$	$\frac{\ell}{m} = \frac{1}{2}$	$\frac{\ell}{m} = \frac{2}{5}$	$\frac{\ell}{m} = \frac{1}{3}$	$\varepsilon = 0.5$	$\varepsilon = 0.6$
$\overset{*}{P}_{1,1}$	1.818	2.575	1.959	1.891	1.802	1.749	1.705
$\Psi_1\|_{max}$	1.35	2.50	1.20	1.23	1.25	1.32	1.35
$\Phi_1\|_{max}$	1.35	0.45	0.85	0.95	1.00	1.15	1.20
$[\cdot]$of Eq. 4.35	0.01311	0.03466	0.01266	0.01252	0.01213	0.01243	0.01239
$[\cdot]$of Eq. 4.36	385.16	326.47	342.56	349.31	337.86	388.86	377.03
v_{s0} (ft/sec)	772.8	967.8	827.0	804.0	789.5	801.7	782.7
G_0 ($\times 10^6$ psf) ($=\rho v_{s0}^2$)	2.41	3.77	2.75	2.60	2.51	2.58	2.46
$\Gamma_{1,1}\|_{max}$	1.0	0.18	0.42	0.48	0.53	0.58	0.65
$[\cdot]$of Eq. 4.37	0.00797	0.01129	0.00859	0.00829	0.00790	0.00767	0.00747
$[\cdot]$of Eq. 4.38	774.9	309.1	400.2	417.4	424.0	462.9	482.2

In the above equations, $w(t)_{max}$ is the maximum relative displacement in each hysteresis loop, and $(\ddot{w}(t) + \ddot{w}_g(t))_{max}$ is the maximum absolute acceleration in each hysteresis loop. Figure 5.3 shows the filtered records (1971 earthquake) of both the absolute acceleration (crest record) and the relative displacement (the crest response with respect to the base). It is important to note that the first 3.0 - 3.5 secs of the base record were lost due to double exposure (1,4). The time dependence of the hysteretic behavior was determined for only the first 25 secs of the 1971 record and for only the first 6 secs of the 1976 record. Each trajectory was plotted every 0.02 sec, and each loop was plotted every second (about every cycle and a half). Samples of the hysteresis loops (of the first mode of longitudinal vibration) of Santa Felicia Dam are shown in Fig. 5.4. (Appendix A shows unfiltered records.)

It is readily apparent that the slope of the hysteresis loop and the area inside the loop are dependent on the magnitude of the response level for which the hysteresis loop is determined.

The estimated shear strain and stress for each hysteresis loop are shown (as circles) in Fig. 5.5; the data show an initial slope, G_{max}, at the origin ranging from 3.5 to 4.10 ($\times 10^6$ psf). The nonlinear stress-strain curves of the Masing type, i.e., the Ramberg-Osgood (R-O) curves (31,32) are adopted here to fit the data (shown as solid curves on Fig. 5.5). For shearing stresses increasing from zero these strain-softening curves are described by

$$\tau = \gamma G_{max} \Bigg/ \left[1 + \alpha \left| \frac{\tau}{C_1 \tau_{max}} \right|^{R-1} \right] \quad , \tag{5.5}$$

where α and R are parameters which adjust the position and shape of the curves, and C_1 is a factor which relates the "yield" value τ_y in the original R-O expression to τ_{max} (i.e., $\tau_y = C_1 \tau_{max}$). For practical and

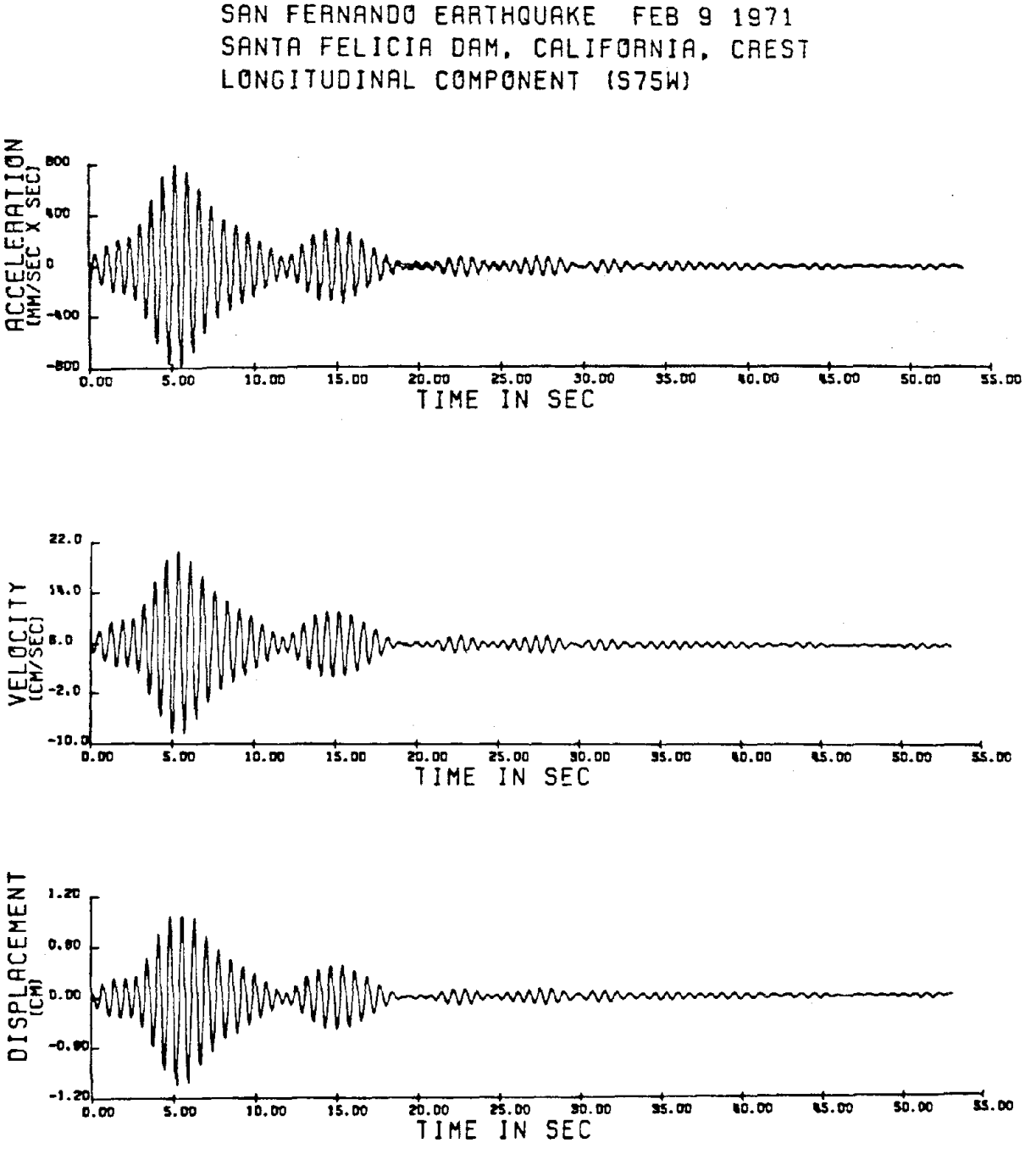

Fig. 5.3-a The filtered records (1971 earthquake) of the crest of Santa Felicia Dam.

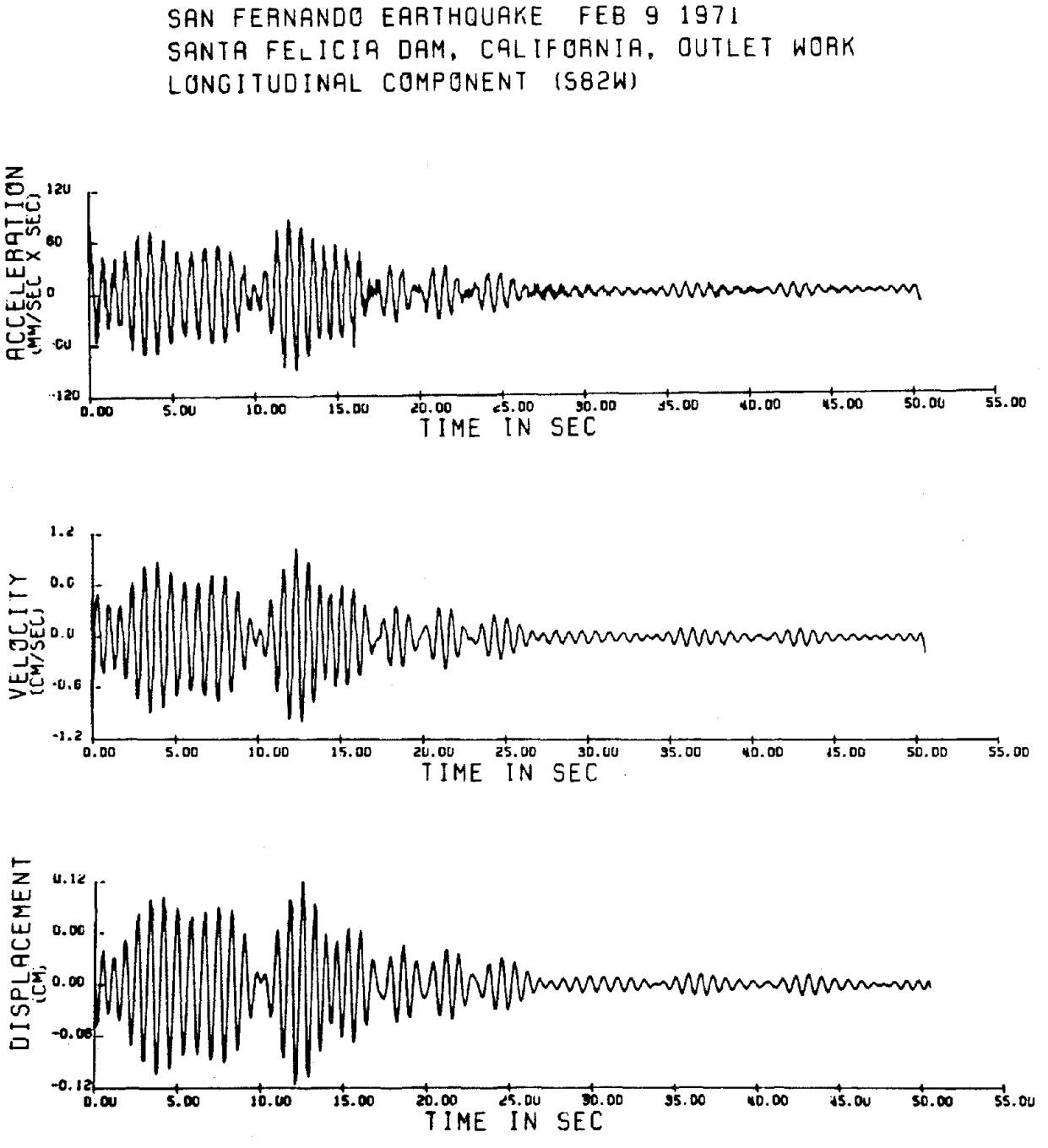

Fig. 5.3-b The filtered records (1971 earthquake) of the abutment of Santa Felicia Dam.

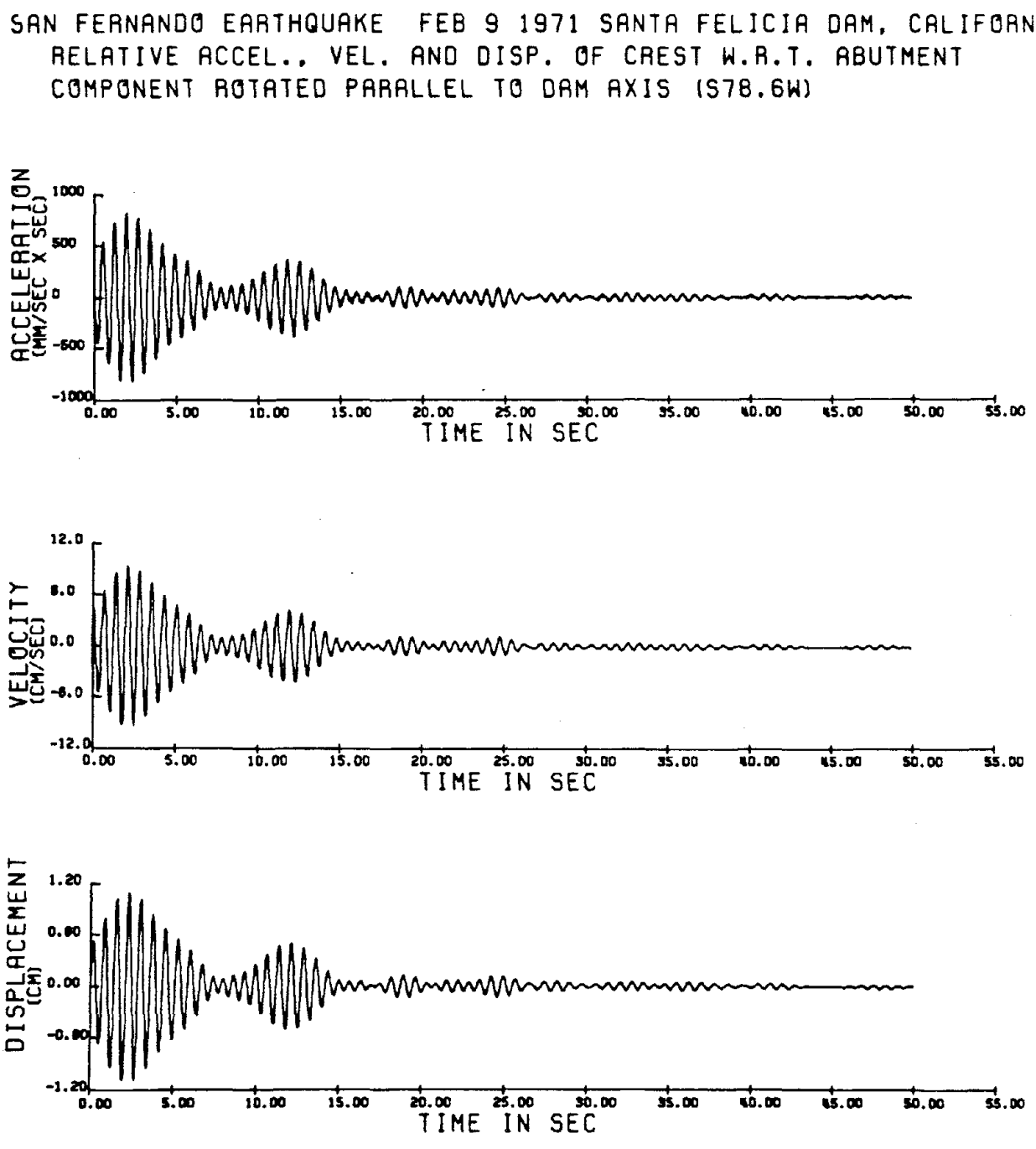

Fig. 5.3-c The filtered records (1971 earthquake) of the relative motion (the crest response with respect to the base) of Santa Felicia Dam.

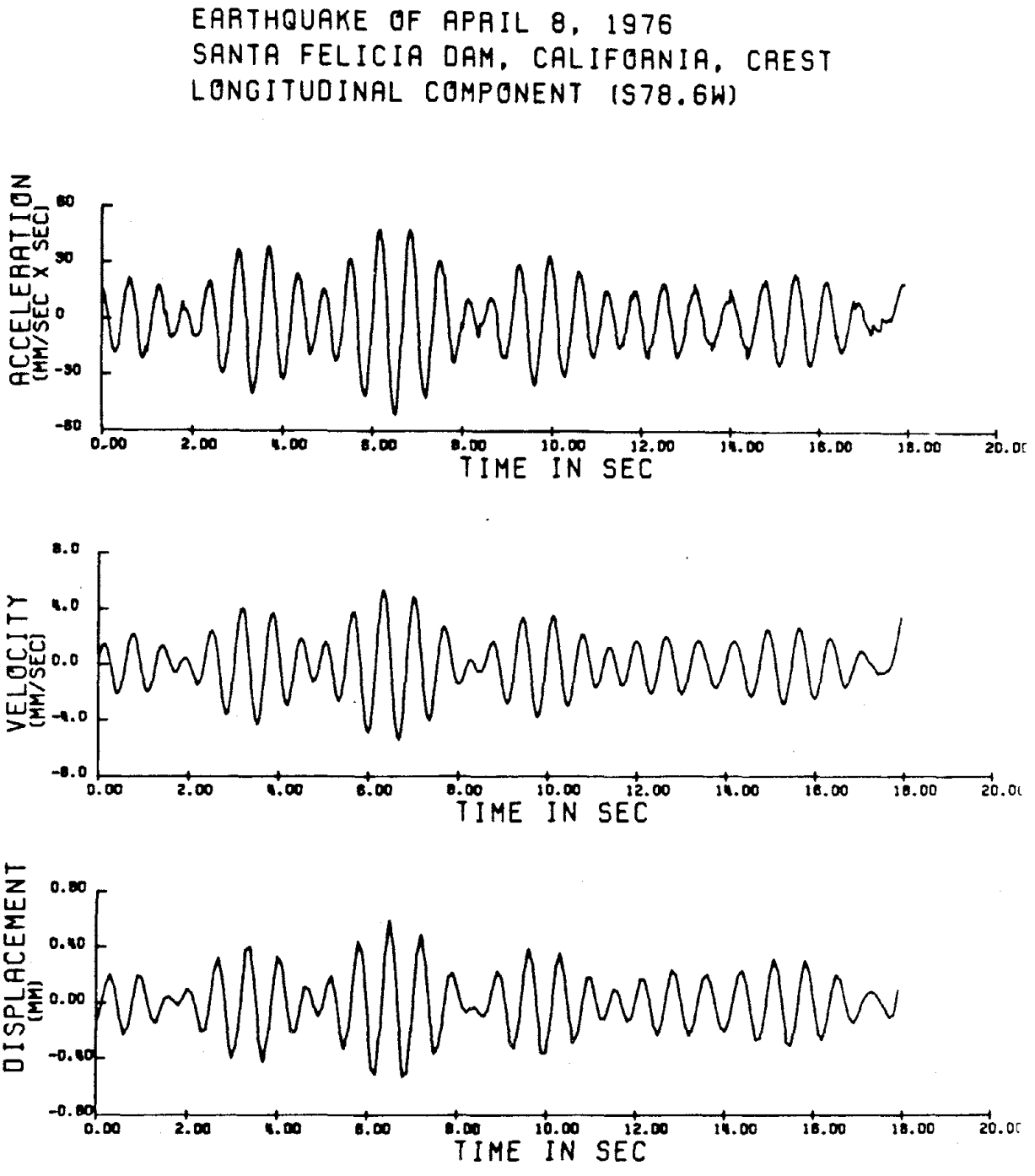

Fig. 5.3-d The filtered records (1976 earthquake) of the crest of Santa Felicia Dam.

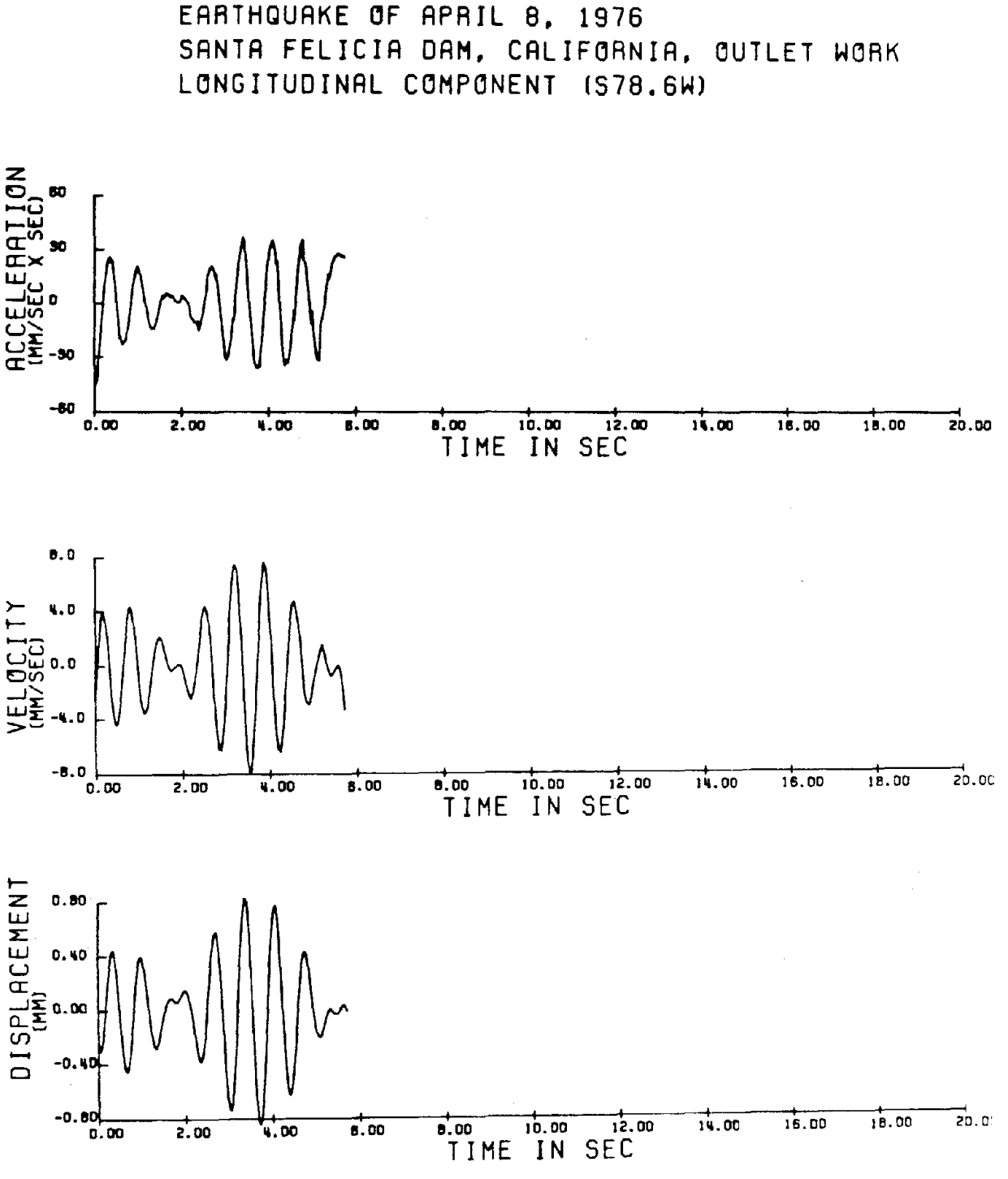

Fig. 5.3-e The filtered records (1976 earthquake) of the abutment of Santa Felicia Dam.

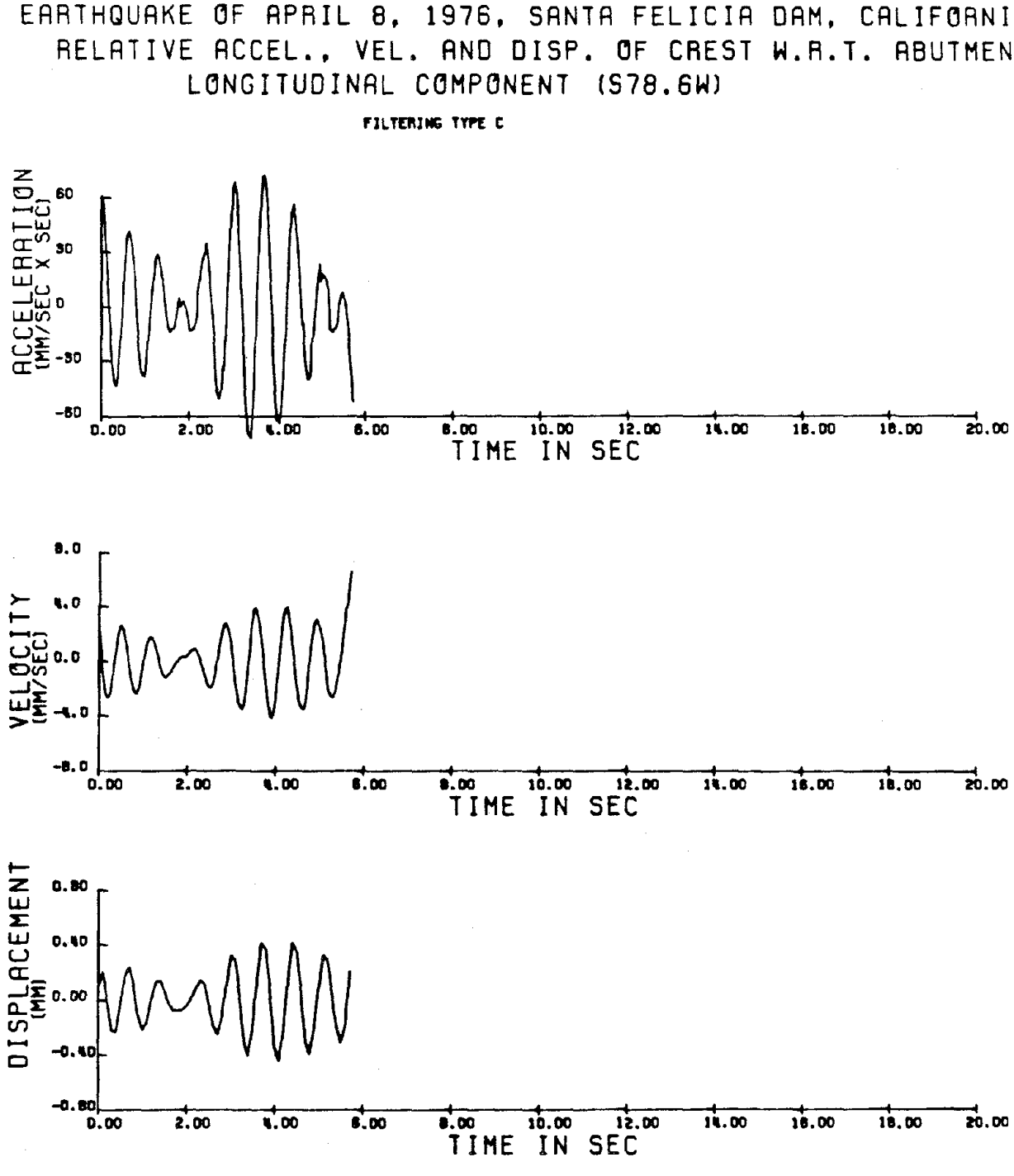

Fig. 5.3-f The filtered records (1976 earthquake) of the relative motion (the crest response with respect to the base) of Santa Felicia Dam.

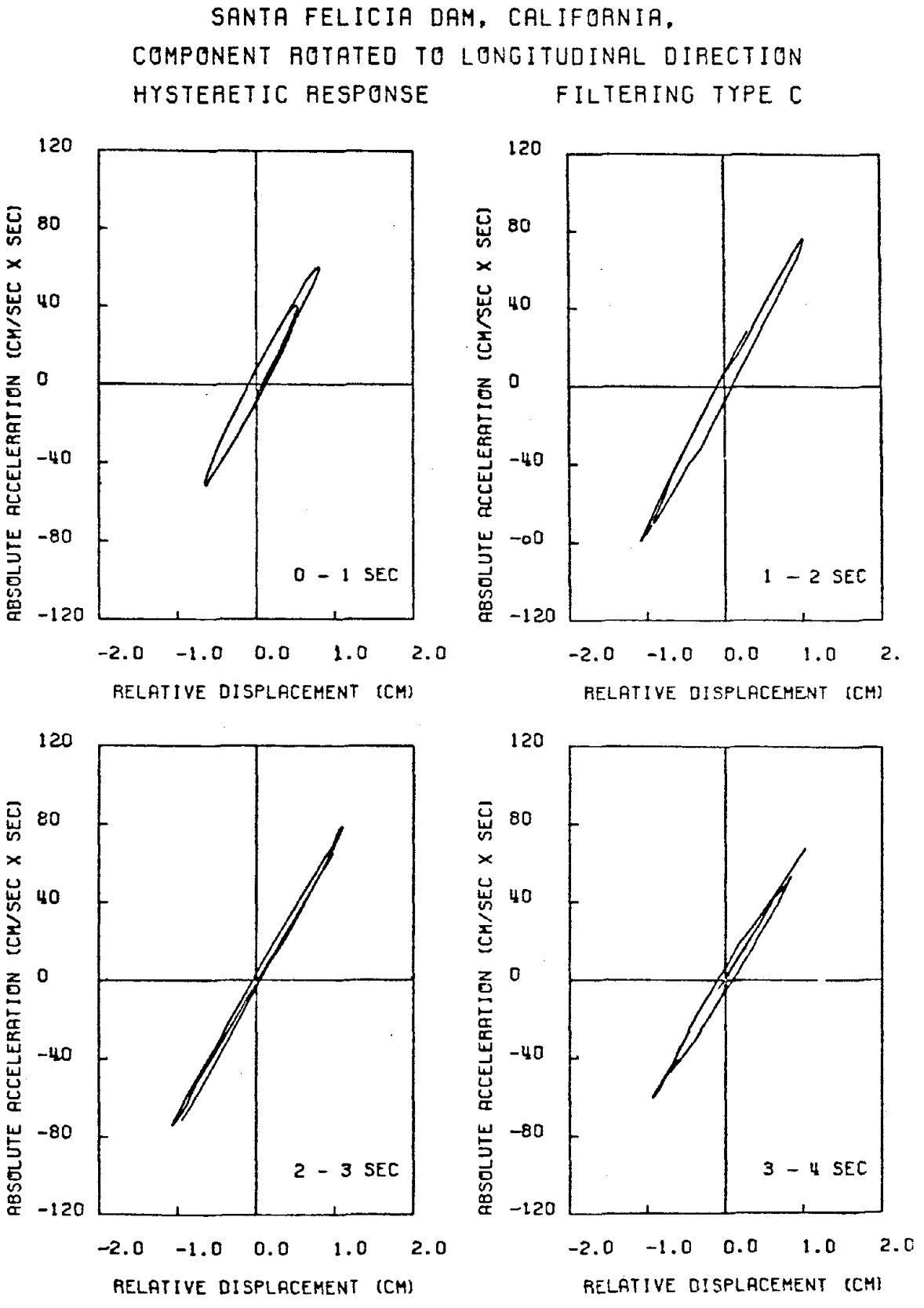

Fig. 5.4-a The hysteresis loops (of the first mode of longitudinal vibration) of Santa Felicia Dam (1971 earthquake).

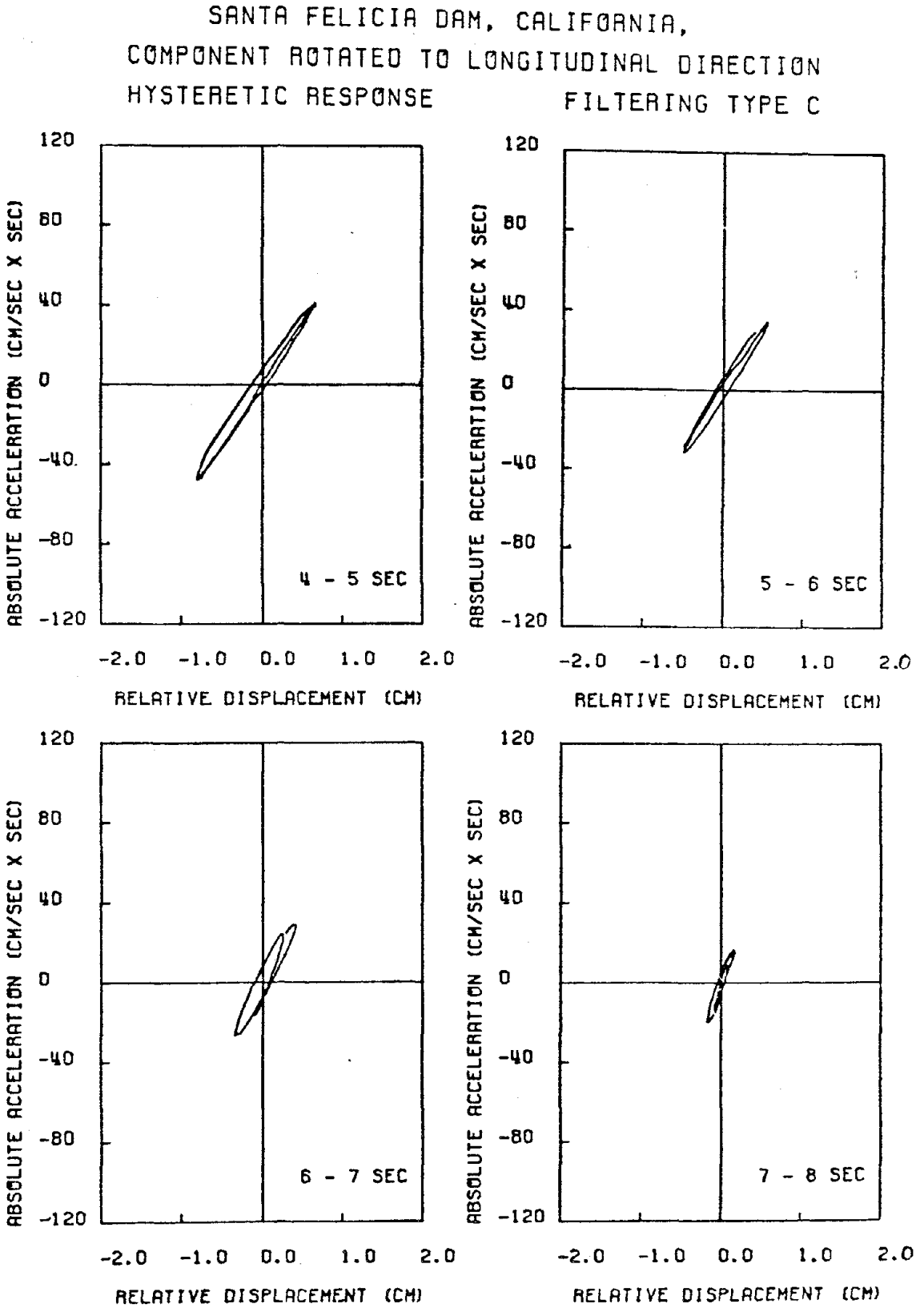

Fig. 5.4-a (continued)

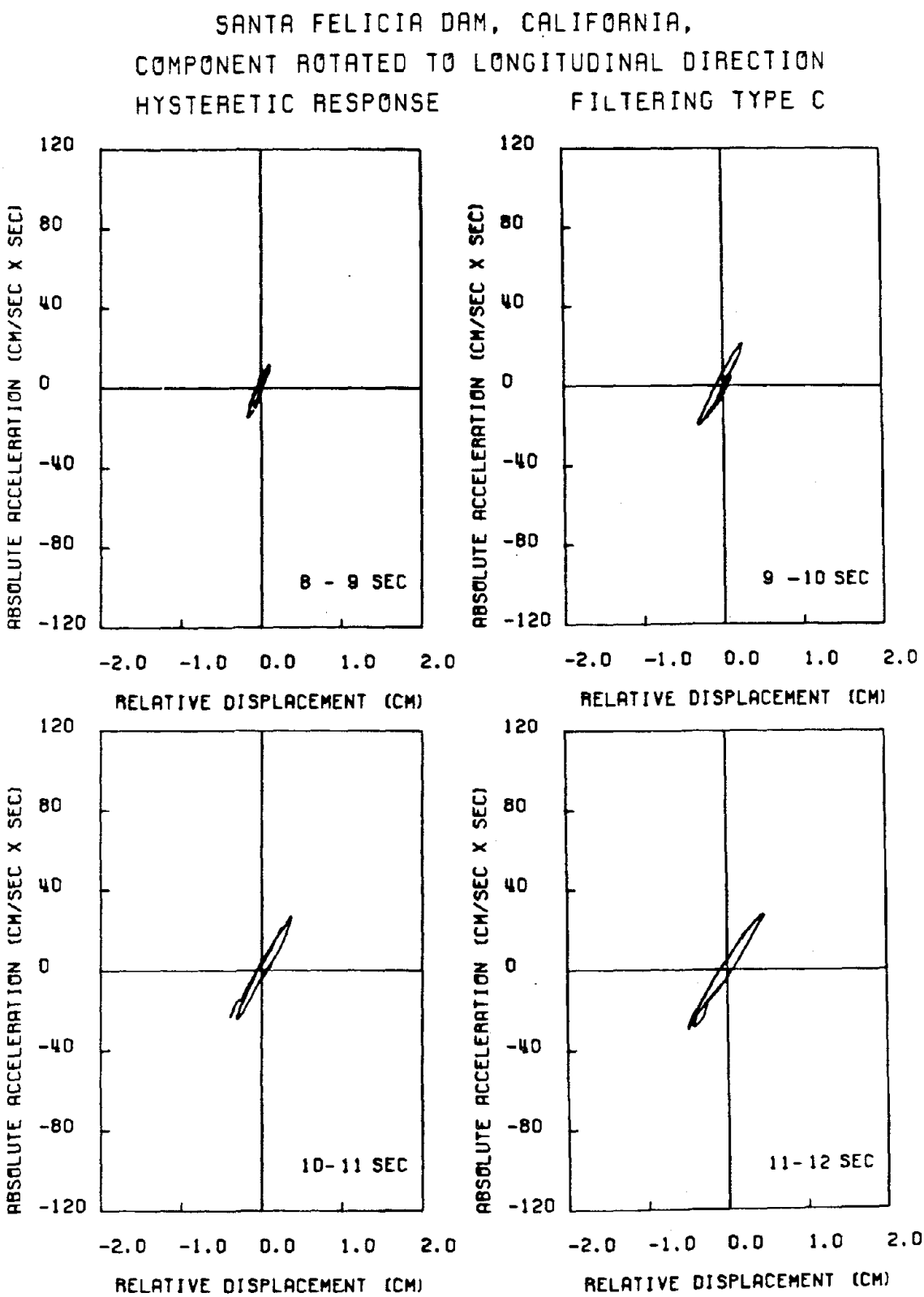

Fig. 5.4-a (continued)

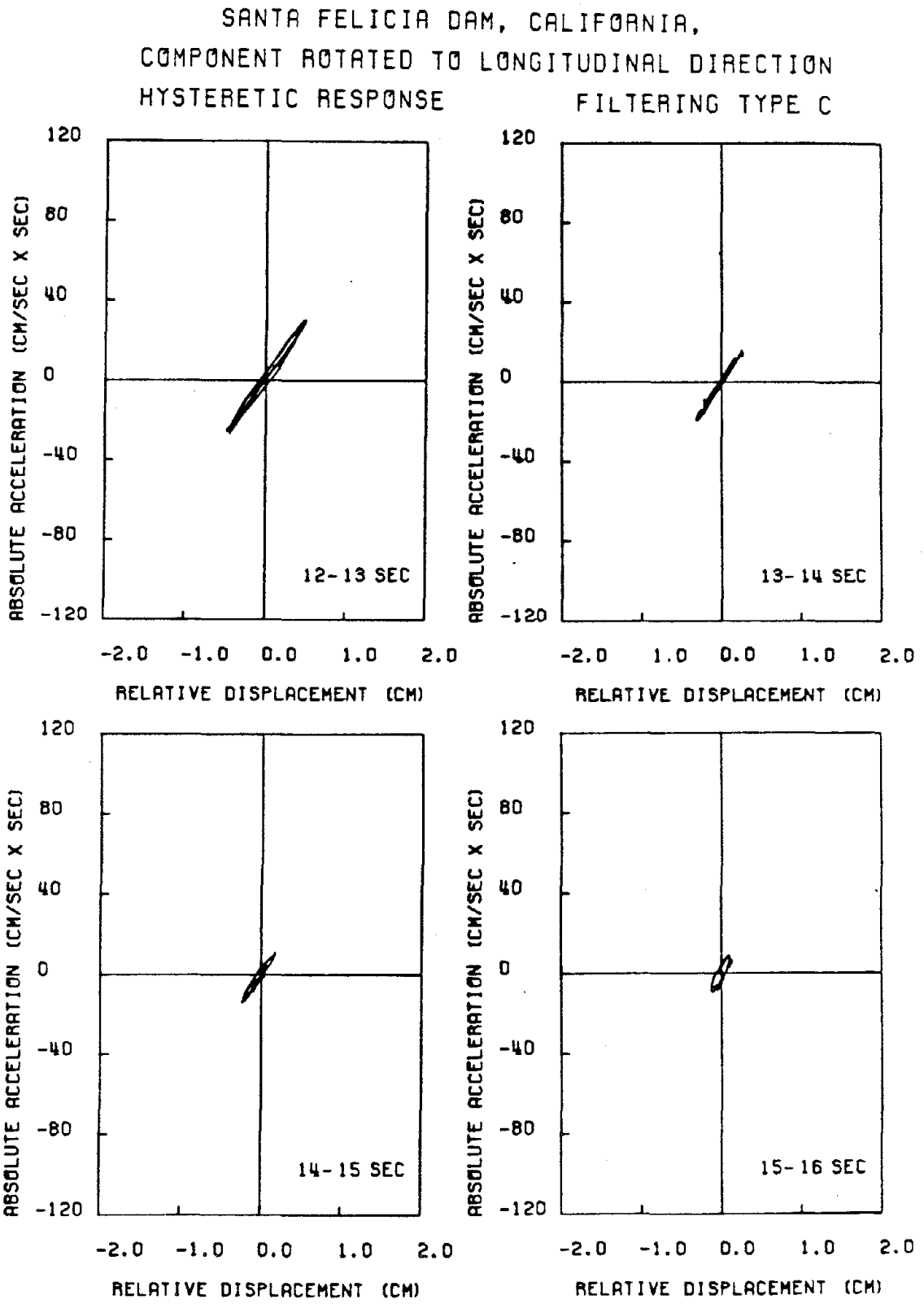

Fig. 5.4-a (continued)

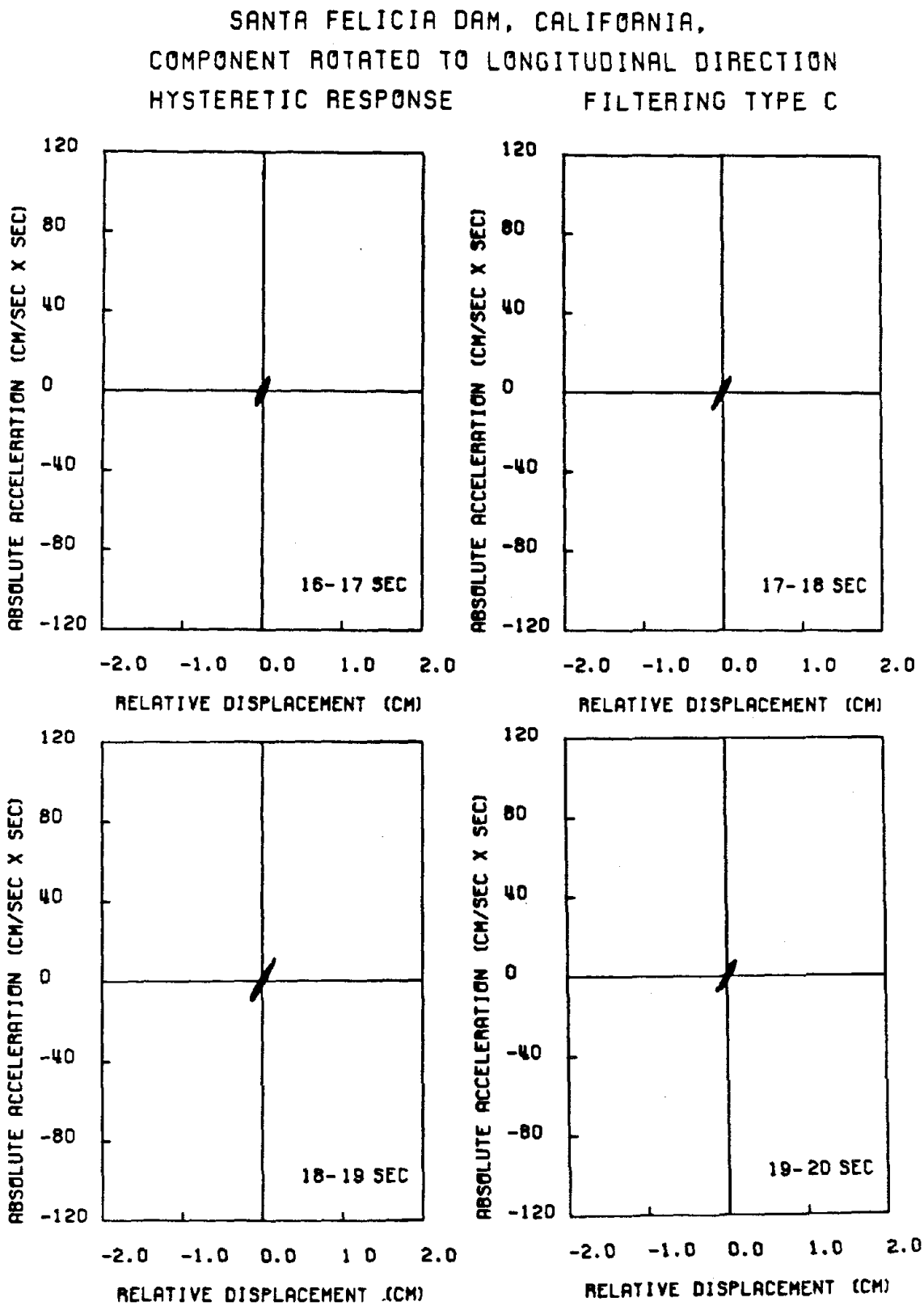

Fig. 5.4-a (continued)

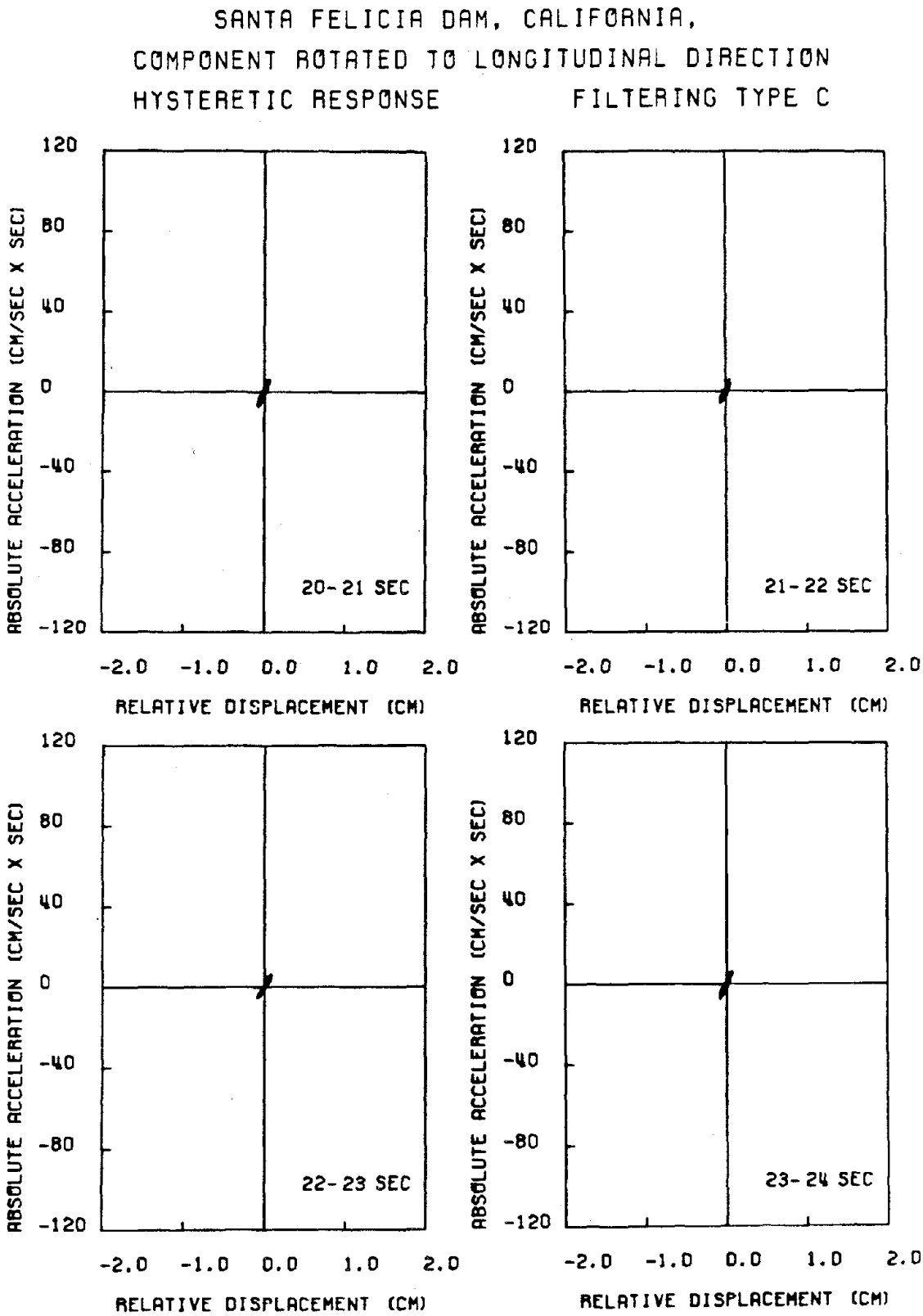

Fig. 5.4-a (continued)

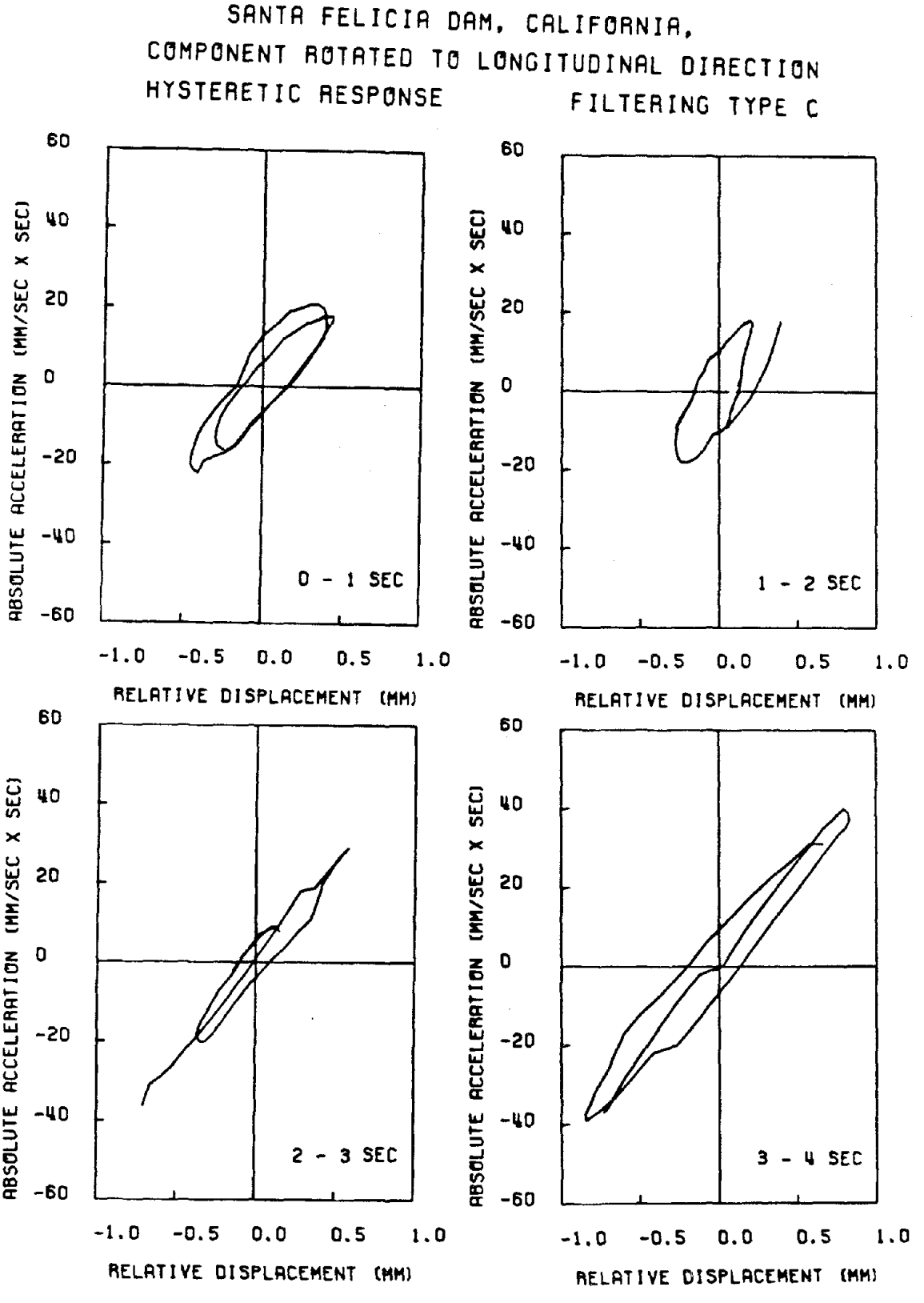

Fig. 5.4-b The hysteresis loops (of the first mode of longitudinal vibration) of Santa Felicia Dam (1976 earthquake).

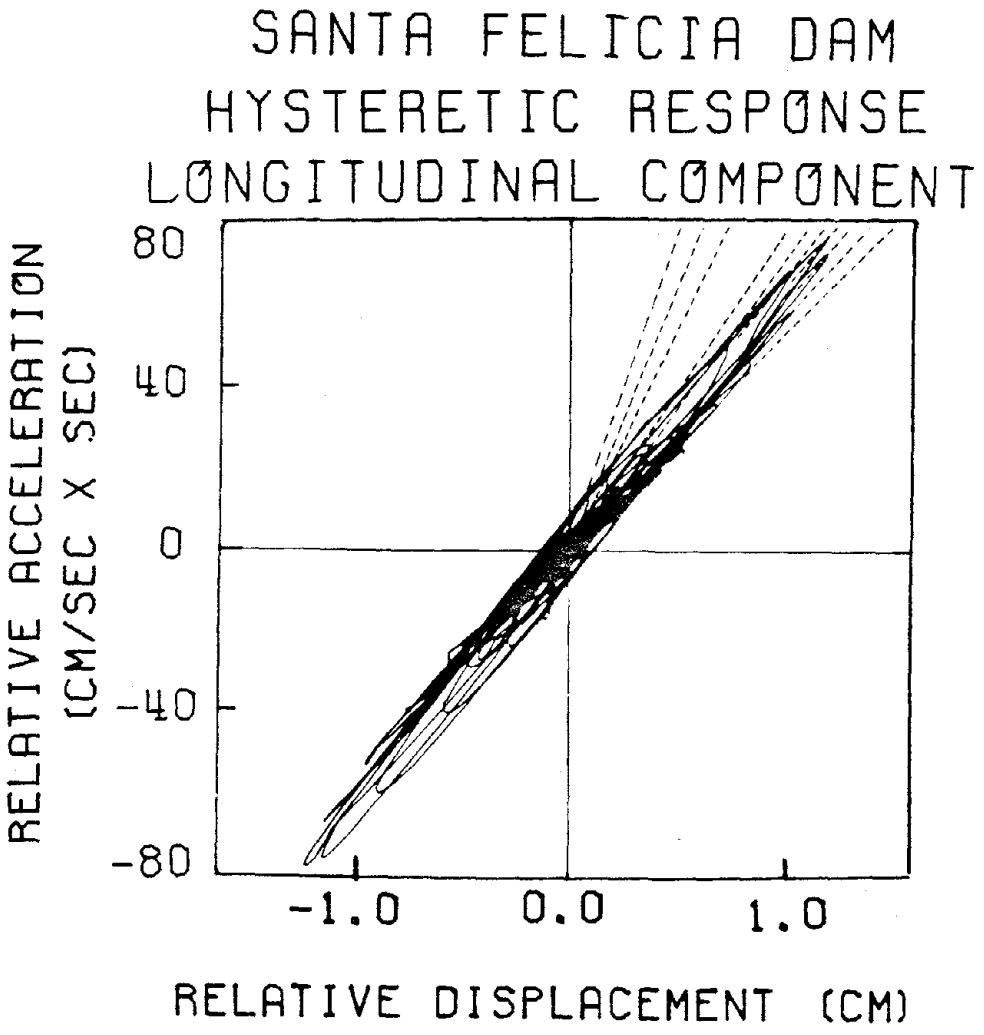

Fig. 5.4-c The accumulative hysteretic response (of the first mode of longitudinal vibration) of Santa Felicia Dam (1971 earthquake).

analytical purposes, the R-O curves with R = 1.8 - 2.0, α = 1.7 - 1.75, and $C_1\tau_{max}$ = 800 to 1,200 psf (with C_1 = 0.8) can be chosen, from Fig. 5.5 and from the normalized curves of Fig. 5.6, to represent the relations for earth dam materials.

Taking G_{max} and τ_{max} from curves 1, 2, and 3 of Fig. 5.5, continuous hyperbolic shearing stress-shearing strain curves (dotted curves) are determined (and are also shown in Fig. 5.5); the curves are given by

$$\tau = \gamma \Big/ \left[\frac{1}{G_{max}} + \frac{\gamma}{\tau_{max}}\right] \quad . \tag{5.6}$$

The hyperbolic fit deviates considerably after the low-strain range, indicating the R-O curves are a better match for the overall behavior.

V-2.2. Shear Moduli and Damping Factors for Santa Felicia Earth Dam

The secant shear modulus, G, for each hysteresis loop, can be obtained by dividing Eq. 4.36 by Eq. 4.35. The relationship between the estimated shear modulus and the dynamic shear strain is shown by the semilog plots of Fig. 5.7 for the first 25 secs of the 1971 earthquake and the first 6 secs of the 1976 earthquake. (Note that the number at each point corresponds to the time in seconds at which the point was computed.) Again, it is apparent that the modulus depends on the magnitude of the strain in the hysteresis loop.

The relationship between the estimated equivalent viscous damping factor determined from the area of each hysteresis loop and the corresponding shear-strain amplitude are shown in Fig. 5.8. While there is a considerable scatter in the data, most of the results fall within the dashed curves in Figs. 5.7 and 5.8. The solid curve in each figure represents an estimate of the mean behavior.

At higher strains, additional data on modulus values are needed; however, approximate values for use in some types of response analyses are arrived at by using the estimated values of the modulus at a very low strain level from

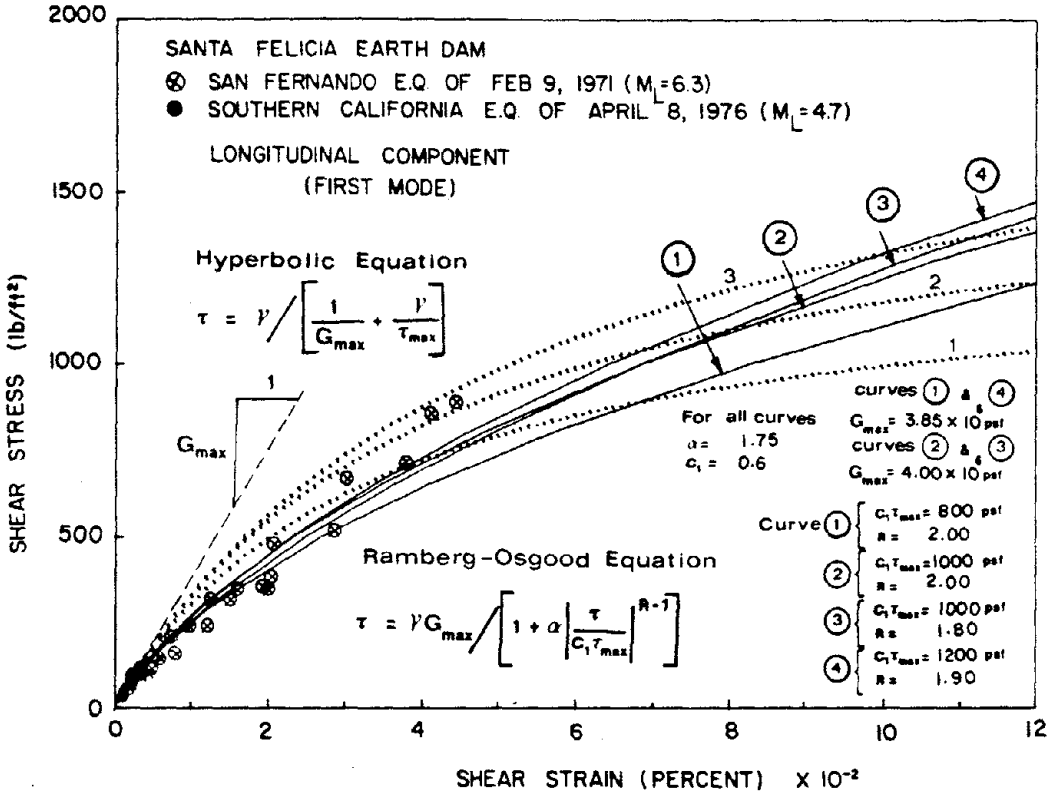

Fig. 5.5 Estimated shear strain and stress for each hysteresis loop and fit of Ramberg-Osgood and hyperbolic curves to earthquake data.

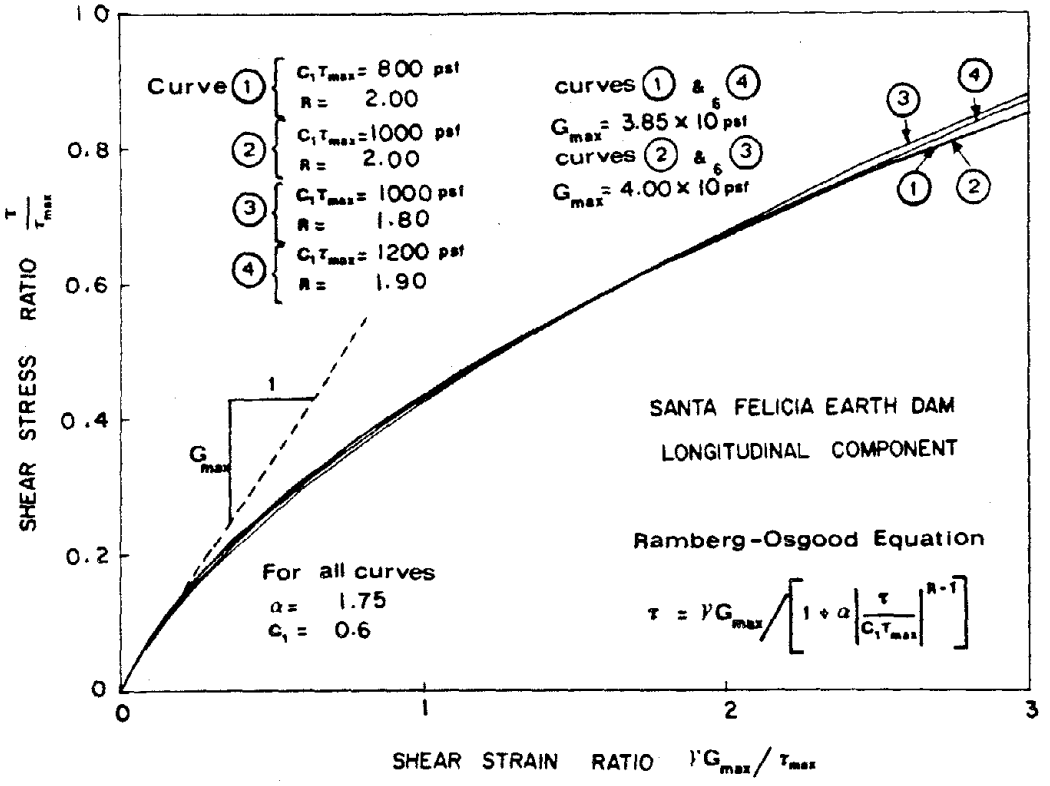

Fig. 5.6 Normalized shear strain-shear stress curves (Ramberg-Osgood Models).

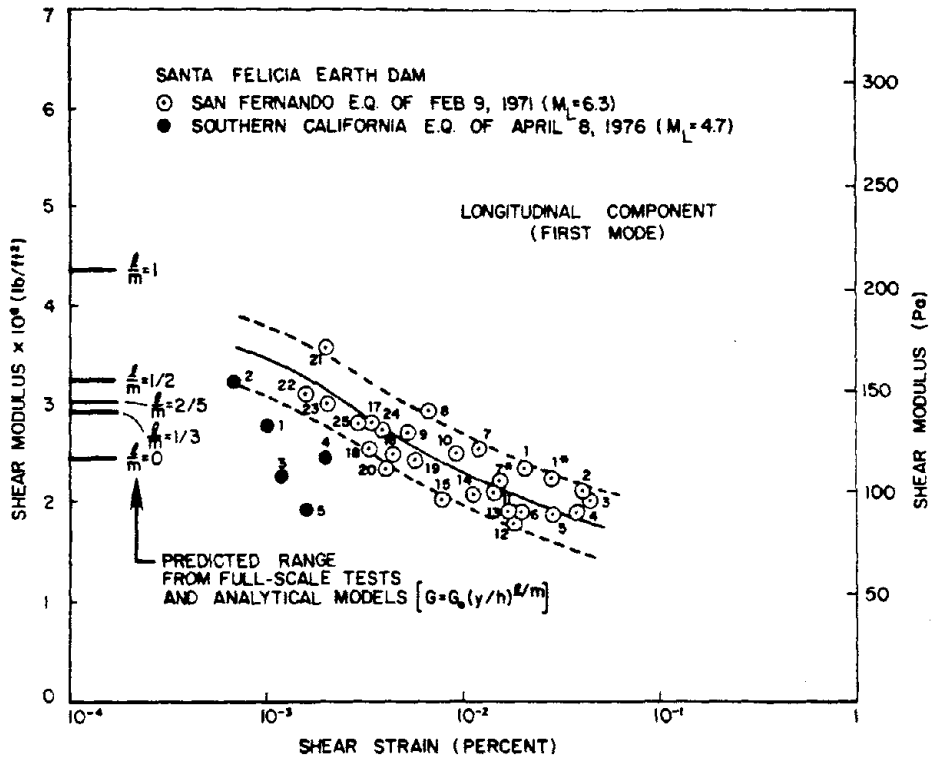

Fig. 5.7 Estimated shear moduli and corresponding dynamic shear strains (evaluated from hysteretic response of two earthquakes).

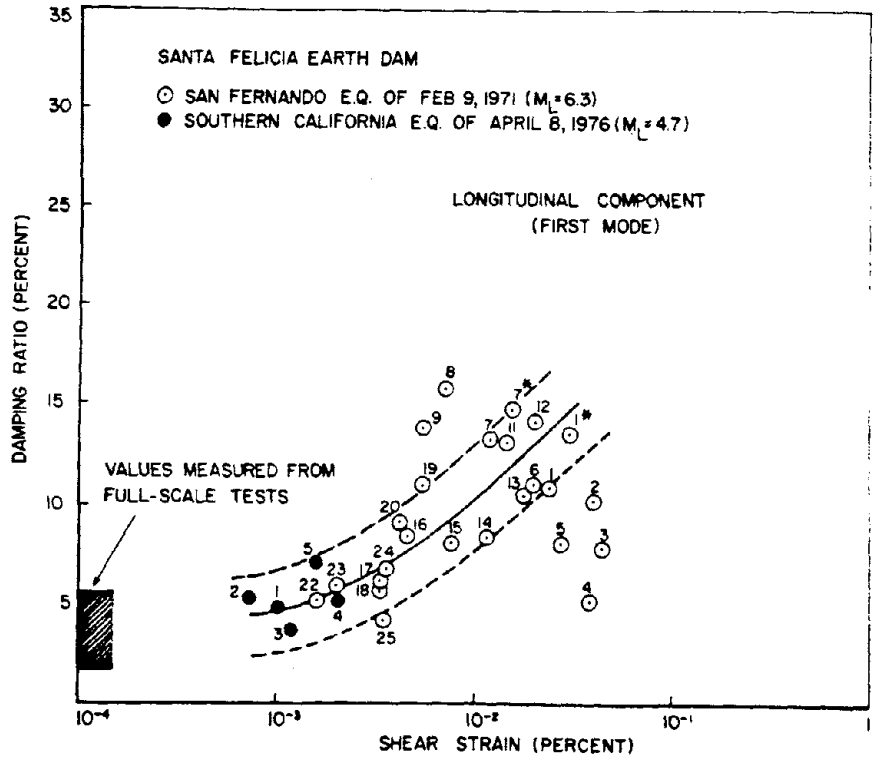

Fig. 5.8 Estimated damping factors and corresponding dynamic shear strains (evaluated from hysteretic response of two earthquakes).

the forced and ambient vibration tests (3) as well as from the in-situ geophysical tests (1,4), with the aid of the analytical models, as indicated in Figs. 5.7 and 5.8. Both figures indicate that the dynamic properties of the dam's constituent material estimated from low-strain full-scale tests are consistent with those determined from the relatively larger strains induced by the two earthquakes (if one extrapolates the data of Figs. 5.7 and 5.8 to the low-strain range). Furthermore, the low-strain analytical models in which the elastic moduli of the dam material vary along the depth are the most appropriate representations for predicting the dynamic properties, as indicated by Fig. 5.7 (where an average value of the cases where $\frac{\ell}{m} = \frac{1}{3}, \frac{2}{5}, \frac{1}{2}, 1$ would be a reasonable extension of the earthquake data, which also were based on an average value of various models (as shown by Table 5.1)).

From the R-O curve (Eq. 5.5) the decrease in secant modulus, $G(= \tau/\gamma)$, with an increase in shearing stress ratio, τ/τ_{max}, is

$$G = G_{max} \left[1 + \alpha \left| \tau/C_1\tau_{max} \right|^{R-1}\right] \quad . \tag{5.7}$$

Figure 5.9 shows the decrease of secant modulus, G, with strain, γ, for the same special values of G_{max}, α, $C_1\tau_{max}$, and R of curves 1, 2, 3, and 4 of Fig. 5.5; shown also on Fig. 5.9 are the data of Fig. 5.7. The R-O curves match both the estimated earthquake results and the results of low-strain full-scale tests very well indicating both the reliability of the developed longitudinal analytical models in predicting earthquake induced stresses and strains (in the first mode) and the applicability of the R-O curves to represent the stiffness relations for earth dams. The normalized curves of the shear modulus (with respect to G_{max}) versus shear strain are shown in Fig. 5.10.

Finally, the damping factors are evaluated, by integration, from the

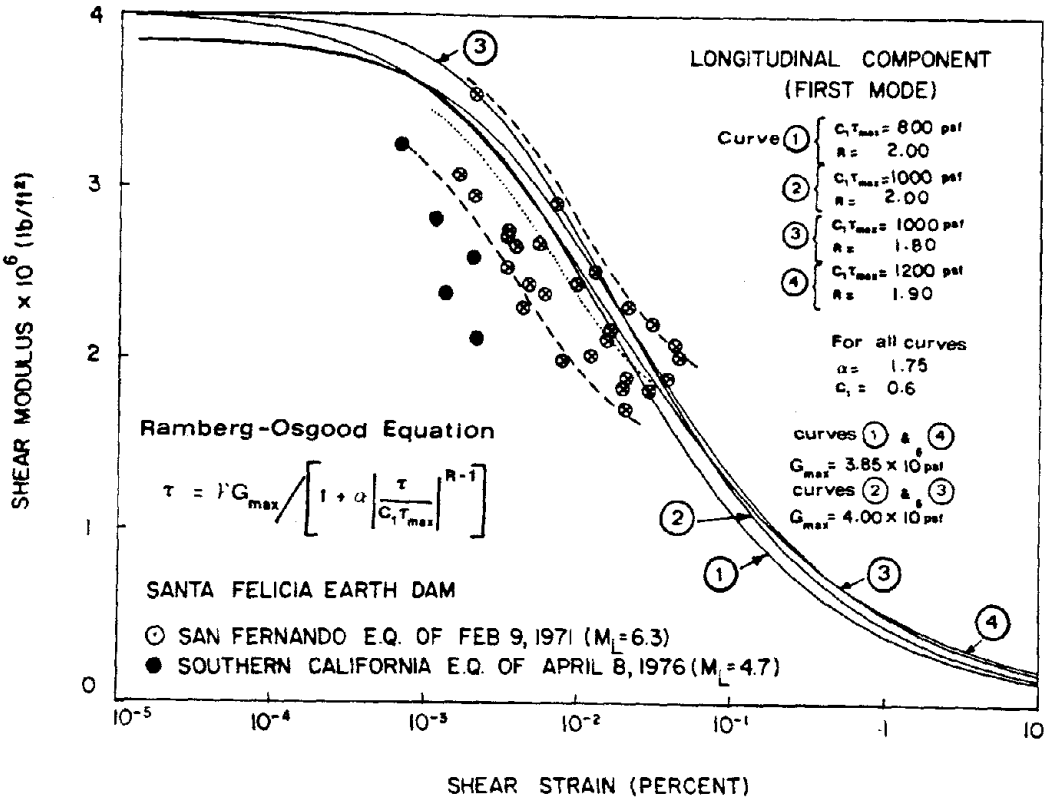

Fig. 5.9 Fit of Ramberg-Osgood curves to estimated values of strain-dependent shear moduli.

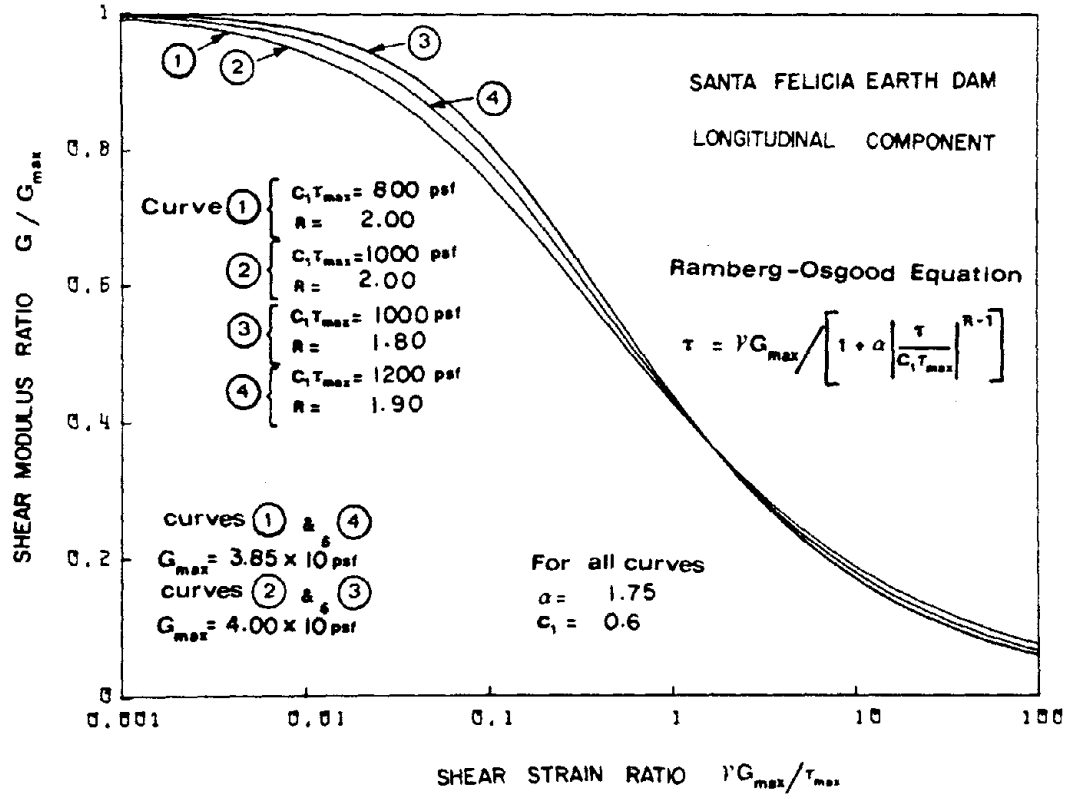

Fig. 5.10 Normalized shear strain-shear modulus (Ramberg-Osgood Models).

R-0 curves (where the area of the hysteresis loop formed is a measure of the hysteretic damping occurring in the dam materials) for the same special conditions of curves 1, 2, 3, and 4 of Fig. 5.5. The results are shown on Fig. 5.11 which displays the earthquake data (of Fig. 5.8) as well. The R-0 curves, which represent the best fit of the three sets of data of Figs. 5.5, 5.7, and 5.8 represent a lower bound of the earthquake damping data. The normalized version of Fig. 5.11 is shown in Fig. 5.12.

V-2.3. Axial Strains and Stresses of Santa Felicia Dam

Unfortunately, there were no accelerographs on the dam crest near its ends (where the maximum axial strains and stresses occur); only two siesmoscopes were located on the east and west abutments (not on the crest) of the dam. The existence of such accelerographs would be very helpful in assessing the amplitude dependence of axial strains and stresses and also in explaining, more accurately, the transverse crack caused by the 1971 earthquake. However, the standard response spectra technique is utilized to quantify the order of magnitude of these axial stresses and strains. Table 5.2 shows the values of these strains and stresses resulting from the spectral peaks of the recorded ground motions (at the base of the dam) during the two earthquakes, assuming uniform input ground motions.

It is necessary to very carefully compare the stresses given in Table 5.2 with the tensile strength of the dam material in order to assess or predict a crack in a dam. As mentioned previously, the occurrence of cracks is in consequence not only of the transient state of stress of the dam during an earthquake, but also of the state of stress before an earthquake. It is also necessary to further investigate the mechanism of cracking in earth fill material under the action of irregular loads.

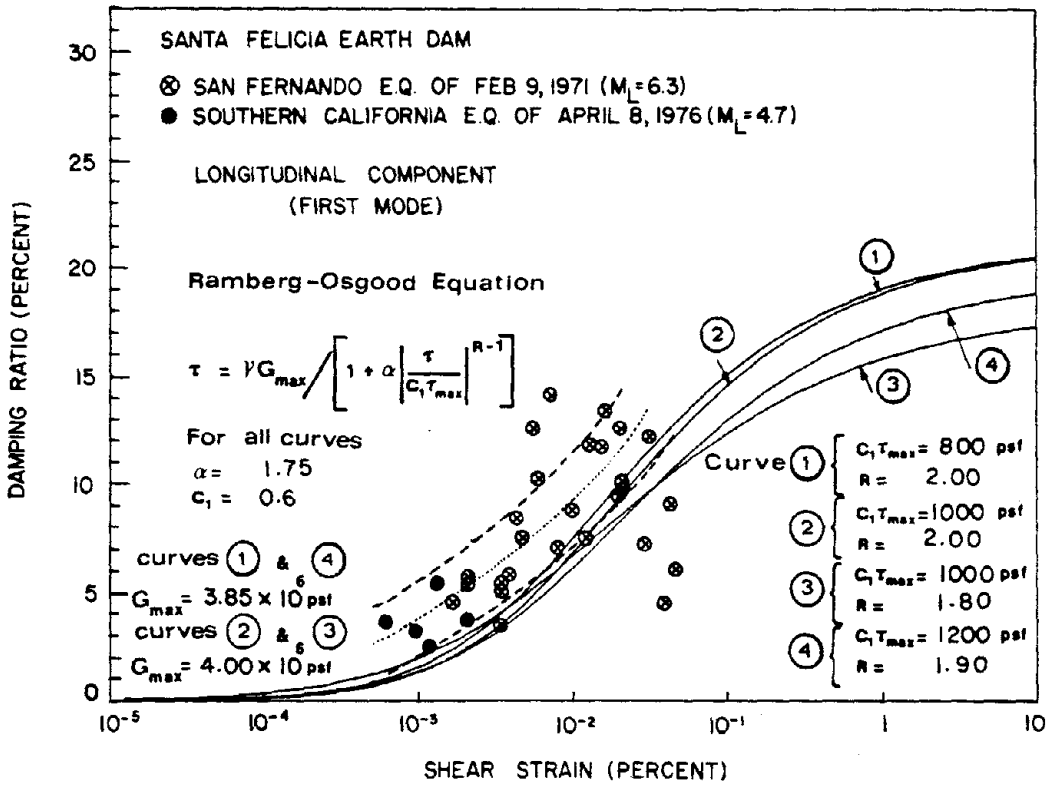

Fig. 5.11 Fit of Ramberg-Osgood curves to estimated values of strain-dependent damping factors.

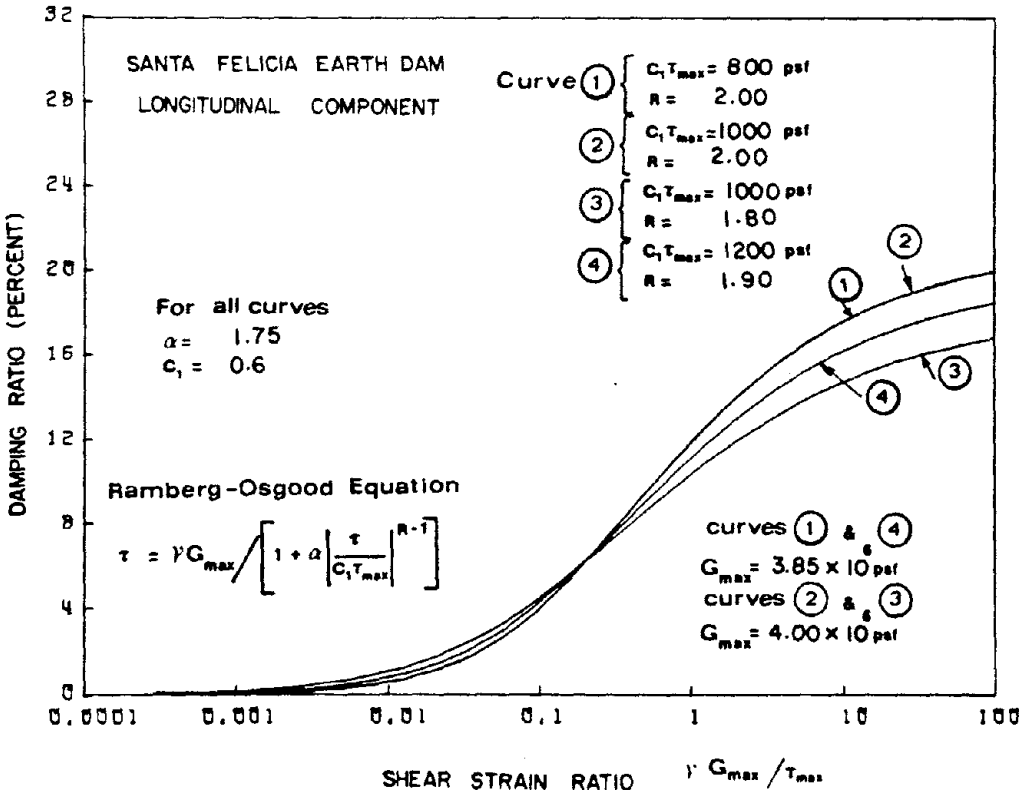

Fig. 5.12 Normalized shear strain-damping ratio (Ramberg-Osgood Models).

Table 5.2

Estimated Axial Strains and Stresses in Santa Felicia Dam
Using Response Spectra Technique

PARAMETER	ASSUMED DAMPING RATIO (PERCENT)		
	2%	5%	10%
1. 1971 San Fernando Earthquake, $T_{1,1}$ = 0.74 sec			
S_d	1.65 cm	1.27 cm	1.02 cm
S_a	98.0 cm/sec^2	78.4 cm/sec^2	63.7 cm/sec^2
$\epsilon_{1,1}\|_{max}$	0.0458 (percent)	0.0352 (percent)	0.0282 (percent)
$\sigma_{1,1}\|_{max}$	1,504.7 psf	1,203.8 psf	978.1 psf
2. 1976 Earthquake $T_{1,1}$ = 0.79 sec			
S_d	0.71 cm	0.41 cm	0.33 cm
S_a	39.2 cm/sec^2	27.4 cm/sec^2	19.6 cm/sec^2
$\epsilon_{1,1}\|_{max}$	0.0197 (percent)	0.0114 (percent)	0.0092 (percent)
$\sigma_{1,1}\|_{max}$	601.9 psf	420.7 psf	301.0 psf

CONCLUSIONS

The analytical models developed here and the data presented will provide information of practical as well as academic significance about the dynamic characteristics of earth dams vibrating in a direction parallel to their longitudinal axis. Real earthquake observations of earth dams and experimental results have confirmed that the models which take into account the effect of variation with depth of both the shear modulus and the modulus of elasticity of the dam material provide the most appropriate representation for predicting the dynamic characteristics in the longitudinal direction. These models are shown to be accurate enough so that they can be used for estimating earthquake induced longitudinal strains and stresses (both shear and normal or axial) on earth dams.

In addition, the formula and curves presented here will enable the determination, for many practical purposes, of the dynamic strains and stresses (both shear and normal) induced in a wide class of earth dams by the longitudinal component of earthquake ground motions. Reasonable estimates of the dynamic stress-strain curves (nonlinear strain-softening type) and the strain-dependent elastic moduli and damping for earth dam materials can be obtained by using the proposed dynamic analysis procedure, earthquake records (on and in the vicinity of dams), and the adoption of the Ramberg-Osgood-type curves. These estimates would be useful for any study of the dam's earthquake-response characteristics; in addition, the variation of material properties with depth should be taken into account for any realistic dynamics study. Figures 5.5 to 5.12 should provide a good guide to the material properties in the dynamic analysis of any earth dam composed predominantly of rolled-fill, essentially cohesionless material, with or without a relatively thin core. Despite the value of this study, however, further research to accurately assess and mitigate potentially adverse effects of seismic shaking on earth dams is needed.

REFERENCES

1. Abdel-Ghaffar, A. M., and Scott, R. F., "An Investigation of the Dynamic Characteristics of an Earth Dam," EERL-78-02, Earthquake Engineering Research Laboratory, California Institute of Technology, Pasadena, CA, August 1978.

2. Abdel-Ghaffar, Ahmed M., "Engineering Data and Analyses of the Whittier, California Earthquake of January 1, 1976," EERL-77-05, Earthquake Engineering Research Laboratory, California Institute of Technology, Pasadena, CA, November 1977.

3. Abdel-Ghaffar, A. M., Scott, R. F. and Craig, M. M., "Full-Scale Experimental Investigation of a Modern Earth Dam," EERL-80-01, Earthquake Engineering Research Laboratory, California Institute of Technology, Pasadena, CA, February 1980.

4. Abdel-Ghaffar, Ahmed M., and Scott, Ronald F., "Analysis of Earth Dam Response to Earthquakes," Journal of the Geotechnical Engineering Division, ASCE, Vol. 105, No. GT12, Proc. Paper 15033, December 1979, pp. 1379-1404.

5. Abdel-Ghaffar, Ahmed M. and Koh, Aik-Siong, "Longitudinal Vibration of Nonhomogeneous Earth Dams," to appear in the International Journal of Earthquake Engineering and Structural Dynamics, 1981.

6. Abdel-Ghaffar, Ahmed M., and Scott, Ronald F., "Shear Moduli and Damping Factors of Earth Dams," Journal of the Geotechnical Engineering Division, ASCE, Vol. 105, No. GT12, Proc. Paper 15034, December 1979, pp. 1405-1426.

7. Abdel-Ghaffar, Ahmed M., and Scott, Ronald F., "Vibration Tests of a Full-Scale Earth Dam," Journal of the Geotechnical Engineering Division, ASCE, Vol. 107, No. GT3, March 1981.

8. Abdel-Ghaffar, Ahmed M., and Scott, Ronald F., "Comparative Study of Dynamic Response of an Earth Dam," Journal of the Geotechnical Engineering Division, ASCE, Vol. 107, No. GT3, March 1981.

9. Ambraseys, N. N., "On the Shear Response of a Two-Dimensional Wedge Subjected to an Arbitrary Disturbance," Bulletin of the Seismological Society of America, Vol. 50, No. 1, January 1960, pp. 45-56.

10. Ambraseys, N. N., "On the Seismic Behavior of Earth Dams," Proceedings of the Second World Conference on Earthquake Engineering, Japan, 1960, Vol. I, pp. 331-354.

11. Chopra, A. K., "Earthquake Response of Earth Dams," Journal of Soil Mechanics and Foundations Division, ASCE, Vol. 93, No. SM2, 1967.

12. Chopra, A. K., Dibaj, M., Clough, R. W., Penzin, J., and Seed, H. B., "Earthquake Analysis of Earth Dams," Proceedings, Fourth World Conference on Earthquake Engineering, Santiago, Chile, January 1969.

13. Clough, R. W. and Chopra, A. K., "Earthquake Stress Analysis in Earth Dams," Journal of Engineering Mechanics Division, ASCE, Vol. 92, No. EM2, April 1966, pp. 198-211.

14. Clough, R. W. and Woodward, R. J., "Analysis of Embankment Stresses and Deformations," Journal of Soil Mechanics and Foundations Division, ASCE, Vol. 93, SM4, pp. 529-549, 1967.

15. Duke, C. M., "Foundation and Earth Structures in Earthquakes," Proceedings of the Second World Conference on Earthquake Engineering, Japan, 1960, Vol. 1, pp. 435-456.

16. Gazetas, G., and Abdel-Ghaffar, A. M., "Earth Dam Characteristics from Full-Scale Vibrations," Proceedings of the X International Conference on Soil Mechanics and Foundation Engineering, Stockholm, Sweden, June 15-19, 1981.

17. Gazetas, G., "3-Dimensional Lateral and Longitudinal Seismic Stability of Earth and Rockfull Dams," Proceedings of the Seventh World Conference on Earthquake Engineering, Istanbul, Turkey, September 1980.

18. Hatanaka, M., "Fundamental Consideration on the Earthquake Resistant Properties of the Earth Dam," Bulletin No. 11 Disaster Prevention Research Institute, Kyoto University, Japan, 1955.

19. Hatano, T. and Watanabe, H., "Seismic Analysis of Earth Dams," Proc. 4th World conference on Earthquake Engineering, Santiago, Chile, 1969.

20. Ishizaki, H. and Hatakeyama, N., "Consideration on the Dynamical Behaviors of Earth Dams," Disaster Prevention Res. Inst., Kyoto University, Bulletin No. 52, 1962.

21. Keightley, W. O., "Vibrational Characteristics of an Earth Dam," Bulletin of the Seismological Society of America, Vol. 56, No. 6, December 1966, pp. 1207-1226.

22. Makdisi, F. I. and Seed, H. B., "Simplified Procedure for Estimating Dam and Embankment Earthquake Induced Deformations," Journal of Geotechnical Engineering Division, ASCE, Vol. 104, No. GT7, July 1978, pp. 850-867.

23. Martin, G. R., "The Response of Earth Dams to Earthquakes," thesis presented to the University of California, At Berkeley, CA, in 1965, in partial fulfillment of the requirements for the degree of Doctor of Philosophy.

24. Medvedev, S. and Sinitsyn, A., "Seismic Effects on Earth Fill Dams," Proceeding 3rd World Conference on Earthquake Engineering, New Zealand, 1965, Paper IV/M/18.

25. Minami, I., "On Vibration Characteristics of Fill Dams in Earthquakes," Proceedings 4th World Conference on Earthquake Engineering, 1968, Santiago, Chile, paper A-5, pp. 101-115.

26. Mori, Y. and Kawakami, F. "Dynamic Properties of the Ainono Earth Dam and the Ushino Rockfill Dam," Proceedings, Jap. Soc. Civ. Eng., No. 240, 1975, pp. 129-136.

27. Seed, H. B. and Idriss, I. B., "Soil Moduli and Damping Factors for Dynamic Response Analysis," Report No. EERC 70-10, Earthquake Engineering Research Center, University of California, Berkeley, CA, December, 1970.

28. Seed, H. B., "A Method for Earthquake-Resistant Design of Earth Dams," Journal of the Soil Mechanics and Foundations Division, ASCE, Vol. 92, No. SM1, January 1966, pp. 14-41.

29. Seed, B. H., Makdisi, F. I. and DeAlba, P., "Performance of Earth Dams During Earthquakes," Journal of the Geotechnical Engineering Division, ASCE, Vol. 104, No. GT7, July 1978, pp. 968-994.

30. Sherard, J. L., Woodward, R. J., Gizienski, S. F. and Clevenger, W. A., Earth and Earth-Rock Dams, John Wiley & Sons, Inc., New York, 1963.

31. Richart, F. E., "Foundation Vibrations," Journal of the Soil Mechanics and Foundations Division, Proceedings ASCE, August 1960, pp. 1-34.

32. Richart, F. E., Jr., and Wylie, E. B., "Influence of Dynamic Soil Properties on Response of Soil Masses," Structural and Geotechnical Mechanics, a volume honoring Nathan M. Newmark, Editor W. J. Hall, Prentice-Hall, Englewood Cliffs, NJ, pp. 141-162, 1977.

APPENDIX A

STANDARD (UNFILTERED) EARTHQUAKE RECORDS OF SANTA FELICIA DAM

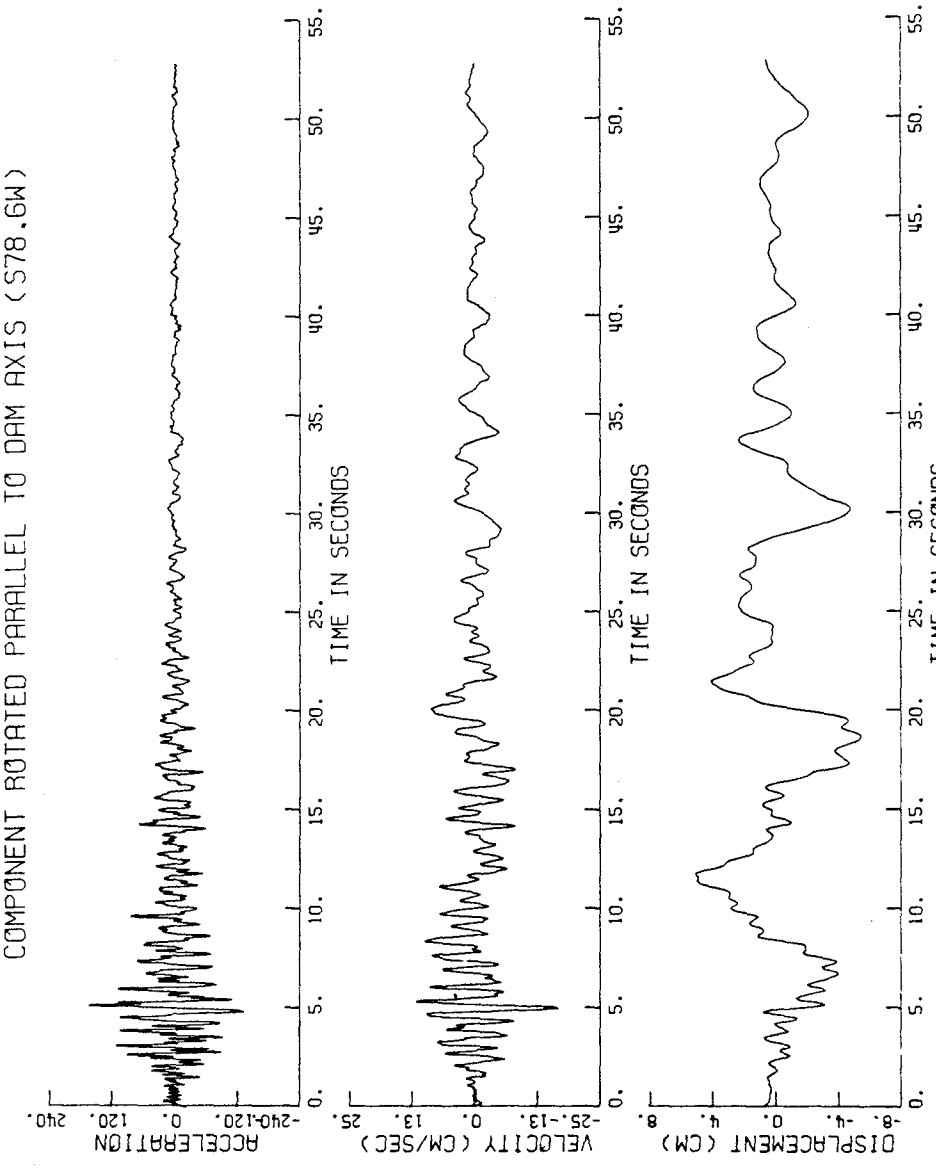
SAN FERNANDO EARTHQUAKE FEB. 9, 1971
SANTA FELICIA DAM, CALIFORNIA, CREST
COMPONENT ROTATED PARALLEL TO DAM AXIS (S78.6W)
ACCELERATION
-240. -120. 0. 120. 240.
VELOCITY (CM/SEC)
-25. -13. 0. 13. 25.
DISPLACEMENT (CM)
-8. -4. 0. 4. 8.
0. 5. 10. 15. 20. 25. 30. 35. 40. 45. 50. 55.
TIME IN SECONDS

Fig. A-1.

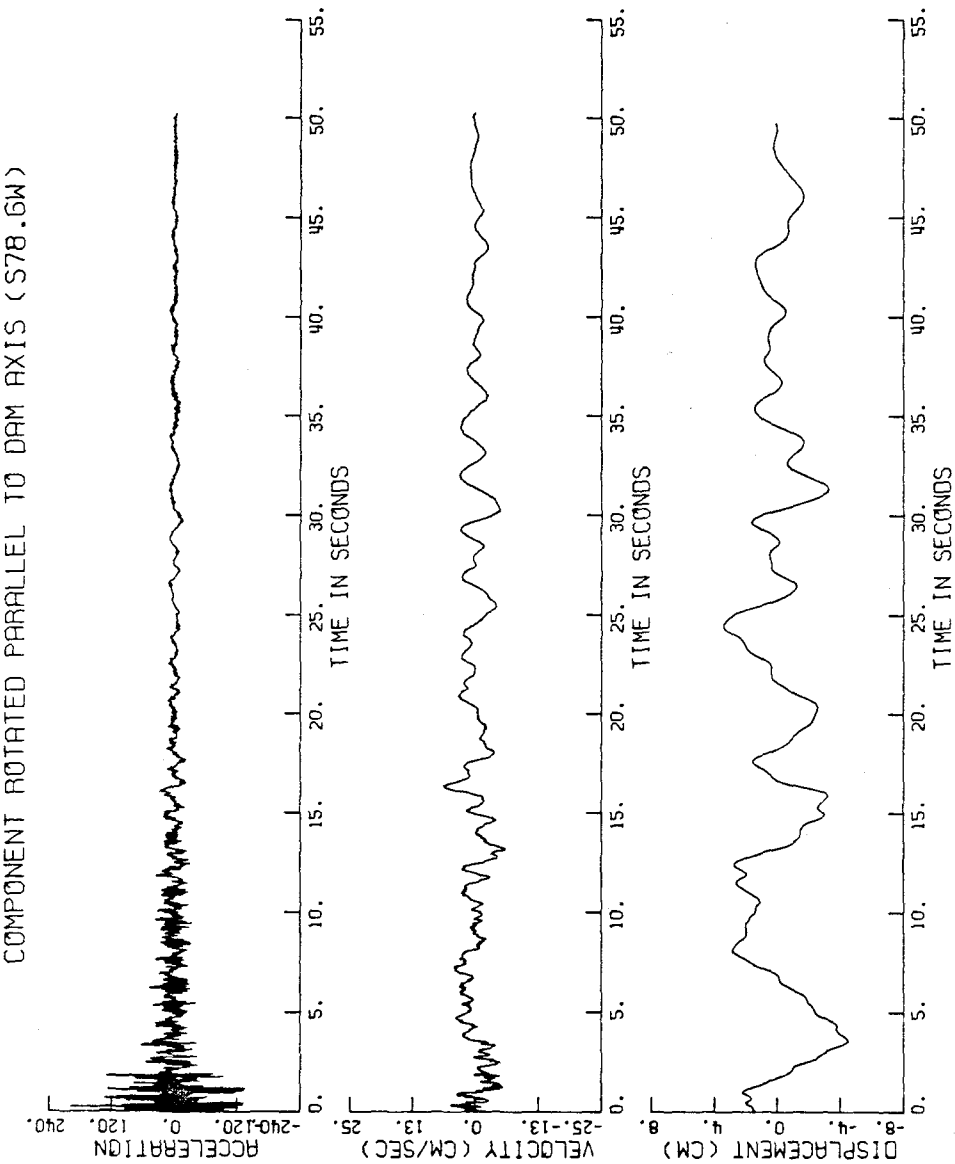
SAN FERNANDO EARTHQUAKE FEB. 9, 1971
SANTA FELICIA DAM, CALIFORNIA, OUTLET WORKS
COMPONENT ROTATED PARALLEL TO DAM AXIS (S78.6W)
ACCELERATION
-240. -120. 0. 120. 240.
VELOCITY (CM/SEC)
-25. -13. 0. 13. 25.
DISPLACEMENT (CM)
-8. -4. 0. 4. 8.
0. 5. 10. 15. 20. 25. 30. 35. 40. 45. 50. 55.
TIME IN SECONDS

Fig. A-2.

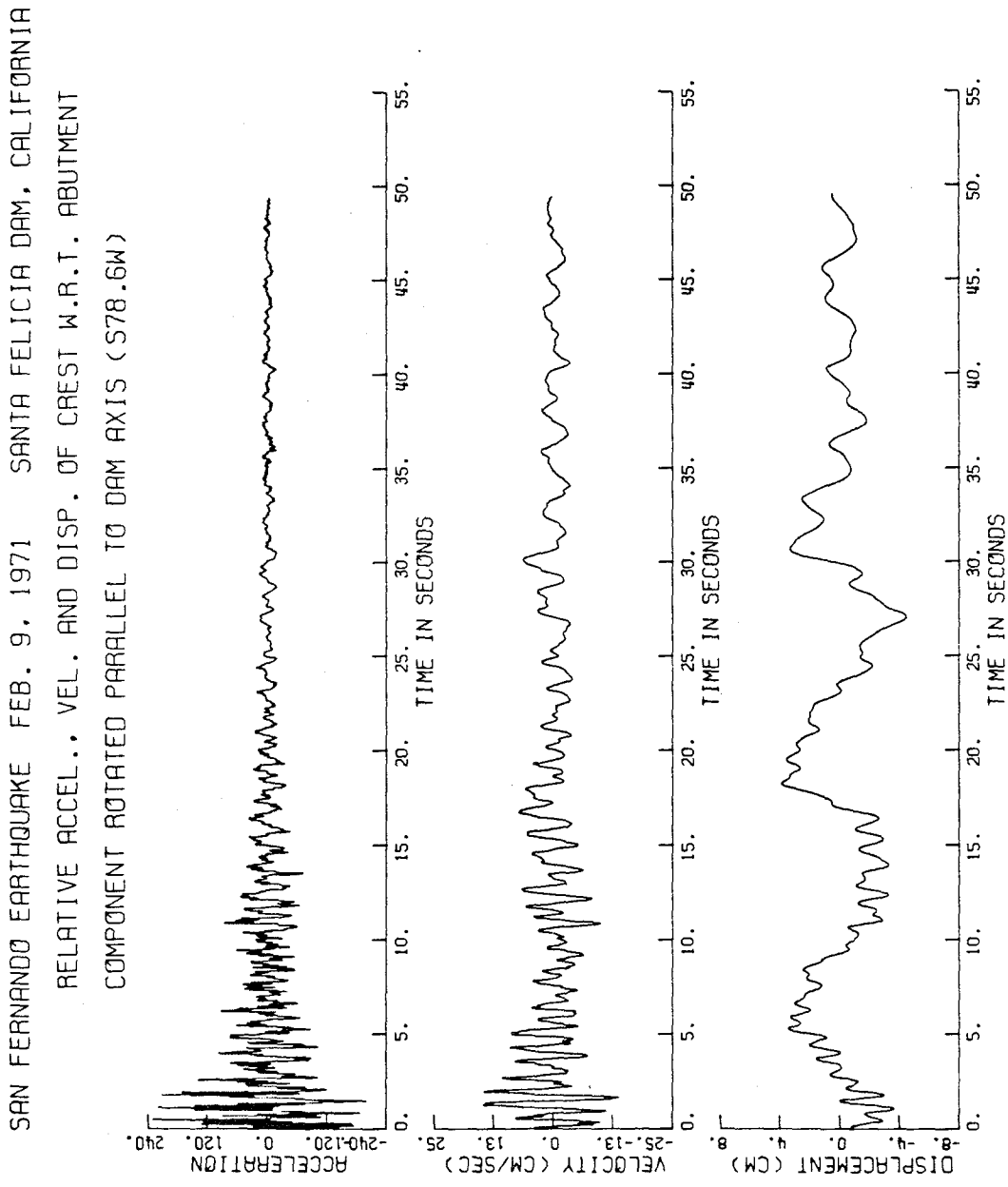
SAN FERNANDO EARTHQUAKE FEB. 9, 1971 SANTA FELICIA DAM, CALIFORNIA
RELATIVE ACCEL., VEL. AND DISP. OF CREST W.R.T. ABUTMENT
COMPONENT ROTATED PARALLEL TO DAM AXIS (S78.6W)
ACCELERATION
VELOCITY (CM/SEC)
DISPLACEMENT (CM)
TIME IN SECONDS

Fig. A-3.

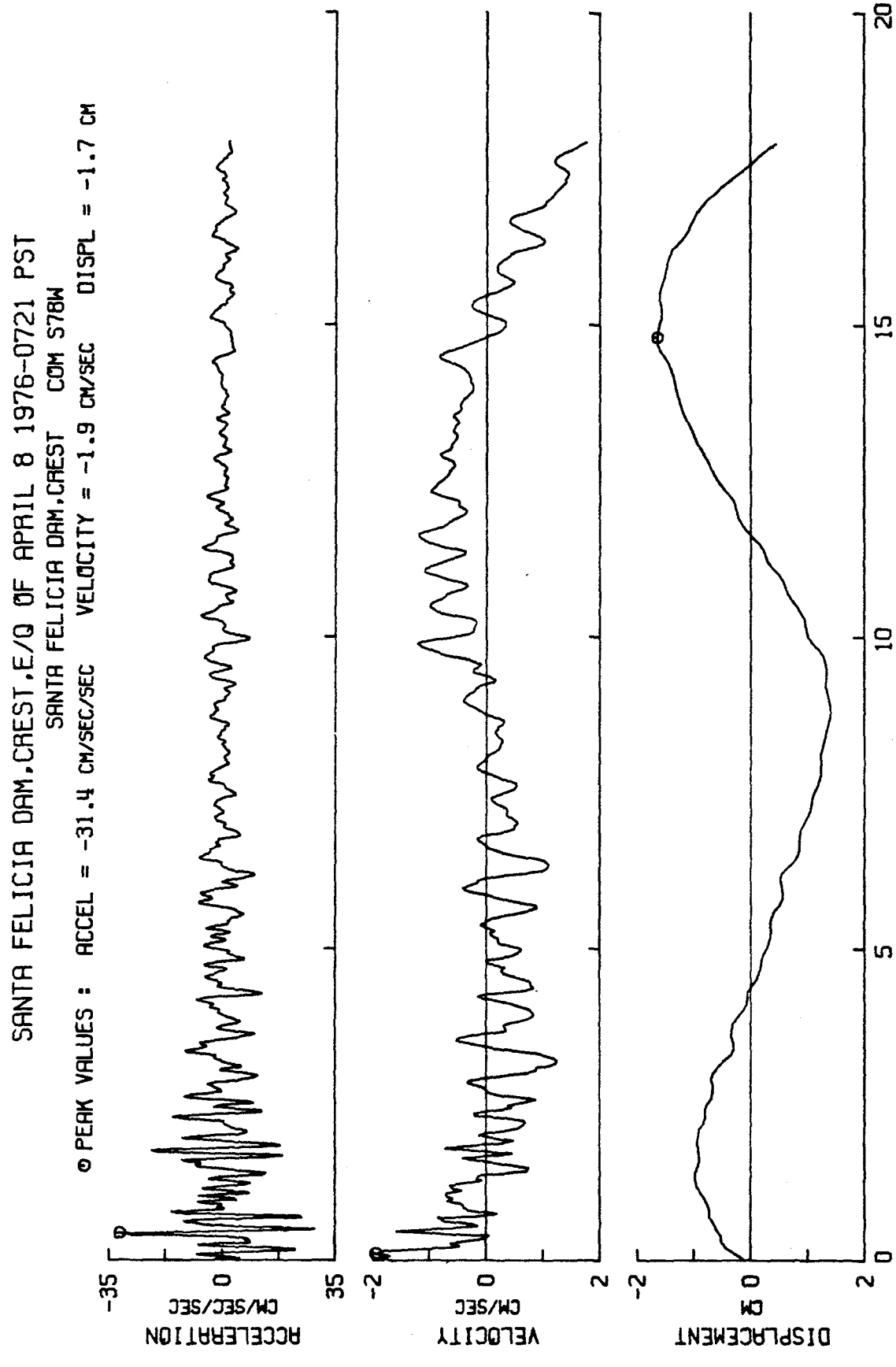
SANTA FELICIA DAM,CREST,E/Q OF APRIL 8 1976-0721 PST
SANTA FELICIA DAM,CREST COM S78W
Φ PEAK VALUES : ACCEL = -31.4 CM/SEC/SEC VELOCITY = -1.9 CM/SEC DISPL = -1.7 CM
ACCELERATION
CM/SEC/SEC
-35
0
35
VELOCITY
CM/SEC
-2
0
2
DISPLACEMENT
CM
-2
0
2
0
5
10
15
20
TIME - SECONDS

Fig. A-4.

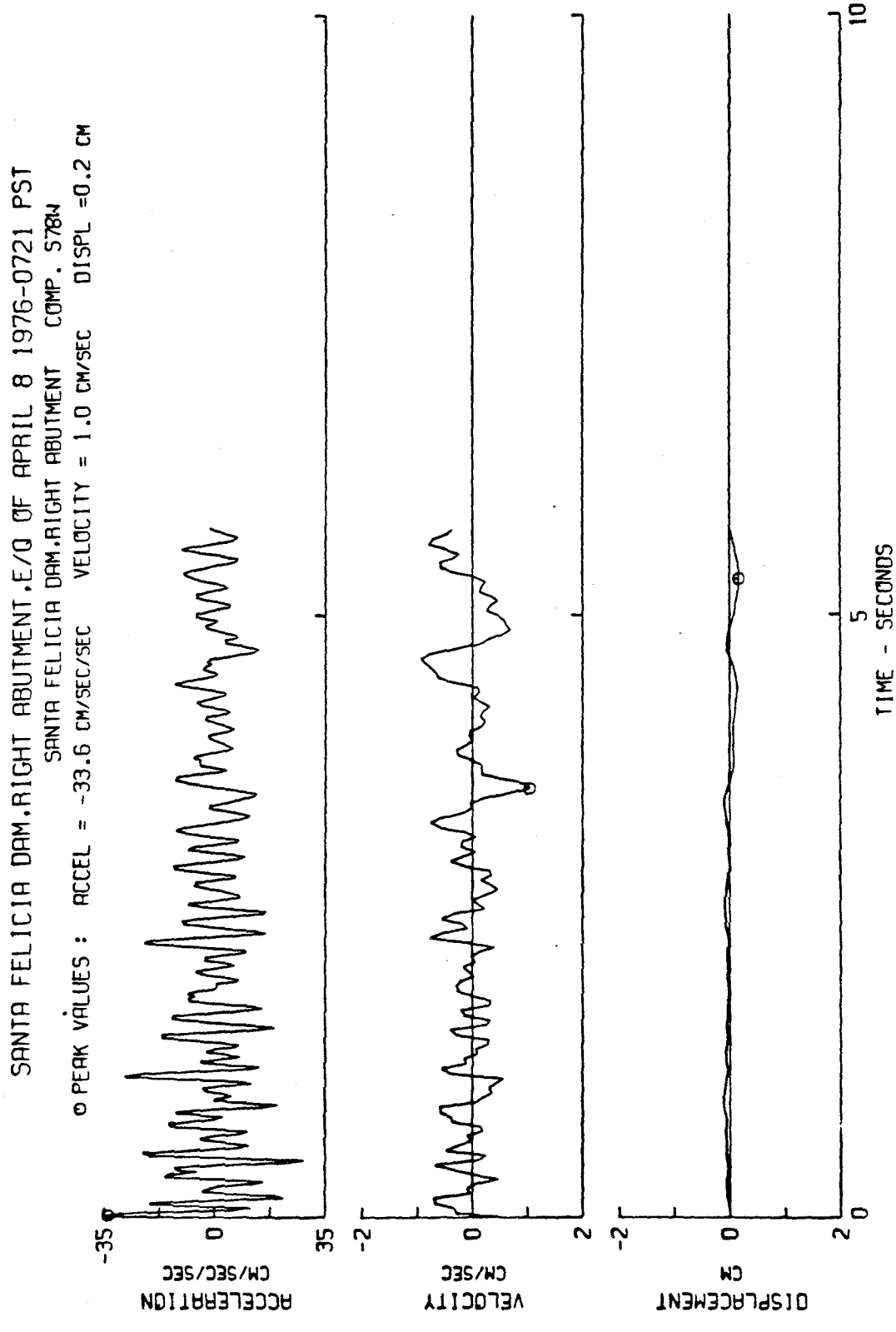
SANTA FELICIA DAM,RIGHT ABUTMENT,E/Q OF APRIL 8 1976-0721 PST
SANTA FELICIA DAM,RIGHT ABUTMENT COMP. S70W
PEAK VALUES : ACCEL = -33.6 CM/SEC/SEC VELOCITY = 1.0 CM/SEC DISPL =0.2 CM
ACCELERATION
CM/SEC/SEC
-35
0
35
VELOCITY
CM/SEC
-2
0
2
DISPLACEMENT
CM
-2
0
2
0
5
10
TIME - SECONDS

Fig. A-5

APPENDIX B

TABLES OF SHEAR STRAINS AND STRESSES INDUCED BY THE TWO EARTHQUAKES

Table B-1

Estimated Longitudinal Shear Strains and Stresses and the Corresponding Shear Moduli

San Fernando Earthquake of February 9, 1971

Cycle No.	Time Secs	Max.Accel. $(\ddot{x} + \ddot{w}_g)_{max}$ (cm/sec^2) +ve	Max.Accel. $(\ddot{x} + \ddot{w}_g)_{max}$ (cm/sec^2) -ve	Max.Displ. x_{max} cm +ve	Max.Displ. x_{max} cm -ve	Average $(\ddot{x} + \ddot{w}_g)_{max}$ cm/sec^2	Average x_{max} cm	Slope $\frac{(\ddot{x} + \ddot{w}_g)_{max}}{x_{max}}$ /sec^2	Equiv. Stress lb/ft^2	Equiv. Strain Percent ($\times 10^{-2}$)	Equivalent Shear Modulus lb/ft^2 ($\times 10^6$)
1	0.0-0.75	40.0	--	0.50	--	40.0	0.50	80.0	471.2	2.04	2.31
1*	.50-1.0	60.0	52.0	0.80	0.66	56.0	0.73	76.7	659.8	2.93	2.21
2	1.0-2.0	72.8	72.0	1.00	1.00	72.2	1.00	72.2	849.9	4.08	2.08
3	2-3	75.0	75.0	1.08	1.08	75.0	1.08	69.4	883.5	4.40	2.01
4	3-4	60.5	60.0	0.91	0.92	60.3	0.92	65.9	710.3	3.75	1.89
5	4-5	40.0	46.5	0.63	0.75	43.3	0.69	62.8	510.1	2.81	1.82
6	5-6	34.0	30.0	0.47	0.50	32.0	0.49	65.3	377.0	2.00	1.89
7	6-6.75	25.0	27.0	0.25	0.35	26.0	0.30	90.0	306.3	1.22	2.51
7*	6.5-7.0	30.0	27.0	0.40	0.35	28.5	0.38	75.0	335.7	1.55	2.17
8	7-8	17.0	17.0	0.15	0.18	17.0	0.17	100.0	200.3	0.69	2.90
9	8-9	14.0	10.0	0.13	0.13	12.0	0.13	92.0	141.4	0.53	2.67
10	9-10	21.0	18.0	0.25	0.20	19.5	0.23	84.8	229.7	0.94	2.44
11	10-11	27.5	25.0	0.38	0.33	26.3	0.36	73.1	309.8	1.47	2.11
12	11-12	28.0	29.0	0.47	0.48	28.5	0.48	59.4	335.7	1.96	1.71
13	12-13	30.0	29.0	0.46	0.46	29.5	0.46	64.1	345.9	1.89	1.83
14	13-14	19.8	20.0	0.27	0.29	19.9	0.28	71.1	233.8	1.16	2.02
15	14-15	12.8	13.0	0.18	0.19	12.9	0.19	67.9	151.4	0.76	1.99
16	15-16	9.0	9.5	0.10	0.11	9.3	0.11	84.6	109.6	0.45	2.44
17	16-17	6.6	8.5	0.07	0.09	7.6	0.08	94.4	89.5	0.33	2.71
18	17-18	7.0	7.2	0.08	0.08	7.1	0.08	88.8	83.5	0.33	2.53
19	18-19	12.0	11.0	0.14	0.14	11.5	0.14	82.1	135.5	0.57	2.38
20	19-20	8.0	8.0	0.10	0.10	8.0	0.10	80.0	94.4	0.41	2.30
21	20-21	6.0	6.0	0.05	0.06	6.0	0.05	109.0	70.7	0.20	3.54
22	21-22	4.2	4.2	0.04	0.04	4.2	0.04	105.0	49.1	0.16	3.07
23	22-23	5.0	5.0	0.05	0.05	5.0	0.05	100.0	58.9	0.20	2.95
24	23-24	8.4	8.4	0.09	0.09	8.4	0.09	93.3	98.5	0.37	2.66
25	24-25	7.7	7.7	0.08	0.08	7.7	0.08	96.3	90.8	0.33	2.75

Table B-2

Estimated Longitudinal Shear Strains and Stresses
and the Corresponding Shear Moduli

Southern California Earthquake of April 6, 1976

Cycle	Time secs	Max.Accel. $(x + w_g)_{max}$ (cm/sec^2)	Max.Displ. x_{max} cm	Equiv. Stress lb/ft^2	Equiv. Strain Percent $(x10^{-2})$	Equiv. Shear Modulus lb/ft^2 $(x\ 10^6)$
1	0-1	2.4	0.025	28.27	0.102	2.77
2	1-2	1.9	0.017	22.38	0.069	3.24
3	2-3	2.3	0.030	27.09	0.122	2.22
4	3-4	4.2	0.050	49.48	0.204	2.42
5	4-5	2.6	0.040	30.63	0.163	1.88